

IEEE ICRA 2010 Full Day Workshop



Snakes, Worms and Catheters: Continuum and Serpentine Robots for Minimally Invasive Surgery

Monday May 3, 2010
Anchorage, Alaska USA

Organizers:
Pierre E. Dupont
Mohsen Mahvash

Workshop Contents

1- Introduction

2- Abstract of Invited Talks

• Neal Tanner, Hansen Medical (commercialization)	3
• David Camarillo, Hansen Medical (robotic catheters)	5
• Howie Choset, Carnegie Mellon University (snakes)	6
• Pierre Dupont, Children's Hospital Boston, HMS (continuum robots)	8
• Koji Ikuta, Nagoya University (robotic catheters)	9
• Joseph Madsen, MD, Children's Hospital, Harvard Med (clinical perspective)	11
• Mohsen Mahvash, Children's Hospital Boston, HMS (continuum robots)	12
• Rajni Patel, University of Western Ontario (robotic catheters)	14
• Cameron Riviere, Carnegie Mellon University (worm robots)	16
• Nabil Simaan, Columbia University (NOTES)	17
• Russell Taylor, Johns Hopkins University (snake robots)	19
• Robert Webster, Vanderbilt University (continuum robots)	20
• Guang-Zhong Yang, Imperial College (snake robots)	23

3- Short Papers

• A Highly Articulated Robotic System (CardioARM) is Safer than a Rigid System for Intrapericardial Intervention in a Porcine Model	24
• Towards a Minimally Invasive Neurosurgical Intracranial Robot	27
• Uncertainty Analysis in Continuum Robot Kinematics	30
• Ultrasound Image-Controlled Robotic Cardiac Catheter System	33
• Steerable Continuum Robot Design for Cochlear Implant Surgery	36
• Modular Needle Steering Driver for MRI-guided Transperineal Prostate Intervention	39
• Distributed Parameter Statics of Magnetic Catheters	42
• A Pilot Study on Using a Flexible Cannula Robot for Micro-Vascular Stenting	45
• Closed-Loop Control of Needle Steering for Percutaneous Kidney Access	48
• Stochastic Modeling and Path Planning for Steerable Needles	51
• A 4-DOF Bendable Endoscope Mechanism For Single Port Access Surgery	54
• Robotization of a Ureteroscope for Efficient Semi-automatic Vaporization of Kidney Stones	57

Introduction

Abstract:

A broad variety of serpentine and continuum robots have been developed for minimally invasive surgical applications. These vary in size from less than a millimeter to several centimeters in diameter and include flexible needles, robotic catheters, multi-segmented sheaths for NOTES applications, snake-like robots capable of suturing and inchworm devices that can move over the heart. While these devices share many common features, little effort has been devoted to exploring and exploiting these commonalities. This workshop focuses on bringing together interested researchers in academia and industry to identify unifying research questions and approaches for these types of devices.

Motivation:

Many surgical applications require reaching tissue deep within the body. Examples include surgery in the throat, inside the heart and in the stomach. Achieving minimally invasive access to these locations imposes unique constraints on robot design. Many ingenious serpentine and continuum robot mechanisms have been developed to satisfy these constraints. Some of these designs consist of multiple miniaturized stages that are connected in series. Many others employ flexible links that function as both link and joint. Developing any of these robots for clinical use poses a common set of problems: design optimization, choice of sensing, kinematic modeling, procedure planning and real-time control. To date, however, researchers interested in a particular design have pursued solutions to these problems independently. This workshop will bring researchers together to identify unifying themes and solution strategies for this class of medical robots. What methods can be shared to enhance telemanipulation capabilities, access to confined surgical spaces and safety? Is there a general kinematic modeling framework that encompasses steerable catheters and snake-like robots? What are the common challenges to clinical acceptance and commercial success for such robots? The goals of the workshop will be to identify such common themes and strategies, to build new partnerships between researchers and to spark new ideas for moving the field forward.

Topics:

- Active catheters
- Continuum robots
- Serpentine robots
- Snake-like robots
- Worm-like robots

Intended Audience:

The primary audience of the workshop consists of those researchers and their students who are currently investigating serpentine and continuum robots for surgical applications. The secondary audience consists of those researchers who are interested in applying this class of robots to medical applications.

Pierre E. Dupont
Director of Pediatric Cardiac Bioengineering
Visiting Professor of Surgery
Children's Hospital Boston, Harvard Medical School
Pierre.Dupont@childrens.harvard.edu

Mohsen Mahvash
Instructor of Surgery
Children's Hospital Boston, Harvard Medical School
mohsen.mahvash-mohammady@childrens.harvard.edu

Robotic Catheter-based Minimally Invasive Procedures: The Sensei X Case Study

Neal Tanner, PhD
Engineering Fellow
Hansen Medical, Inc.

Abstract: While traditionally used for simple tasks, such as fluid administration, catheters have evolved into powerful tools for diagnosis and therapy delivery. This is mainly due to their minimally invasive nature, which allows them to reach patients' anatomy through natural ducts and vessels. While this can be an advantage for the patient, it often translates into a more complicated procedure for the physician, which in turn may affect outcomes. Robotics may be able to play a role in facilitating such procedures by creating more capable flexible tools as well as more intuitive interfaces to control them. The talk will focus on some of the opportunities and challenges one may be faced with when building such a system.

Relevant Web Links:

<http://www.hansenmedical.com/home.aspx>
<http://ai.stanford.edu/~barbagli/>



The Sensei X Robotic Catheter System

Control of Robotic Catheters for Cardiac Ablation

David B. Camarillo
UCSF, Dept of Biochemistry and Biophysics
Stanford University, Depts of ME, CS, SURG, & BIOE
Hansen Medical, Inc.

Abstract:

Atrial fibrillation affects 4% of adults over age 60 and puts these patients at risk for stroke. Cardiac catheter ablation can cure this disease, but it is technically very difficult to achieve continuous lesions with manual catheter control. A robotic system may simplify, shorten, and ultimately improve effectiveness of this procedure by providing an intuitive user interface and a precisely controllable catheter.

Hansen Medical, Inc. has developed a catheter control system for atrial fibrillation and other electrophysiology applications. One of the major challenges in this endeavor was to design a catheter that would be sufficiently repeatable so that a relatively simple model could achieve precise control. The result has been one of the most sophisticated catheters in commercial production, and a new modeling framework that accounts for the multiple compliant modes found in a catheter.

In this talk, I will discuss the approach taken by Hansen Medical and collaborators to achieve precise catheter control. In addition, I will reflect on the clinical feedback for the performance of this system and lessons learned in the process.



Artisan Extend™ Control Catheter

References:

1. Camarillo DB, Carlson CR, Salisbury JK. "Configuration Tracking for Continuum Manipulators with Coupled Tendon Drive." *IEEE Transactions on Robotics*. vol. 25, no. 4, pp 798-808, 2009.
2. Camarillo DB, Milne CF, Carlson CR, Zinn MR, Salisbury JK. "Mechanics Modeling of Tendon Driven Continuum Manipulators." *IEEE Transactions on Robotics*. vol. 24, no. 6, pp 1262-1273, 2008.
3. Camarillo DB, Krummel TM, Salisbury JK. "Robotic Technology in Surgery: Past, Present and Future." *American Journal of Surgery*. vol. 188. no. 4A, pp. 2S-15S, 2004.
4. Camarillo DB, Carlson CR, Salisbury JK. "Task-space Feedback Control of Continuum Manipulators with Coupled Tendon Drive." *Springer Tracts in Advanced Robotics*. vol. 54 pp. 270-280. Athens, Greece. 2008
5. Camarillo DB, Loewke KE, Salisbury JK. "Vision Based 3-D Shape Sensing of Flexible Manipulators." *Proceedings of the IEEE International Conference on Robotics and Automation*, Pasadena, CA, 2008.

Relevant Web Links: www.hansenmedical.com/

Enabling Medical Robotics for the Next Generation of Minimally Invasive Procedures

Howie Choset

Robotics Institute, Carnegie Mellon University

Marco Zenati, M.D.

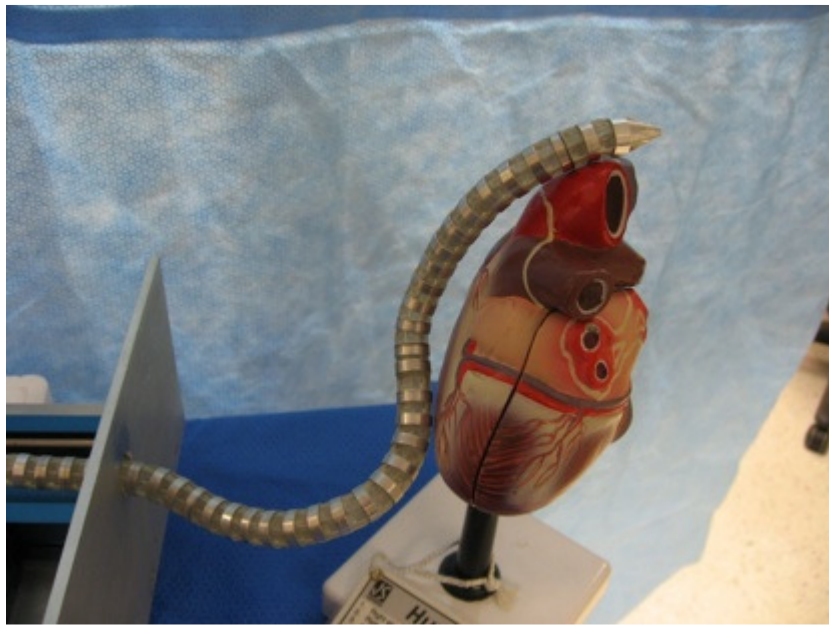
Department of Surgery, University of Pittsburgh

Abstract:

Minimally invasive surgery is the greatest advance to the art and science of surgery since Lister introduced antiseptic techniques 150 years ago. By accessing anatomical targets through a small incision with specialized tools, the clinical benefits to patients are profound: less soft tissue disruption, reduced pain, faster healing and recovery, and fewer complications. However, despite their proven track record, minimally invasive devices are still quite limited in that they are rigid or only reach superficial regions in the body. One reason for this is that they are mechanical, lacking true computational capabilities that we have enjoyed in other fields. By developing and combining the mechanical and computational, the robotics field can make true advances to all medical interventions.

Already, we have seen robotics enter the operating room. Without a doubt, the da Vinci™ surgical robot by Intuitive Surgical represents the greatest success in medical robotics with hundreds of systems installed throughout the world. Ultimately, however, we envision future medical robots will be ubiquitous and so well integrated into the OR that they will not be recognizable by today's standards of what we call a robot. We will see everyday tools become robotic, such as Hansen Medical's Sensei™ Robotic Catheter System. The Hansen device is just the beginning, especially when one considers navigating outside the luminal spaces.

In this talk, we will describe a surgical snake robot called the CardioARMTM which was invented at Carnegie Mellon and is undergoing commercial development by a new startup called Cardiorobotics, co-located in Pittsburgh, PA and Newport, RI. The CardioARM has 102 degrees of freedom and is capable of following a curve in three dimensions. We have performed several experiments on live pigs and human cadavers to establish the efficacy of the CardioARM for minimally invasive cardiac surgery. In addition to describing the technology, we will also talk about our "story" which led us to start Cardiorobotics and ultimately to a commercial product.



CardioARM articulating around a model of a heart

References:

- 1.“Highly Articulated Robotic Surgical System for Minimally Invasive Surgery.” Ota T, Degani A, Schwartzman D, Zubiate B, McGarvey J, Choset H, Zenati MA. Ann Thorac Surg, 2009.
- 2.“A Novel Highly Articulated Robotic Surgical System for Cardiac Ablation.” Takeyoshi Ota, MD, PhD, Amir Degani, David Schwartzman, Brett Zubiate, Jeremy McGarvey, Howie Choset, and Marco A. Zenati. International Conference of the IEEE Engineering in Medicine and Biology Society, Vancouver, British Columbia, Canada, 20th - 24th August, 2008.
- 3.“Highly Articulated Robotic Probe for Minimally Invasive Surgery,” Amir Degani, Howie Choset , Marco Zenati, Take Ota and Brett Zubiatte. International Conference of the IEEE Engineering in Medicine and Biology Society, Vancouver, British Columbia, Canada, 20th - 24th August, 2008.
- 4.“Epicardial Atrial Ablation Using a Novel Highly Articulated Robotic Probe through a Subxiphoid Approach,” T. Ota, A. Degani, A. Wolf, H. Choset, and M. Zenati. Am J Cardiol 2006; 98(8):248M.

Concentric Tube Robots – from Lab Bench to Operating Room

Pierre E. Dupont
Children's Hospital, Boston
Harvard Medical School

The question to be answered in medical robotics is, “which came first – the clinical need or the cool technology?” While the venture capitalist wants to hear that it is the clinical need, for the engineer, it is often the cool technology. The engineer’s challenge is then to bring the technology to the point where its clinical superiority can at least be inferred if not demonstrated outright for a small set of specific procedures. This is a substantially more difficult task than the typical academic laboratory project and involves solving a set of coupled design problems. For example, should the robot carry out the targeted procedure using the same tools and techniques as are done manually? Or should the surgical techniques be reinvented to fit the capabilities of the robot? Furthermore, what sensors and imaging systems are needed to carry out the procedure? Identifying the appropriate procedures and answering these questions necessitates partnership with savvy clinicians. This talk will describe some of the challenges the speaker’s group has faced in developing the technology of concentric tube robots for applications in beating-heart intracardiac surgery. Since the principles developed are based on the capabilities and limitations of concentric-tube technology, they can be extrapolated to other types of procedures.

Related Publications

1. Sears P, Dupont P. A Steerable Needle Technology Using Curved Concentric Tubes. Conf Proc IEEE/RSJ Intelligent Robots and Systems (IROS) 2006:2850-2856.
2. Huang J, Triedman J, Vasilyev N, Suematsu Y, Cleveland R, Dupont P. Imaging Artifacts of Medical Instruments in Ultrasound-Guided Interventions. Journal of Ultrasound in Medicine 2007;26:1303-1322.
3. Dupont P, Lock J, Itkowitz B, Butler, E. Design and Control of Concentric Tube Robots. IEEE Transactions on Robotics 2010; in press.
4. Dupont P, Lock J, Itkowitz, B. Real-time Position Control of Concentric Tube Robots. Conf Proc IEEE International Conference on Robotics and Automation 2010, in press.



Pre-operative Testing of Concentric-tube Robot

Relevant Web Link: biorobotics.bu.edu

From SMA Active Endoscope to Micro Catheter

Koji Ikuta Ph.D.

Biomicro Mechatronics and Robotics Lab.

Department of MicroNano System Engineering

Graduate School of Engineering

Nagoya University

ikuta@mech.nagoya-u.ac.jp

Abstract:

Author has been investigating a series of work on active snake like robot for medical applications from 1982. Both new device concepts and new mechatronic technologies have been developed by the author's group. The world's first active endoscope driven by the shape memory alloy servo actuator was demonstrated at Tokyo Institute of Technology in 1986 during Prof.Ikuta's Ph.D research. Active catheter using same concept was developed later. The electric current leakage free active catheter was proposed and developed in 2000. The new idea of micro band-pass valve enable to realize multi-degrees of freedom active catheter. Although the original diameter was 2.5mm, the micro fabrication process developed by us can reduce the size down to 0.3mm. Most unique feature of our research is based on the approach from both new material development and new fabrication process. Author has been believed "New principle based mechatronics" will open the future medical robotics.

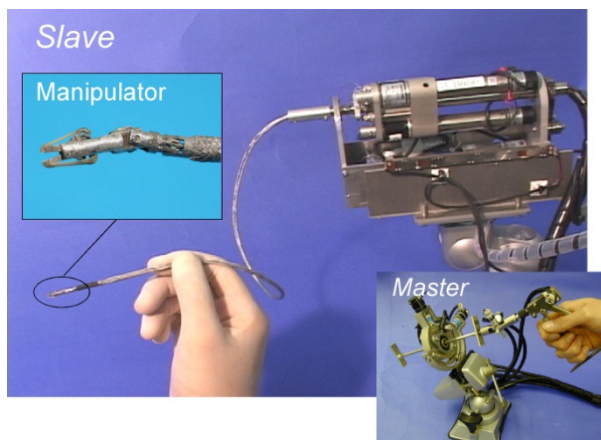
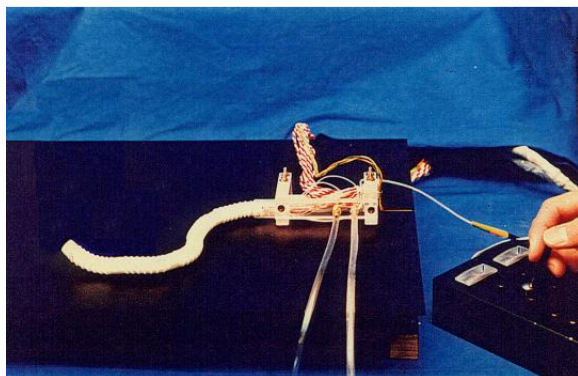
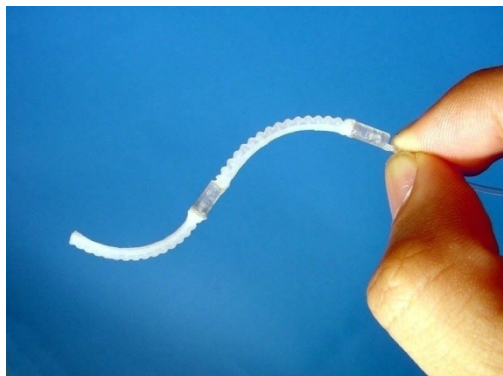
References:

- (1) S.Hirose, K.Ikuta, M.Tuskamoto, "Development of a Shape Memory Alloy Actuator (Measurement of Material Characteristics and Development of Active Endoscope)", Advanced Robotics, Vol.4, No.1, pp.3-27, (1990)
- (2) K.Ikuta, M.Nokata, S.Aritomi, "Biomedical Micro Robots Driven by Miniature Cybernetic Actuator", Proc. of IEEE International Workshop on Micro Electro Mechanical System (MEMS-94), pp.263-268 (1994)
- (3) K.Ikuta, "Shape Memory Alloy Servo Actuator System with Electric Resistance Feedback and Application for Active Endoscope", Computer-Integrated Surgery, MIT Press, (1995)
- (4) K.Ikuta, T.Kato, S.Nagata, "Development of micro-active forceps for future microsurgery", Minimally Invasive Therapy Volume10 Number4/5 October 2001 ISSN 1364-5706,pp.209-213. (2001)
- (5) Koji Ikuta, Hironobu Ichikawa, Katuya Suzuki, "Safety-active Catheter with Multiple-segments Driven by Micro Hydraulic Actuators", In Medical Image Computing and Computer-Assisted Intervention (MICCAI2002),LNCS2488,pp.182-191,2002.

(6) K.Ikuta, H.Ichikawa, K.Suzuki and D.Yajima, Multi-degree of Freedom Hydraulic Pressure Driven Safety Active Catheter, 2006 IEEE International Conference on Roboticsand Automation (ICRA'06), Orlando, Florida, USA, May 15-19, 2006.

(7) M. Ikeuchi, K. Ikuta, "Membrane Micro Emboss following Excimer Laser Ablation (MeME-X) Process" for Pressure-driven Micro Active Catheter, 21st IEEE International Conference on Micro Electro Mechanical Systems (MEMS2008), Tucson, USA, January 13-17, 2008

Relevant web links (URL:<http://www.bmse.mech.nagoya-u.ac.jp>)

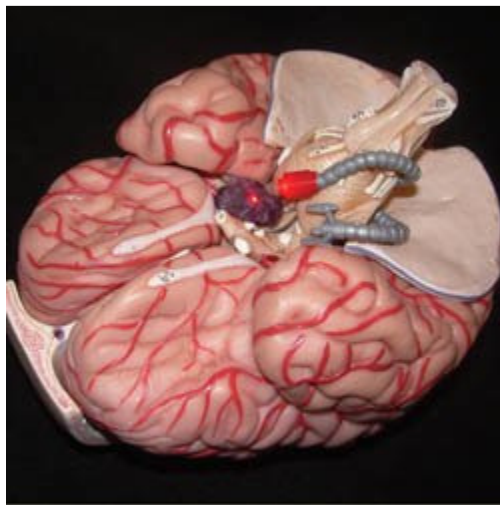


Evolution of the Surgical Robot: the Case for Slithering

Joseph R. Madsen, MD
Department of Neurosurgery
Children's Hospital, Boston
Harvard Medical School

Abstract:

Surgical robots potentially improve clinical care by introducing miniaturization, standardization of repeated movements, elimination of unwanted movements (such as tremor), and the potential of telesurgery. In the current early developmental stage of surgical robotics, devices are favored which mimic human eyes, hands, and arms. A snakelike geometry would allow different classes of surgical problems to be approached with robotic assistance. This review from a clinician's vantage point will highlight body cavities appropriate for such snakelike and wormlike devices throughout the body. The potential for neurosurgical robotics will be stressed. Large exposures with potential morbidity accompany many neurosurgical procedures currently, which might be eliminated by appropriate steerable technology. Optimal integration of visualization and coordinated motion will guide design strategies, and close collaboration between clinical experts and robotic engineers will be essential.



Conceptual Robotic Snakes for Neurosurgery

Relevant Web Links:

www.childrenshospital.org/vector/vector_spr08/from_battlefield_to_brain.html

Active Stiffness Control of Surgical Continuum Robots

Mohsen Mahvash

Instructor of Surgery

Children's Hospital Boston, Harvard Medical School

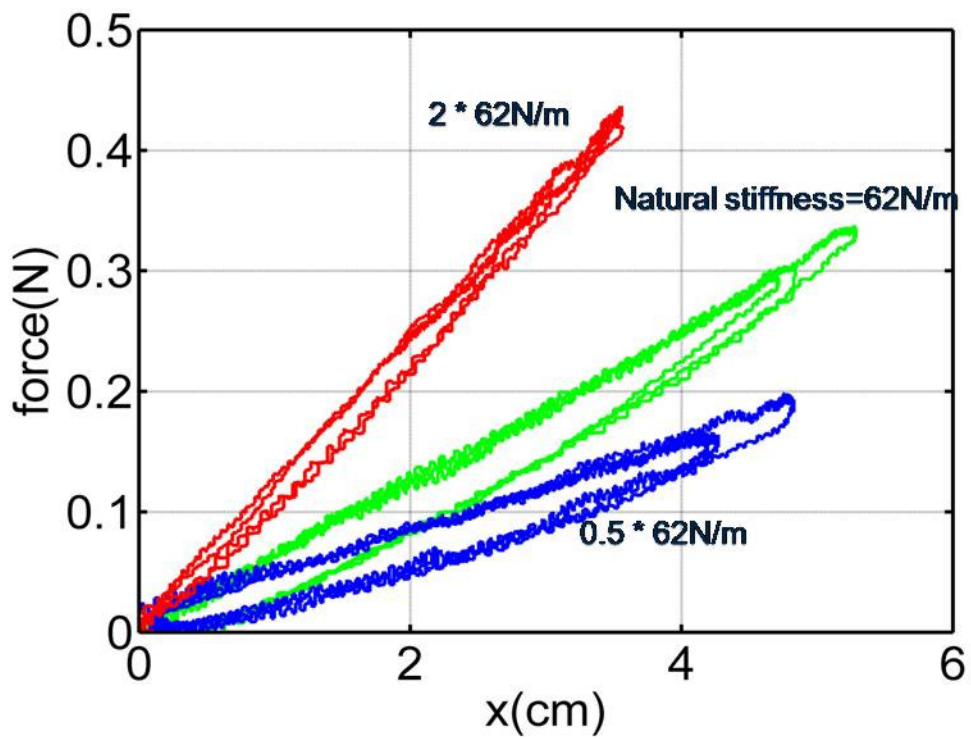
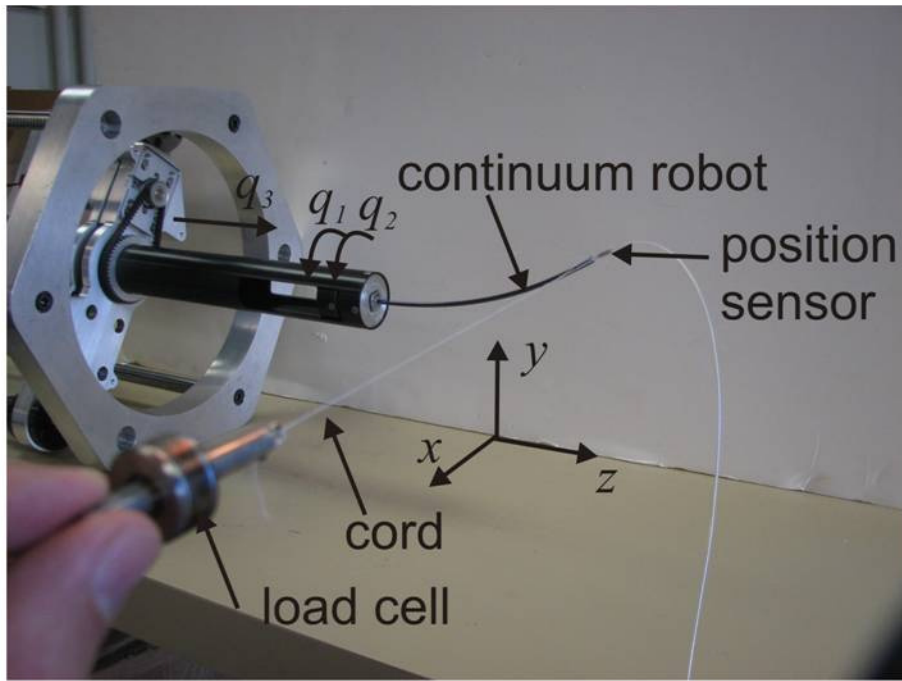
mohsen.mahvash-mohammady@childrens.harvard.edu

Historically, the study of robot-environment interaction has focused on industrial robots interacting with stiff environments in manufacturing tasks. In these applications, robot position control is infeasible since uncertainties in both the position and stiffness of the environment lead to excessive contact forces as well as to the jamming and wedging of parts. A variety of techniques have been developed to address these problems. These include the addition of passive compliant components to the end effector as well as the active control of contact using hybrid force / motion control or stiffness control.

Recently, continuum robots including steerable catheters, multi-backbone snake-like robots and concentric tube robots have been introduced for surgical applications. Despite the inherent passive compliance of these robots, interactions with soft biological environments can still lead to excessive and damaging contact forces. Consequently, hybrid force / motion control and stiffness control can offer the same benefits for continuum robots that these control approaches provide in industrial robot applications. Implementing such controllers on continuum robots is a challenging problem, however, since the kinematic and force mappings are coupled, complex and highly dependent on the type of continuum robot.

In this talk, I will explore our vision for creating real-time control laws that are applicable to broad classes of continuum robots. As an example, I will discuss our results developing active stiffness controllers. We have employed two unifying principles in developing these controllers. First, we use flexion of the robot itself to measure and control tip forces. Second, we utilize a unified kinematic model that can represent many types of continuum robots in contact with their environment. I will explain these ideas in the context of an experimental implementation of stiffness control on a concentric tube robot.

1. M. Mahvash, and P. E. Dupont, Stiffness control of surgical continuum manipulators, *IEEE Transactions on Robotics*, under review.
2. P. Dupont, J. Lock, B. Itkowitz, and E. Butler, "Design and control of concentric tube robots," *IEEE Transactions Robotics*, in press.
3. M. Mahvash and P. Dupont, "Bilateral Teleoperation of Flexible Surgical Robots." *New Vistas and Challenges in Telerobotics Workshop*, IEEE 2008 International Conference on Robotics & Automation, Pasadena, CA, 19-23 May, 2008.



Active stiffness control of a concentric tube robot: (a) experimental setup (b) controller can both increase and decrease natural tip stiffness of robot.

Robot-Assisted Active Catheter Control

Jagadeesan Jayender (jayender@bwh.harvard.edu)

Department of Radiology, Harvard Medical School, CIMIT Image Guidance Laboratory,
Massachusetts General Hospital
Boston, MA

Mahdi Azizian (mazizian@uwo.ca)

Department of Electrical & Computer Engineering, University of Western Ontario
Canadian Surgical Technologies and Advanced Robotics (CSTAR)
London, Ontario, Canada.

Rajni Patel (rvpatel@uwo.ca)

Dept. of Elect. & Comp. Engineering, Dept. of Surgery, University of Western Ontario
Canadian Surgical Technologies and Advanced Robotics (CSTAR)
London, Ontario, Canada.

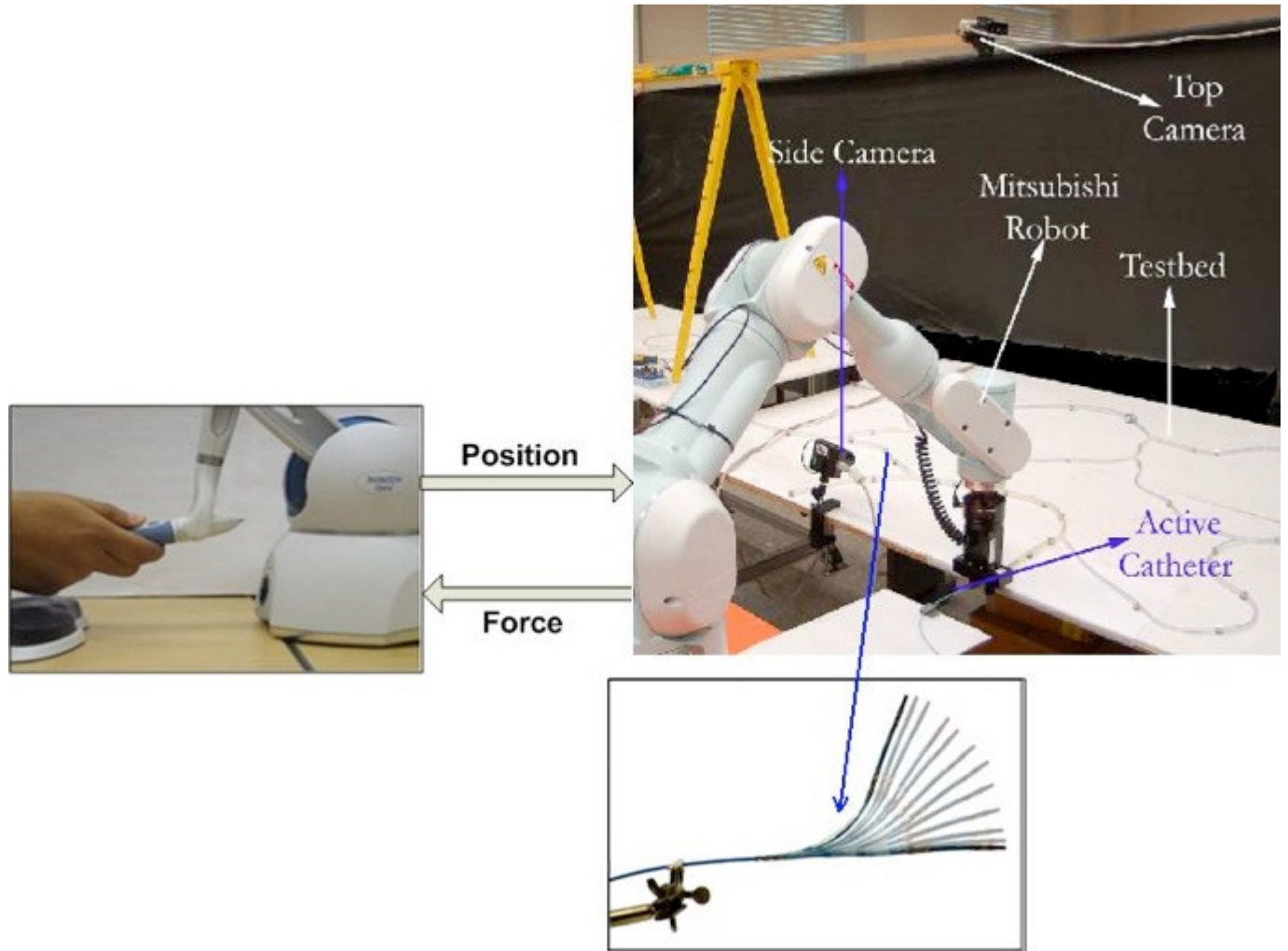
Abstract:

Interventional cardiologists are at a great risk of radiation exposure due to lengthy percutaneous catheter-based procedures performed under X-ray radiation. In addition, excessive force applied by the catheter tip on the artery walls or plaque buildup could lead to rupturing of the artery or dislodging of plaque with potentially dangerous consequences. These problems can be overcome by teleoperated reliable and accurate control of the distal end of the catheter. We have therefore focused on developing robot-assisted control of an active catheter under image guidance. We have developed an active catheter instrumented with Shape Memory Alloy (SMA) actuators, a 5-DOF electromagnetic (EM) position/orientation sensor, and a 3-DOF strain gauge based force sensor [1], [2]. Furthermore, we have demonstrated that a robotic manipulator can be used to control the proximal end of the catheter which inserts or retracts the catheter into the body [3], [4], [5]. We have developed unilateral [6] and bilateral teleoperation algorithms [1], [7] to control the position of the distal end of the catheter. Strain gauges installed close to the tip of the catheter provide force feedback to a haptic device for teleoperated (master-slave) control of the active catheter. A combination of image-based and EM tracking is used for position control [8]. The master-slave control of the catheter enables a clinician to remotely manipulate the catheter, thereby minimizing the clinician's exposure to X-ray radiation. We have also developed a force control algorithm for the active catheter [1] to ensure that the contact force on the distal end of the catheter is regulated to enable smooth insertion of the catheter without damaging the artery walls or dislodging plaque. Our ongoing work is focusing on techniques to improve the control of the active catheter by developing a continuum model for the active catheter [9].

References:

- 1.J. Jayender and R. V. Patel. Wave-variables based bilateral teleoperation of an active catheter. 2nd IEEE RAS & EMBS International Conference on Biomedical Robotics and Biomechatronics (BioRob), pages 27-32, 2008.
- 2.J. Jayender, R. V. Patel, and S. Nikumb. Modeling and control of shape memory alloy actuators. IEEE Transactions on Control Systems Technology, 16(2):279-287, 2008.
- 3.J. Jayender, R. V. Patel, and S. Nikumb. Robot-assisted active catheter insertion: Algorithms and experiments. International Journal of Robotic Research, 28(9):1101-1117, 2009.
- 4.J. Jayender, M. Azizian, and R. V. Patel. Autonomous robot-assisted active catheter insertion using image guidance. IEEE/RSJ International Conference on Intelligent Robots and Systems (IROS), pages 889-894, 2007.
- 5.J. Jayender, M. Azizian, and R.V. Patel. Autonomous image-guided robot-assisted active catheter insertion. IEEE Transactions on Robotics, 24(4):858-871, 2008.

- 6.J. Jayender and R. V. Patel. Master-slave control of an active catheter instrumented with shape memory alloy actuators. IEEE/RSJ International Conference on Intelligent Robots and Systems (IROS), pages 759-764, 2007.
- 7.J. Jayender, M. Azizian, and R. V. Patel. Bilateral telemanipulation of a flexible catheter in a constrained environment. IEEE International Conference on Robotics and Automation (ICRA), pages 649-654, 2008.
- 8.M. Azizian, J. Jayender, and R. V. Patel. Image processing algorithms for real-time tracking and control of an active catheter. European Control Conference (ECC), 2007.
- 9.J. Jayender, R. V. Patel, Michaud G., and N. Hata. Optimal transseptal puncture location for robot assisted left atrial catheter ablation. 12th Intl. Conference on Medical Image Computing and Computer Assisted Intervention (MICCAI), 2009.



Master-Slave (Teleoperated) Robot-Assisted Active Catheter Control

Relevant Web Link: <http://www.eng.uwo.ca/people/rpatel/CatheterProject.html>

HeartLander: an Epicardial Crawling Robot for Beating-Heart Surgery

Cameron Riviere, Ph.D.
The Robotics Institute
Carnegie Mellon University

Marco Zenati, M.D.
University of Pittsburgh Medical Center

Abstract:

The goal of accurate minimally invasive surgery on the beating heart presents considerable challenges. The heart beats roughly once per second, and the amplitude of its motion can be over 25 mm. Access is also difficult: the heart is under pressure from the surrounding organs, and any instrument inserted into the pericardial sac must create its own working space. The approach used by many instruments, entering between the ribs, is undesirable because it requires partial deflation of the left lung for access to the heart. To address these challenges, we have developed HeartLander, a tethered miniature mobile robot that adheres to the epicardium using suction, and navigates via inchworm-like locomotion, using flexible nitinol pushwires connected to motors located outside the patient. Due to its flexibility, HeartLander can be inserted through a small incision below the xiphoid process of the sternum, avoiding any interference from the lungs. Clinical procedures envisioned for the system include myocardial injections, epicardial lead placement, and epicardial ablation. In closed-chest beating-heart experiments *in vivo* in a porcine model, HeartLander has demonstrated acquisition of preselected target locations with average error of 1.7 mm. Ongoing work includes research to optimize the locomotion for minimum treatment time and minimum slippage in the wet intrapericardial environment.

References:

- 1.N. A. Patronik, T. Ota, M. A. Zenati, and C. N. Riviere. A miniature mobile robot for navigation and positioning on the beating heart. *IEEE Transactions on Robotics*, 25(5):1109-1124, 2009.
- 2.T. Ota, N. A. Patronik, D. Schwartzman, C. N. Riviere, and M. A. Zenati. Minimally invasive epicardial injection using a semi-autonomous robotic device. *Circulation*, 118:S115-120, 2008.
- 3.C. N. Riviere, J. Gangloff, and M. de Mathelin. Robotic compensation of biological motion to enhance surgical accuracy. *Proceedings of the IEEE*, 94(9):1705-1716, 2006.



The HeartLander epicardial crawling robot on a Chamberlain Group heart model.

Relevant Links: www.cs.cmu.edu/~heartlander/, www.heartlandersurgical.com

Robotic Technologies for NOTES, Single Port Access Surgery, and Minimally Invasive Surgery in Confined Spaces

Nabil Simaan

Associate Professor

Department of Mechanical Engineering

Columbia University

Abstract:

Natural Orifice Transluminal Endoscopic Surgery (NOTES) and Single Port Access (SPA) surgery are new surgical paradigms that promise to further reduce or eliminate the number of access incision ports compared to traditional minimally invasive surgery. While these new paradigms are being explored in a handful of academic centers, their progress and widespread use are hampered by many technological challenges that present research opportunities and challenges for the medical robotics and the surgical communities.

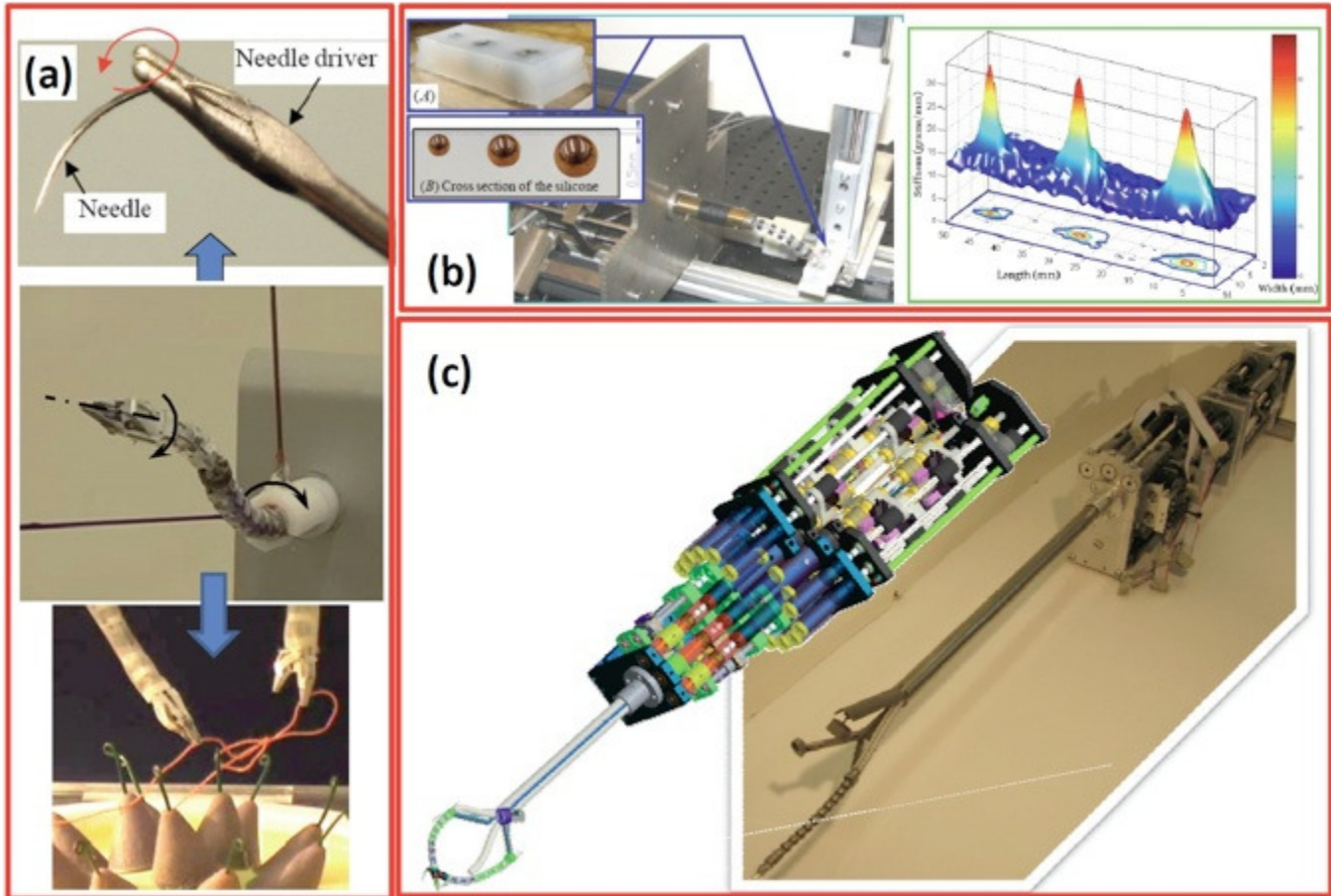
This talk will explore some of these challenges and the necessities of their technological solutions. This talk will identify the challenges associated with addressing the needs of (NOTES) and Minimally Invasive Surgery (MIS) in confined spaces. The focus of the talk will be a discussion of design, control, and deployability considerations for these applications. We will specifically discuss our experience on the design of multi-backbone continuum robots for these applications while focusing on modeling frameworks for evaluating the dexterity of design alternatives, control strategies to mitigate backlash, and new methods for force sensing and feedback using joint-level (intrinsic) information and extrinsic information.

Related Works:

- 1.N. Simaan, "Snake-Like Units Using Flexible Backbones and Actuation Redundancy for Enhanced Miniaturization," in IEEE International Conference on Robotics and Automation Barcelona, Spain, 2005, pp. 3020-3028.
- 2.N. Simaan, R. Taylor, and P. Flint, "High Dexterity Snake-like Robotic Slaves for Minimally Invasive Telesurgery of the Upper Airway," in MICCAI 2004 (7th International Conference on Medical Image Computing and Computer-Assisted Intervention), 2004, pp. 17-24.
- 3.N. Simaan, R. Taylor, and P. Flint, "A Dexterous System for Laryngeal Surgery - Multi-Backbone Bending Snake-like Slaves for Teleoperated Dexterous Surgical Tool Manipulation," in IEEE International Conference on Robotics and Automation New Orleans, 2004, pp. 351-357.
- 4.N. Simaan, R. Taylor, P. Flint, and A. Hillel, "Minimally Invasive Surgery of the Upper Airways: Addressing the Challenges of Dexterity Enhancement in Confined Spaces," in Surgical Robotics - History, Present and Future Applications. vol. Nova Science Publications, R. Faust, Ed., 2007261-280.
- 5.K. Xu, R. Goldman, J. Ding, P. Allen, D. Fowler, and N. simaan, "Design and Deployment Animation of an Insertable Robotic Effector Platform for Single Port Access (SPA) Surgery," in IEEE/RSJ International Conference on Intelligent RObots and_Systems (IROS) St. Louis, 2009, pp. 5546-5552.
- 6.J. Ding, K. Xu, R. Goldman, P. Allen, D. Fowler, and N. Simaan, "Design, Simulation and Evaluation of Kinematic Alternatives for Insertable Robotic Effectors Platforms in Single Port Access Surgery," in IEEE International Conference on Robotics and Automation Anchorage, Alaska, 2010, p. accepted for publication.
- 7.K. Xu and N. Simaan, "Actuation Compensation for Flexible Surgical Snake-like Robots with Redundant Remote Actuation " in IEEE International Conference on Robotics and Automation, 2006, pp. 4148-4154.
- 8.N. Simaan, K. Xu, A. Kapoor, P. Kazanzides, P. Flint, and R. Taylor, "Design and Integration of a Telerobotic System for Minimally Invasive Surgery of the Throat " International Journal of Robotics Research - special issue on Medical Robotics (special Issue on Medical Robotics), pp. Accepted for publication. First published online on published online on May 27th through IJRR OnlineFirst, 2009, 2009.

- 9.K. Xu and N. Simaan, "An Investigation of the Intrinsic Force Sensing Capabilities of Continuum Robots," IEEE Transactions on Robotics, vol. 24, pp. 576-587, 2008.
10. Bajo and N. Simaan, "Finding Lost Wrenches: Using Continuum Robots for Contact Detection and Estimation of Contact Location," in IEEE International Conference on Robotics and Automation (ICRA'2010) Anchorage, Alaska, 2010, accepted for publication.

1.



Robotic Technologies for NOTES (a) Continuum robots performing rotation about their own backbone as a means for dexterous operation in confined spaces, (b) Continuum robots performing force sensing and stiffness imaging using intrinsic (joint-level) information only, (c) continuum robots used in a recently developed system for single port access surgery.

Relevant Web Links:

<http://www.columbia.edu/cu/mece/arma/index.shtml>

A Perspective on Flexible Robots for MIS

Russell H. Taylor

Department of Computer Science

Engineering Research Center for

Computer-Integrated Surgical Systems and Technology (CISST ERC)

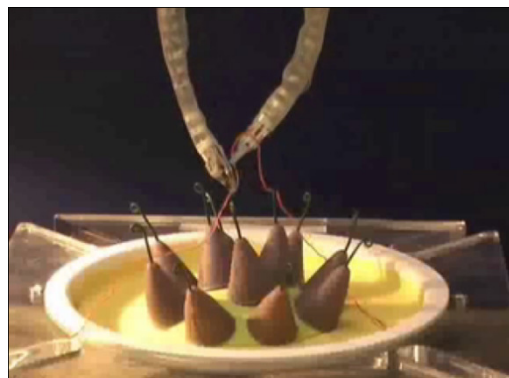
The Johns Hopkins University

Abstract:

This talk is intended to complement the more specific talks by the other speakers in this workshop, which generally report current work on individual systems or projects. Instead, it will try to place flexible robots into the broader theme of medical robotic systems for MIS, in which the robotic device itself is only one component, but which also incorporate imaging, planning, control components, human-machine interfaces, and integration with the broader information infrastructure of the operating room or intervention suite. Within this context, flexible robots, whether "snakes", "continuum" robots such as active cannulas, actively manipulated catheters, or other structures are intended to provide relatively high dexterity or mobility in confined spaces that may not be easily reached by more conventional instrumentation. In many cases, they must be used in conjunction with imaging devices or other sensors and must also accommodate specialized end-effectors or therapy delivery devices. The control for these systems must accommodate both the unique characteristics of the device and higher-level requirements. This talk will draw upon our experience within the CISST ERC and elsewhere to explore some of the research challenges, approaches, and future prospects for these devices as they relate to emerging systems and applications.

Selected References:

- 1.R. H. Taylor, "A Perspective on Medical Robotics", IEEE Proceedings, vol. 94- 9, pp. 1652-1664, September 2006
- 2.R. Taylor, A. Menciassi, G. Fichtinger, and P. Dario, "Medical Robotics and Computer-Integrated Surgery". in Springer Handbook of Robotics: Springer, 2008, pp. 1199-1222.
- 3.M. Loser, N. Navab, B. Basile, and R. Taylor, "Visual servoing for automatic and uncalibrated percutaneous procedures", in Proc. SPIE Medical Imaging, 2000, pp. 270-281
- 4.N. Simaan, K. Xu, A. Kapoor, W. Wei, P. Kazanzides, P. Flint, and R. Taylor, "A System for Minimally Invasive Surgery in the Throat and Upper Airways", Int. J. Robotics Research (special issue on medical robotics), vol. 28- 9, pp. 1134-1153, June 2009.<http://ijr.sagepub.com/cgi/content/abstract/28/9/1134> DOI 10.1177/0278364908104278 NIHMSID 114080.



Bimanual suturing with snake robot

Relevant Web Links: <http://cs.jhu.edu/~rht> , <http://www.cisst.org/>

Modeling, shape sensing, image guidance, and therapeutic applicator integration: Enabling technologies for clinical continuum robots

Robert Webster
Mechanical Engineering
Vanderbilt University

Abstract:

Continuum devices have been key enablers of less invasive surgical and diagnostic access within the human body. The procedures achievable by catheters, bronchoscopes, colonoscopes, etc. illustrate the clinical benefits possible with even relatively simple designs. Thinner and more maneuverable continuum devices promise to enable novel, less-invasive procedures. Coordinating the many degrees of freedom afforded by these new devices often requires a move away from manual control, toward robotic solutions. In the Medical & Electromechanical Design lab at Vanderbilt, we are developing methods of design optimization, sensing, modeling, planning, and real-time control to meet these needs. Though many of our results are broadly applicable, of particular interest to us is one of the thinnest surgical continuum robots developed to date, namely the concentric tube active cannula design.

In particular, we will discuss modeling of continuum robots using rod theory. Recent results account for externally applied forces and moments. In the case of active cannulas, our models also account for general precurvatures of component tubes, and both bending and torsion throughout the device. With respect to shape sensing, we will describe use of self-organizing maps to speed reconstruction of the 3D robot curve from stereo camera images. Toward practical implementation in surgery we will describe use of preoperative medical images to guide the active cannula, enabled by laser surface scans. We will also describe recent motion planning results that determine active cannula configurations 1) to avoid obstacles while reaching a desired target, and 2) within branching lumens in the human lung. Lastly, we will describe initial work toward what appears likely to be the first human clinical application of active cannulas (likely within 2-3 years). We intend to treat large and geometrically complex tumors via acoustically induced hyperthermia, through a single entry point in the organ surface, under three-dimensional ultrasound guidance.

References:

- 1.D. C. Rucker, B. A. Jones, and R. J. Webster III. A Geometrically Exact Model for Externally Loaded Concentric Tube Continuum Robots. *IEEE Transactions on Robotics*. (Accepted)
- 2.R. J. Webster III and B. A. Jones. Design and Modeling of Constant Curvature Continuum Robots: A Review. *International Journal of Robotics Research*. (Accepted)
- 3.D. C. Rucker, R. J. Webster III, G. S. Chirikjian, and N. J. Cowan. Equilibrium Conformations of Concentric-Tube Continuum Robots. *International Journal of Robotics Research*. (Accepted)
- 4.D. C. Rucker and R. J. Webster III. Parsimonious Evaluation of Concentric-Tube Continuum Robot Equilibrium Conformation. *IEEE Transactions on Biomedical Engineering*, 56(9), 2308-2311, 2009.
- 5.D. C. Rucker, J. M. Croom, and R. J. Webster III. Aiming Surgical Lasers With an Active Cannula. *ASME Journal of Medical Devices*, 3(2), pp. 027506, 2009. (Abstract only)
- 6.R. J. Webster III, J. M. Romano, and N. J. Cowan. Mechanics of Precurved-Tube Continuum Robots. *IEEE Transactions on Robotics*, 25(1), 67-78, 2009.
- 7.R. J. Webster III, J. S. Kim, N. J. Cowan, G. S. Chirikjian, and A. M. Okamura. Nonholonomic Modeling of Needle Steering. *International Journal of Robotics Research*, 25(5–6), 509-525, 2006.
- 8.D. C. Rucker, B. A. Jones, and R. J. Webster III. A Model for Concentric Tube Continuum Robots Under Applied Wrenches. *IEEE International Conference on Robotics and Automation*. (Accepted)

- 9.L. A. Lyons, R. J. Webster III, and R. Alterovitz. Planning Active Cannula Configurations Through Tubular Anatomy. IEEE International Conference on Robotics and Automation. (Accepted)
- 10.R. A. Lathrop, D. C. Rucker, and R. J. Webster III. Guidance of a Steerable Cannula Robot in Soft Tissue Using Preoperative Imaging and Conoscopic Surface Contour Sensing. IEEE International Conference on Robotics and Automation. (Accepted)
- 11.J. M. Croom, D. C. Rucker, J. M. Romano, and Robert J. Webster III. Visual Sensing of Continuum Robot Shape Using Self-Organizing Maps. IEEE International Conference on Robotics and Automation. (Accepted)
- 12.J. Das, D. C. Rucker, and R. J. Webster III. A Testbed for Multi-Lumen Steerable Needle Experiments. ASME Design of Medical Devices Conference. (Accepted).
- 13.E. C. Burdette, D. C. Rucker, P. Prakash, C. J. Diederich, J. M. Croom, C. Clarke, P. J. Stolka, T. Juang, E. M. Boctor, and R. J. Webster III. The ACUSITT Ultrasonic Ablator: The First Steerable Needle with an Integrated Interventional Tool. Proceedings of SPIE 2010. (Accepted)
- 14.E. M. Boctor, P. Stolka, C. Clarke, D. C. Rucker, J. M. Croom, E. C. Burdette, and R. J. Webster III. Precisely Shaped Acoustic Ablation of Tumors Utilizing Steerable Needle and 3D Ultrasound Image Guidance. Proceedings of SPIE 2010. (Accepted)
- 15.L. A. Lyons, R. J. Webster III, and R. Alterovitz. Motion Planning for Active Cannulas. IEEE/RSJ International Conference on Intelligent Robots and Systems, 801–806, 2009.
- 16.D. C. Rucker and R. J. Webster III. Mechanics of Bending, Torsion, and Variable Precurvature in Multi-Tube Active Cannulas. IEEE International Conference on Robotics and Automation, 2533-2537, 2009.
- 17.R. J. Webster III, J. P. Swensen, J. M. Romano, and N. J. Cowan. Closed-Form Differential Kinematics for Concentric-Tube Continuum Robots with Application to Visual Servoing. 11th International Symposium on Experimental Robotics 2008, Springer Tracts in Advanced Robotics 2009, 54, 485-494, 2008.
- 18.D. C. Rucker and R. J. Webster III. Mechanics-Based Modeling of Bending and Torsion in Active Cannulas. IEEE RAS/EMBS International Conference on Biomedical Robotics and Biomechatronics, 704-709, 2008.
- 19.R. J. Webster III, J. M. Romano, and N. J. Cowan. Kinematics and Calibration of Active Cannulas. IEEE International Conference on Robotics and Automation, 3888-3895, 2008.
- 20.R. J. Webster III, A. M. Okamura, and N. J. Cowan. Toward Active Cannulas: Miniature Snake-Like Surgical Robots. IEEE/RSJ International Conference on Intelligent Robots and Systems, 2857-2863, 2006.

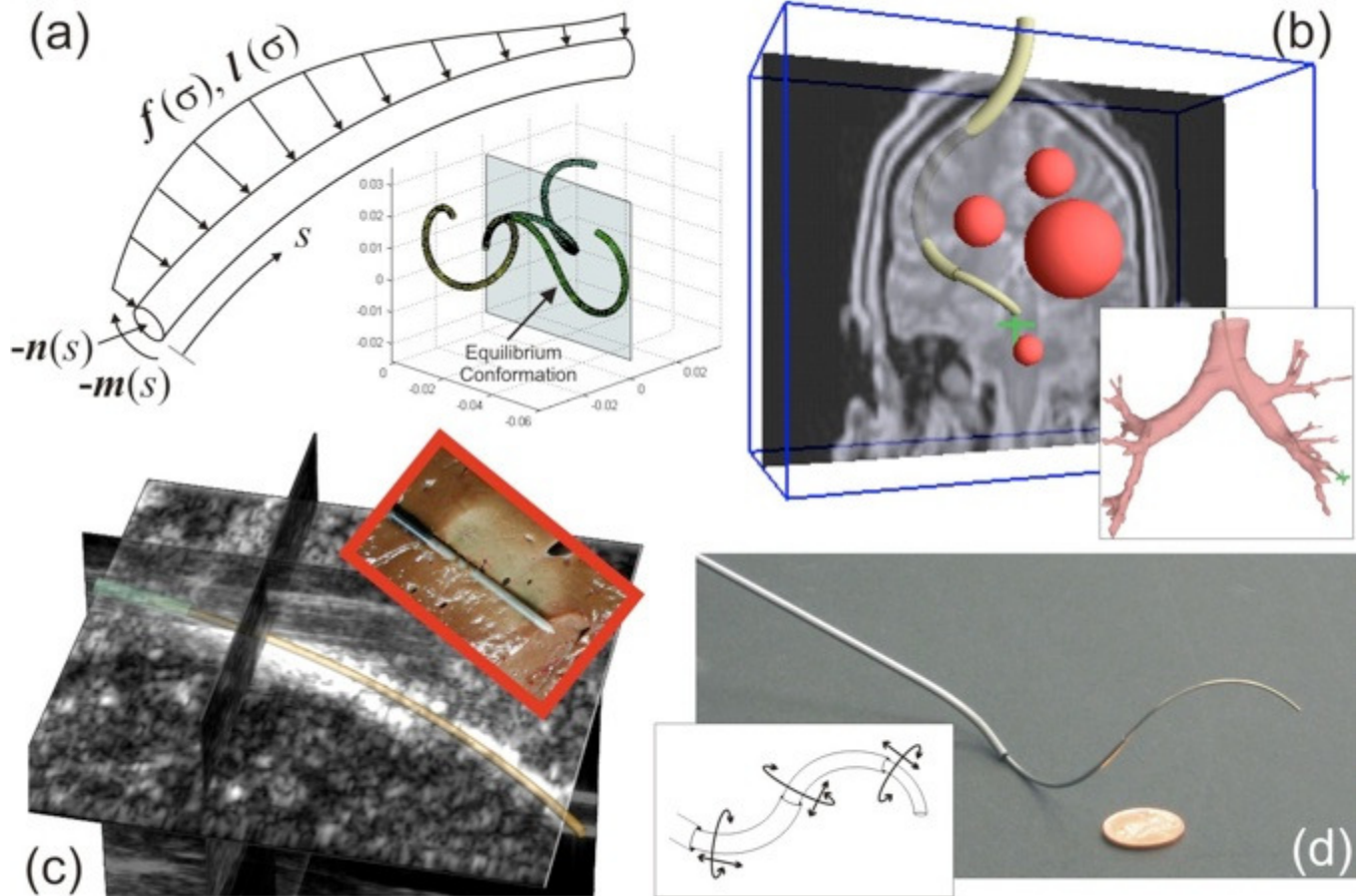


Figure Caption: (a) The most general mechanics-based models of active cannula shape account for point and distributed forces and moments along the robot, and can also handle general precurved tube shapes. (b) Motion planners have been developed which plan paths in the presence of obstacles (e.g. for brain surgery) and within tubes (e.g. for lung biopsy). (c) Recent soft tissue applications include acoustic ablation under 3D ultrasound guidance for liver cancer treatment. (d) Photograph of a prototype active cannula composed of three precurved Nitinol tubes with a line drawing showing degrees of freedom.

Relevant Web Links: <http://research.vuse.vanderbilt.edu/MEDLab/>

Realtime *in situ* *in vivo* surgical sensing and imaging

Guang-Zhong Yang
Imperial College London, UK

Abstract:

Recent technological advances in surgery have resulted in a broad range of new techniques for reducing patient trauma, shortening hospitalisation, and improving diagnostic accuracy and therapeutic outcome. This talk addresses the current paradigm shift and clinical demand in bringing cellular and molecular imaging modalities to an *in vivo* *in situ* setting to allow for real-time tissue characterisation, functional assessment, and intraoperative guidance with articulated surgical robots. It will also cover details on new multimodality imaging methods based on excitation/emission spectral resolution suitable for endoscopy and laparoscopy.

A Highly Articulated Robotic System (CardioARM) is Safer than a Rigid System for Intrapericardial Intervention in a Porcine Model

M. P. Chapman, T. Yokota, T. Ota, S. Tully, D. Schwartzman, B. Zubiate, C. Wright, H. Choset, M. A. Zenati

Abstract— Minimally invasive surgical access to the heart is facilitated using a subxiphoid approach to the pericardial space. We have successfully utilized this methodology using a rigid video-guided device to deliver a variety of epicardial interventions, but this approach is associated with significant hemodynamic compromise and occasionally fatal arrhythmia. A subxiphoid approach to the pericardial space was carried out in two groups (N=5 each) of large porcine subjects. In group A the CardioARM was used to navigate to 6 intrapericardial anatomical targets via 7 routes. In group B (N=5) the SubX approach and navigation to the same 6 targets was performed with the rigid shaft FlexView device. Generally, hemodynamic parameters were only minimally decreased compared to baseline in Group A, while we observed significant compromise in Group B, for targets located deep inside the pericardial space. Moreover, significant arrhythmias were noted in group B only, resulting in the death of one individual. No such arrhythmias were present in the CardioARM group. We conclude that the CardioARM highly articulated robotic system provides superior results to the rigid SVP approach both with respect to hemodynamics and arrhythmogenicity which may well translate into superior patient safety in future, human applications.

I. INTRODUCTION

ACCESS to the heart through a small surgical incision sparing the bony structures of the chest wall is an important technique in modern cardiac surgery. The principle motivation for development minimally invasive cardiac surgery (MICS) techniques has been to improve post-surgical recovery times and reduce the complications of surgery inherent in an open approach, such as pain, infection and wound dihiscence. The subxiphoid approach, utilizing a small abdominal incision is one such technique that shows much promise as it avoids thoracotomy entirely, and could

This work was supported in part by the National Heart, Lung and Blood Institute grant R01HL079940 (to M. A. Zenati).

M. P. Chapman, T. Yokota, T. Ota, and M. A. Zenati (corresponding author, e-mail: zenatim@upmc.edu) are with the Division of Cardiac Surgery, University of Pittsburgh, Pittsburgh, PA 15213 USA.

D. Schwartzman is with the Atrial Arrhythmia Center, University of Pittsburgh, PA, 15213 USA

B. Zubiate and C. Wright are with Cardiorobotics, Inc., (e-mail: bzubiate@cardiorobotics.com)

S. Tully and H. Choset (email: choset@cs.cmu.edu) are with the Robotics Institute at Carnegie Mellon University, Pittsburgh, PA, 15213 USA

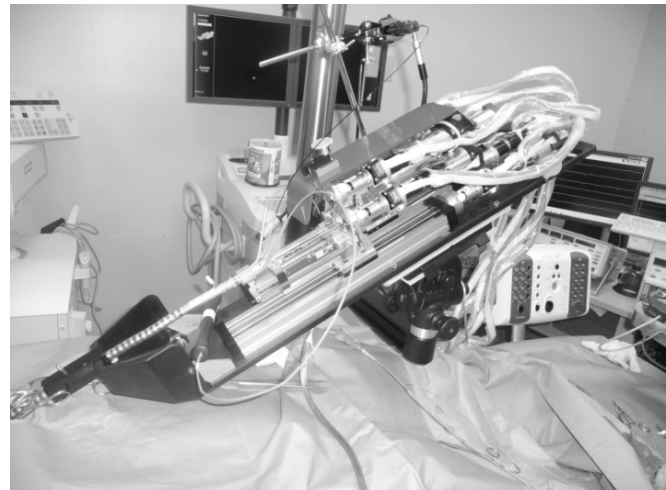


Fig. 1. The CardioARM highly-articulated snake-like robot, mounted a pole in the operating room, in position for the subxiphoid approach

spare a human patient general endotracheal anesthesia and lung deflation.¹ We have previously demonstrated the feasibility of interventions in the pericardial space, including left atrial appendage exclusion, pacing lead implantation and epicardial mapping; utilizing this route with both traditional rigid surgical implements and a highly articulated robotic device, the CardioARM.²⁻⁶

In our previous work, we observed a negative impact on several hemodynamic parameters of our porcine subjects using the rigid subxiphoid videopericardoscopy (SVP). Potentially life-threatening arrhythmias were also observed. These phenomena were most pronounced during interventions at remote targets within the pericardium, requiring significant levering action on the heart or pericardium and were largely absent during anterior approach to the left atrial appendage. We concluded that mechanical compression of the heart and its vessels with the rigid shaft of the videopericardioscopy device was responsible for the observed disturbances in hemodynamic parameters compared to baseline.³

We hypothesized these life-threatening intraoperative difficulties might be overcome by using a flexible, highly articulated device. Our recent development of a highly articulated snake-like robot device designed for epicardial intervention presented itself as a potential solution.^{3,7} The objective of this study is to compare the effect on the intraoperative hemodynamics of porcine subjects during navigation to six intrapericardial targets via a single

subxiphoid port, utilizing either a rigid (VPS) technique or a highly articulated robotic system (CardioARM).

I. METHODS

A. Experimental Setup

The study comprised two groups (Group A: CardioARM; Group B: rigid SVP) each consisting of five large healthy Yorkshire swine (either sex, median weight, 45 kg).. All subjects were sacrificed at the end of the experiment. The study protocol was approved by the Institutional Animal Care and Use Committee of the University of Pittsburgh.

All animals were anesthetized with intramuscular injections of 20 mg/kg ketamine and 2 mg/kg xylazine, and 1% to 5% isoflurane was delivered using a face mask. The animal was placed in the supine position and endotracheally intubated. For both the CardioARM (Group A) and rigid SVP (Group B) subjects, a 15-mm subxiphoid incision was made, and the underlying tissue was dissected to the pericardial level. A small pericardiotomy (5 mm) was created under direct visualization. The respective devices were then introduced into the pericardial space.

Heart rate and rhythm were monitored with electrocardiography. The right carotid artery and jugular vein were exposed through an incision on the right side of the neck, and the right carotid artery was cannulated with a 6-Fr catheter to monitor the arterial BP. The jugular vein was cannulated with a 7-Fr Swan-Ganz catheter to monitor the CVP, pulmonary artery pressure, and SvO_2 . Baseline hemodynamics (systolic, diastolic and mean arterial pressure; systolic, diastolic and mean pulmonary artery pressure; central venous pressure; mixed venous oxygen saturation) were recorded and compared after each target was visually acquired.

B. CardioARM Device and Image Guidance Method

The CardioARM device and the computed tomography (CT) image guidance technique has been described in detail elsewhere.^{2,6} Briefly, the CardioARM consists of a 12 mm by 30 cm snake-like body comprised of 50 links connected by spherical joints with two degrees of freedom. Four cables marionette the motion of the robot to follow a curve in a three-dimensional space allowing it to maneuver in the pericardial space. The current device has a minimum radius of curvature of 4.5 cm and three working channels with ports sufficiently sized for passage of 7 Fr. (approx. 2.5 mm OD) surgical tools and catheters. The user commands motion via joystick.

Navigation was accomplished using CT image guidance indexed to nine metal fiducial landmarks emplaced in skin of the animal's ventral thorax at the time of imaging. The working head of the robot is tracked with respect to these fiducials using a three-axis magnetic tracking coil delivered to the head of the robot via a working channel and an external electromagnetic tracking system (Aurora, NDI). 3-

D CTA images were obtained using an Helical CT scanner (64-Slice LightSpeed VCT; GE Health-care, Milwaukee, WI). CT scanning (120kV, 800mA, pitch of 0.16:1, 350ms/rotation gantry speed) with a thickness of 0.6mm was performed after intravenous injection of an iopamidol contrast agent. Images were reconstructed and real-time guidance was supplied utilizing dedicated software (Blue Belt Technologies, Pittsburgh, PA). Navigational targets were previously identified on the CTA image and were identical to those described for the rigid technique (below).

C. Rigid SVP Device and Technique

An SVP device (FLEXView System; MAQUET Cardiovascular, San Jose, CA) consisting of a 7-mm extended length endoscope with two proximal entry service ports was inserted into the pericardial cavity via a subxiphoid approach. The surgeon manipulated the SVP device under video guidance to six anatomic targets: right atrial appendage (RAA), superior vena cava (SVC), ascending aorta (AO), left atrial appendage (LAA), transverse sinus (TrvS), and atrio-ventricular groove (AVG). Additionally, the left atrial appendage can be targeted via the anterior approach (LAA-A) or posterior approach (LAA-P). In the anterior approach, the SVP device runs along the surface of the anterior left ventricle from the subxyphoid incision toward the left atrial appendage, and in the posterior approach, the SVP device runs over the surface of the posterolateral left ventricle from the subxiphoid incision toward the left atrial appendage. When the device reached a target, it was drawn out to the subxiphoid incision.

D. Data Analysis

The quantitative results were expressed as the mean percent change from each subjects baseline of a given parameter \pm the standard error of the mean (SEM) and analyzed using a software package for statistical analysis (Stata/IC software, version 10.0; Stata Corp., College Station, TX). These percentage changes were compared between groups A and B for each location/route and for each of eight hemodynamic parameters. Wilcoxon's signed-rank test was used to determine the significance of the difference. P values of less than 0.05 were considered statistically significant. Arrhythmogenicity was reported qualitatively in a binary manner as either the presence or absence of operator-identifiable arrhythmia on EKG.

II. RESULTS

Both devices were able to successfully navigate through the epicardial space of the beating heart to all 6 anatomical targets via 7 distinct routes. All 5 animals in group A (CardioARM) survived to conclusion of the experiment. One of five (20%) animals in group B (rigid SVP) suffered a fatal ventricular arrhythmia during exposure of the atrio-ventricular groove. Episodes of arrhythmia were noted during the rigid approach via all 7 routes except for the

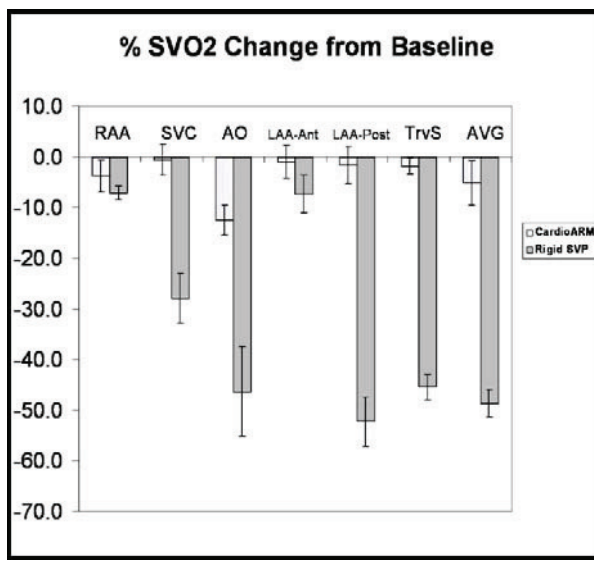


Fig. 2. Percentage change in SvO_2 compared to baseline is greater for rigid SVP (dark grey bars) than CardioARM (speckled bars) at 6 intrapericardial targets (LAA access via two routes). Error bars represent SEM.

anterior approach to the LAA. No arrhythmias were observed using the CardioARM. No gross damage was observed to the heart or other mediastinal structures utilizing either approach. We believe the most likely explanation for the fatal episode of ventricular fibrillation (VF) encountered with rigid navigation to the AV groove to be kinking of the left anterior descending coronary artery and/or compression of the left ventricular outflow tract.

The quantitative hemodynamic data parallels the qualitative arrhythmogenicity data; in that the rigid approach produces far greater disturbances in cardiac function than the CardioARM. A total of eight hemodynamic parameters were measured for the purpose of physiological studies which will be presented elsewhere. The most clinically relevant parameter we measured is the oxygen saturation of the central venous blood (SvO_2), which is a proxy for cardiac output, as this parameter falls as tissue perfusion decreases. Significantly greater drops in SvO_2 were noted in the rigid SVP group compared to CardioARM during surgical manipulations at five of seven of the studied routes: SVC, AO, LAA-Post, TrvS, AVG ($p<0.01$; Fig. 2).

We observed similar changes in central venous pressure (CVP). (Fig 3.) In the case of CVP, the parameter is an inverse proxy for cardiac function, such that the value rises as blood backs up into the venous reservoir with pump failure. The effect on CVP only rises to statistical significance for two locations: the TrvS and AVG. This may reflect the insensitivity of the parameter itself or compensatory physiologic changes outside the scope of our measurement. SvO_2 is the best correlated parameter to observed arrhythmias and may have the greatest value as the benchmark for evaluation of future devices and approaches.

III. CONCLUSION

We demonstrated the ability of the CardioARM, a highly articulated robotic system, to navigate through the pericardial space to potential interventional targets on the epicardium, using image guidance alone. Our data demonstrate the clear superiority of CardioARM over a

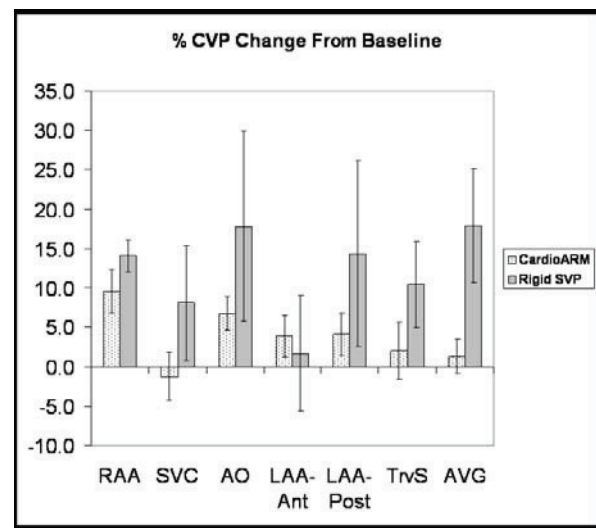


Fig. 3. Percentage change in CVP compared to baseline is greater for rigid SVP (dark grey bars) than CardioARM (speckled bars) at 6 intrapericardial targets (LAA access via two routes). Error bars represent SEM.

conventional rigid device, in terms of hemodynamic stability of the subject during the procedure. These findings suggest that such highly articulated systems may achieve similar improvements over rigid techniques with regard to patient safety during intrapericardial procedures in human patients.

REFERENCES

- [1] R.H. Taylor, A perspective on medical robotics, *Proc.of the IEEE* 94(9), 2006, 1652-1664.
- [2] M.A. Zenati, T. Yokota, D. Schwartzman et. al., "Model-Guided Epicardial Interventions Using a Novel 'Snake' Robot (CardioARM) Through a Subxiphoid Port Acces" in *Proc.14th LASTED Int. Conf.Robotics and Applications*, Cambridge, MA, 2009, pp 242 -246.
- [3] T. Yokota, T. Ota, D. Schwartzman, M. A. Zenati, "Impact of Subxiphoid Video Pericardoscopy With a Rigid Shaft on Cardiac Hemodynamics in a Porcine Model" *Innovations*, vol. 5, no. 1, pp. 51-54, Jan. 2010
- [4] M.A. Zenati, D. Shwartzman , M. Gartner, et al. "Feasibility of a new method for percutaneous occlusion of the left atrial appendage". *Circulation*. vol. 106, no. p. 619.
- [5] T. Ota, D. Schwartzman, M.A. Zenati, "Subxiphoid epicardial left ventricular pacing lead placement is feasible", *J Thorac Cardiovasc Surg* 2009 in press.
- [6] T. Yokota, T. Ota, D. Schwartzman, C. Nikou, B.Jaramaz, H. Choset, M.A. Zenati, "A highly articulated robotic surgery system using an external visualization and navigation system", *Int J CARS* 4(1), 2009, S302.
- [7] A. Degani, H. Choset , A. Wolf, T. Ota, M.A. Zenati, Percutaneous intrapericardial interventions using a highly articulated robotic probe, *Proc. 1st IEEE/RAS-EMBS International Conference on Biomedical Robotics and Biomechatronics*, (BioRob 2006 – Best paper award), Pisa, Italy, 2006, 7-12..

Towards a Minimally Invasive Neurosurgical Intracranial Robot

Mingyen Ho¹, Arvind Ananthanarayanan², Leicester Ehrlich², Rao Gullapalli³, J. Marc Simard³, Satyandra K. Gupta², and Jaydev P. Desai¹

¹*Robotics, Automation, Manipulation, and Sensing (RAMS) Laboratory*

²*Advanced Manufacturing Laboratory (AML)*

^{1,2}*University of Maryland, College Park, MD, USA*

³*University of Maryland School of Medicine, Baltimore, MD, USA*

Email: myho@umd.edu, arvinda@umd.edu, lester.ehrlich@gmx.net, rgullapalli@umm.edu, msimard@surgery1.umaryland.edu, skgupta@umd.edu, jaydev@umd.edu

Abstract— Brain tumors are among the most feared complications of cancer. The prognosis for these patients is poor with a median survival of 4-8 months. The primary reasons are the lack of good continuous imaging modality for intraoperative intracranial procedures and the inability to remove the complete tumor tissue due to its placement in the brain and the corresponding space constraints to reach it. To overcome the above limitations, we envision developing a Minimally Invasive Neurosurgical Intracranial Robot (MINIR). MINIR will be fully MRI compatible, so that the physician can use frequently updated MRI to accurately perform tumor resection. In MINIR, we use two antagonistic shape memory alloy (SMA) wires as actuators for each joint. We also developed a theoretical model based on Tanaka's model to predict the joint motion of the robot by the temperatures of SMA wires. Experimental results from our current prototype of a 2-DOF robot show that we can actuate the SMA wires reliably and hence observe joint motion in a gelatin medium. Finally, we developed a fabrication process using insert molding. In theory, this idea can generate a multi degree of freedom robot in just one processing step without requiring any post molding assembly steps.

I. MATERIALS AND METHODS

A. Robot Design and Actuation

MINIR will be operated under frequently-updated MRI and resect tumor by positioning an instrument that liquefies tissue and washes out the debris. The goal of this project is to develop a prototype of MINIR with demonstrated degrees of freedom and MRI compatible robot body. In current design of MINIR [1] (see Fig. 1), we put all joints on the outside surface of the robot and kept it hollow in the center. Thus, all the wiring and tubes will be kept inside the robot body. This design enables us to route channels for soft-tissue irrigation and electrocautery hardware inside the robot, and which makes the robot more compact, safer and easier to shield. The two probe tips shown in the figure is the envisioned system for electrocauterizing the tumor. The envisioned MINIR has totally nine revolute joints and the motion range of each joint is $\pm 35^\circ$. The workspace of MINIR is shown as Fig. 2, the motion range is $\pm 60\text{mm}$ along x and y directions, and from -20mm to 60mm along the z direction.

Finding a suitable actuator given the above MRI limitation is also challenging. Actuators such as electromagnetic motors are not feasible for use in MRI since they are fabricated from ferromagnetic materials and permanent magnet parts. Several

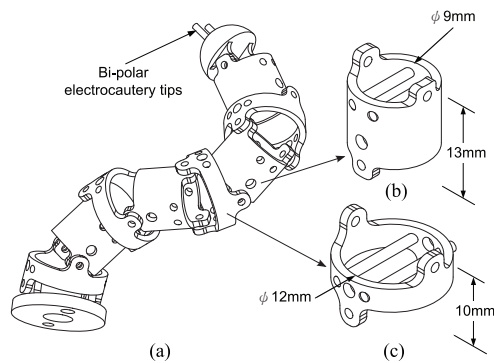


Fig. 1. (a) Envisioned MINIR schematic, (b) Body segment of the prototype and (c) Ring segment of the prototype.

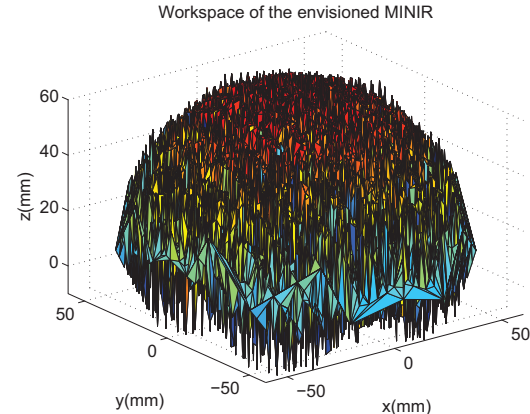


Fig. 2. The workspace of the envisioned MINIR.

other actuation methods are also eliminated due to the special requirements in the MRI environment. Shape memory alloy (SMA) has been proven to be MRI compatible [2] and due to its unique molecular characteristics, it can generate extremely large forces if it encounters any external load during phase transformation. This phenomenon thus provides a unique mechanism for actuation. For each joint of MINIR, we used two antagonistic SMA wires as actuators and each joint could be operated individually. Fig. 3 shows how this actuation mechanism works. In the stationary condition (see Fig. 3(a)),

SMA wires were bent to the desired shape in advance to keep the links straight. When actuating the left side SMA wire, the wire was heated by electric current and it thus recovered its original memorized straight shape. As a result, the body segment will be pushed by the wire and cause a clockwise rotation as shown in Fig. 3(b).

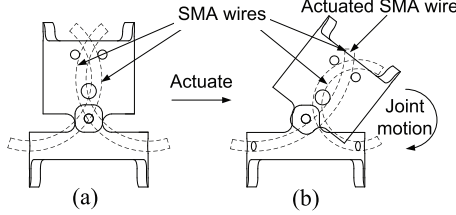


Fig. 3. Actuation mechanism: (a) Stationary (b) Actuated.

B. SMA characterization

The behavior of SMA is a function of three primary variables: stress, strain, and temperature. In our application, we would like to use temperature as a feedback signal to control the motion of an individual joint as well as the end-effector position of the robot. To precisely control the motion of MINIR using temperature feedback, a theoretical model to describe the correlation between temperature and bending displacement (strain) of SMA wires was necessary. We used a widely used constitutive model, namely, Tanaka's model [3], to describe the material behavior (strain-temperature relationship) of the one-way shape memory effect. Under certain conditions, the constitutive equation can be written as a function of martensite phase ratio (ξ) and is given by:

$$\sigma - \sigma_0 = (\varepsilon - \varepsilon_0 - \xi\varepsilon_L)[E_A + \xi(E_A - E_M)] \quad (1)$$

Where σ is the external stress and ε is the strain of SMA. σ_0 and ε_0 are the initial conditions. E_A and E_M are the Young's modulus of SMA in martensite phase and austenite phase respectively. If we assume that the external stress remains constant ($\sigma - \sigma_0 = 0$) and ξ is a function of temperature, then based on Eq. 1, we have the relationship between ε and temperature. Therefore, we can predict the strain of the SMA wire by its temperature.

II. CORRELATING JOINT MOTION WITH TEMPERATURE

After obtaining the strain vs. temperature relationship, the next step is to derive the relationship between the strain and the bending displacement (θ). From the geometry of a link of MINIR (Fig. 4), the following relationship is satisfied:

$$(L\sin\theta + x)^2 + [L\cos\theta + y - (\frac{d}{2\varepsilon} + \frac{d}{2})]^2 = (\frac{d}{2\varepsilon} + \frac{d}{2})^2 \quad (2)$$

Where d is the diameter of the SMA wire and is a known parameter. To summarize, we can measure the temperature of SMA wires by thermocouples and use Eq. (1) to compute the strain in the wire. After obtaining the strain, we can use Eq. (2) to compute the bending displacement of each joint. Thus, we can predict the rotation of each joint

of the robot by knowing the temperature and thus the tip position of MINIR can be computed by forward kinematics. Essentially, this approach enables us to control the tip of the robot by monitoring the temperature of the wire through the thermocouples attached to each SMA actuator.

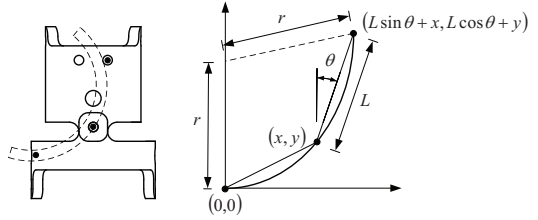


Fig. 4. Correction of the radius of curvature to joint displacement

A. PWM control

Since the motion of the robot can be reliably predicted by temperature, we needed to implement a controller to control the temperatures of SMA wires. PWM is often used to control the supply of electric power to another device. Therefore, we chose PWM to deliver power to heat up individual SMA wires. We used switching circuit, which is comprised of four switches, an on/off discrete control signal, four SMA wires and a DC power supply to realize the PWM control. Note that only one power supply is required to control the four SMA wires. The discrete on/off control signal is used to control the state of the switches and it thus converts the current into an equivalent PWM output command, which activates the corresponding SMA wire and thereby induces joint motion.

B. Robot Fabrication

To provide a cost effective method for fabricating the multiple degree of freedom MINIR, we have developed an in-mold assembly approach using insert molding to prototype MINIR. This approach is illustrated in Fig. 5 using injection molding. This process involves the use of cylindrical metallic parts made of brass as mold inserts. The metallic inserts serve as shut off surfaces between the mold cavities which form the different parts of the revolute joint. Subsequently after cooling, the in-mold assembled revolute joint is ejected from the mold cavity. Using this approach, we have developed a mold design which can be used to fabricate the 9-DOF MINIR.

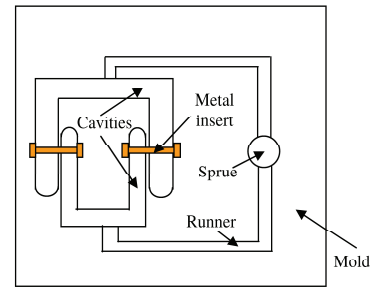


Fig. 5. Mold design concept for In-Mold Assembly using insert molding

III. RESULTS

We did experiments to demonstrate that the motion of an individual joint of MINIR is consistent with the theoretical model described before. These experiments were conducted on a brass prototype which was fabricated using conventional machining and assembly. The SMA wire was pre-strained and attached to the joint. Then constant current was applied to the SMA wire and the thermocouple readings and bending displacement were recorded continuously. The experimental setup is as shown in Fig. 6(a). The experimental result is shown in Fig. 6(b).

In the PWM control test, we heated four SMA wires up to 70°C independently by using only one power supply. The result (see Fig. 7) shows that the controller is capable of heating multiple SMA wires while maintaining the temperatures of other wires and only one power supply is required. Through this temperature control test and the above bending displacement vs. temperature results, we can control the motion of each joint of MINIR simultaneously and independently by using the PWM control scheme with temperature feedback. In neurosurgical application, MINIR

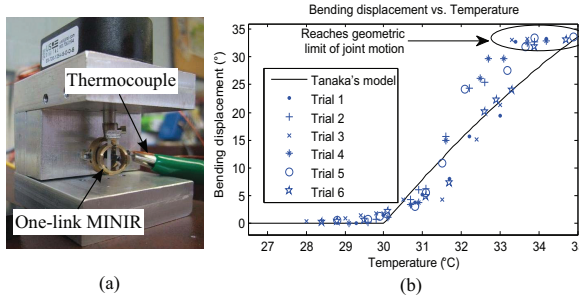


Fig. 6. (a) Experimental setup for the testing of a one-link MINIR, (b) Bending displacement vs. temperature curve of a one-link MINIR.

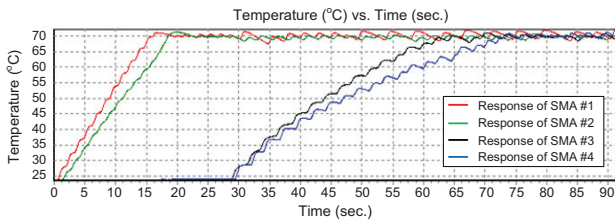


Fig. 7. Test of the PWM controller and the switching circuit for the temperature control of SMA wires.

should be able to move in a tightly enclosed environment (human brain). Thus, a sufficient force is required to move the robot links. Experiment showed that the maximum force can be generated by each link was about 1.5N with a 0.02" SMA wire. Furthermore, we tested the 2-DOF robot in a gelatin slab and the results (see Fig. 8) clearly demonstrate that the 2-DOF robot is able to move in a tightly enclosed environment and push the gelatin away. The horizontal displacement of the robot tip is about 25mm which is of the order of the size of a brain tumor. Using the insert

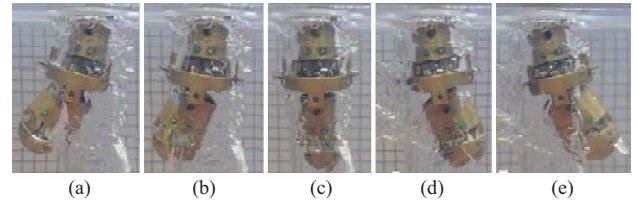


Fig. 8. Test of the 2-DOF robot manufactured using brass in gelatin. (a) Left-most position, (b) Left-middle position, (c) Neutral position, (d) Right-middle position and (e) Right-most position.

molding methods described before, we manufactured a 9-DOF MINIR in a single injection shot. The design of this articulating structure consists of ten independent parts which are connected by metallic mold inserts of 1.58 mm diameter. Fig. 9 shows three different configurations of the 9-DOF articulating structure that we have manufactured. We also



Fig. 9. 9-DOF MINIR manufactured using insert molding.

successfully tested one module of the molded prototype shown in Fig. 9 for actuation using the 0.02" SMA wire. Fig. 10 shows three configurations of the molded module under actuation using SMA wires. As part of our future work, we plan to develop detailed force models for the molded prototype by incorporating the approach we have developed for the MINIR prototype that we have fabricated using brass (as shown in Fig. 8).

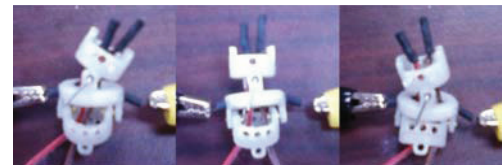


Fig. 10. Test of the 2-DOF robot manufactured using the insert molding process.

REFERENCES

- [1] M. Ho and J. P. Desai, "Characterization of sma actuator for application in robotic neurosurgery," in *Int. Conf. of the IEEE Engineering in Medicine and Biology*, 2009, pp. 6856–6859.
- [2] N. Pappafotis, W. Bejgerowski, R. Gullapalli, M. Simard, S. K. Gupta, and J. P. Desai, "Towards design and fabrication of a miniature mri-compatible robot for applications in neurosurgery," in *Int. Design Eng. Technical Conf. & Computers and Information in Eng. Conf.*, 2008.
- [3] K. Tanaka, "A thermomechanical sketch of shape memory effect: One-dimensional tensile behavior," *Res. Mechanica*, vol. 18, pp. 251–263, 1986.

Uncertainty Analysis in Continuum Robot Kinematics

Sohail Iqbal, Samer Mohammed, Yacine Amirat, and Georges Fried

Abstract—This paper presents a new approach to physical uncertainties in continuum robot kinematics. It considers both physical uncertainties and rounding errors while computing an inverse kinematics using interval analysis. Interval algorithms compute the uncertainty propagation rigorously. Effects of the physical uncertainties can be seen both in joint space and task space. This new insight of the impact of uncertainties can pave the way for the development of guaranteed kinematics schemes mainly for the minimally invasive surgical application. An analysis of the uncertainties in the continuum robot is given and uncertainty impact in joint and task space is shown in simulation. Current analysis is the continuation of our work [1].

Index Terms – Continuum robot, uncertainty analysis, inverse kinematics, interval analysis, surgical robotics.

I. INTRODUCTION

Continuum robots have many distinctive applications including robot navigation in unstructured environment. Special care was given lately for applications dealing with the robotic surgery, where the top priority is the precise control of the both position and orientation of the robot's end-tool [2], [3]. In fact, the current therapeutic trend is development of minimally invasive techniques. This trend is emerged due to clinical needs and has various objectives [4]. First objective is to increase the comfort level for the patient by reducing the pain, traumatism, and recovery time. Second objective is to increase the safety of the patient by enhancing the manipulation precision of surgical instruments, filtering out the surgeon's hand's tremors, and by providing surgeon a scaling factor.

One of the most important concerns to increase the safety of the patient is to take care of the uncertainties that could be there in the surgical system. These uncertainties could be included in the system mainly due to three factors. First factor is the physical errors that could arise in the error tolerance of the robot machining process. Second factor is the error that could arise in the system due to the rounding errors, and third one is the errors that could come in due to the over-simplification of a real system in its model such as considering the homogeneous bending of a continuum robot. To our knowledge, not much research has been conducted on this crucial issue of system uncertainties in the continuum robots. Yet, system uncertainties raise a major concern when these robots are meant to be used for the surgical applications [5].

Sohail Iqbal, Samer Mohammed, Yacine Amirat, and Georges Fried are with LISSI, University of Paris-Est Créteil, 122 rue Paul Armangot, 94400, Vitry Sur Seine, France. {iqbal, samer.mohammed, amirat, fried}@u-pec.fr

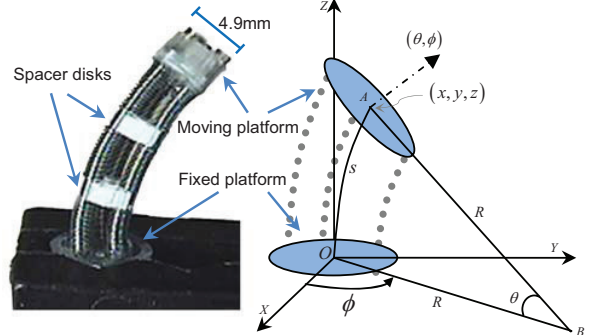


Fig. 1. Continuum robot with diameter 4.9mm, able to attain a maximum bending of 53° with controllable inputs of bellows pressures, designed for the aortic aneurysm treatment along with its model.

This research addresses the crucial issue of system uncertainties in the context of development of an active catheter for the purpose of stent placement to treat Abdominal Aortic Aneurysm (AAA). In this case, the source of error generation could be the tolerance of machining of the holes in the base disk and the spacer disks as well as the local deformation of the continuum robot lying between the spacer disks [6]. This means that the major source of error and uncertainty come from the position of the bellows on the base disk and on the moving platform.

We have already devised a technique of formulating robot's kinematics problem as a Constraint Satisfaction Problem (CSP) to deal with rounding errors [1]. In this paper, we are devising robot's inverse kinematics that takes into account the system uncertainties due to rounding errors as well as the physical uncertainties; however, we are not considering the uncertainties that may be generated due to non-homogeneous bending. Due to small size of our robot this last factor is not a major issue.

These system uncertainties produce discrepancies between the modeled and real behaviors of a robot manipulator. Moreover, closed form formulas are also devised to be used in the proposed interval based algorithm. Interval analysis is a powerful mathematical tool to solve an inverse problem and to find out the global optimal solution while taking care of system uncertainties in a rigorous way [7].

II. PROBLEM DESCRIPTION AND ITS SOLUTION

A. Micro Robot Description

A microrobot of continuum type has been conceived to control the orientation of the distal extremity of a catheter in endovascular surgery. To obtain complex poses in the vascular system, a snakelike structure called MALICA

(Multi Active LInk CAthereter) is developed in our lab, as shown in Fig. 1. The robot is conceived for the catheter placement inside the patient's body suffering from AAA.

The microrobot is composed of two cylindrical platforms connected by three electrodeposited nickel bellows which gives MALICA the required features of compliance and compactness. The prototype has the advantage to be easily integrated in the standard catheters due to its small dimensions (diameter of 4.9mm, length of 20mm). Micro robot can achieve a maximum bending of 53.47°. To satisfy the safety constraints of endovascular surgery, this micro robot does not require any electrical power inside the patient body and is actuated by hydraulic pressure by a biocompatible liquid [4]. The variation of pressure inside bellows will change their lengths, resulting in change in the pose of the robot's moving platform. To avoid buckling of the robot, two spacer disks are introduced between the moving and fixed platform, as shown in the Fig. 1.

B. System Uncertainties

We can decompose the uncertainties raised due to the machining errors in the disk holes (to attach the bellows with platforms) into uncertainties of two parameters. First is the diameter of the robot generating radial uncertainties, and second is the angle of attachment of the bellows on the disk

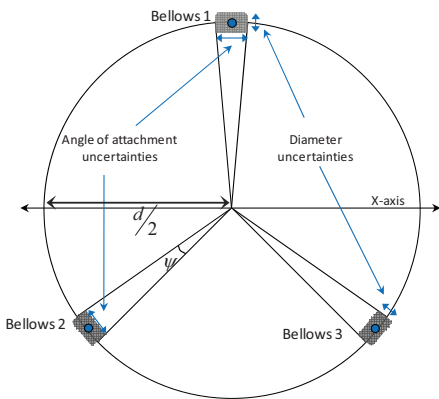


Fig. 2. Uncertainties in the disk are marked with gray color.

generating transversal uncertainties. In Fig. 2, uncertainties in the disk are depicted with the gray color. These gray color areas show the uncertainty region as a function of the tolerance of machining holes in the disk. Thus, with the help of our interval based technique, we can compute a robot's workspace that is certain. By considering all these uncertainties systematically, we are able to compute configurations of the robot manipulator that guarantees us that robot will not access certain sensitive areas. For the surgical application, such type of information is very useful for computing the safe configuration for the patient. Consequently, all the configurations that are not safe can be made inaccessible to the surgeon.

C. Problem Formulation

While computing the continuum robot's kinematics, one module of continuum robot is considered (Fig. 1). Inverse kinematics consists of representing bellows lengths \mathbb{Q} as end tool's position/orientation \mathbb{X} .
 $\mathbb{X} = [\mathbb{X}_p; \mathbb{X}_o] = [x, y, z, \theta, \phi]^T$ and $\mathbb{Q} = [l_1, l_2, l_3]^T$; where
 $\mathbb{X}_p = [x, y, z]^T$ and $\mathbb{X}_o = [\theta, \phi]^T$ represent the Cartesian position and orientation coordinates respectively. Whereas $\mathbb{Q} = [l_1, l_2, l_3]^T$ represent joint coordinates/bellows lengths.
 $[s, R]^T$ represent the length and radius of curvature of the central arc of robot. For orientation control of the robot, computation of inverse kinematics is based only on \mathbb{X}_o . These parameters are connected in the following way [2]:

$$\theta = \frac{2\sqrt{l_1^2 + l_2^2 + l_3^2 - l_1 l_2 - l_2 l_3 - l_3 l_1}}{3d} \quad (1)$$

$$\phi = \tan^{-1} \left(\frac{(l_2 + l_3 - 2l_1)}{\sqrt{3}(l_2 - l_3)} \right) \quad (2)$$

Computing \mathbb{Q} as a function of \mathbb{X}_o will generate an infinite number of solutions, which leaves a room for optimization. The problem of finding the optimized inverse kinematics of continuum robot while taking system into account can be written as:

$$\text{Minimize } f(l_1, l_2, l_3) = \frac{1}{2} \left(\frac{l_1 + l_2 + l_3}{3} - l_d \right)^2 \quad (3)$$

subject to

$$C_\theta := l_1^2 + l_2^2 + l_3^2 + l_1 l_2 + l_2 l_3 + l_3 l_1 - \frac{9d^2}{4} \cdot \theta^2 = 0 \quad (4)$$

$$C_\phi := 2l_1 - (1 - \sqrt{3} \tan(\phi + \psi))l_2 - (1 + \sqrt{3} \tan(\phi + \psi))l_3 = 0 \quad (5)$$

Where l_d is the desired length of the continuum robot and d is the diameter of the robot. Note that diameter d contains the radial uncertainties and ψ shows the transversal uncertainties. We examine the behavior of robot kinematics with uncertain physical behavior by using interval analysis techniques. These techniques always compute the accumulated system errors and uncertainties in such a way that their global behavior remains intact [8].

D. Simulation Results

An algorithm for solving the problem, described in section II-C, is proposed. This algorithm transforms the problem from the joint space to the task space. In the task space two orientation constraints (3) and (4) reduce the number of independent variables from three to one. Then optimized solution is found using interval Newton's method and used

to compute the joint values (bellows lengths). This algorithm is implemented in Matlab®/Intlab® for the computation of a circulator trajectory of the continuum robot while optimizing a quadratic cost function. Time consumption for a sample of 360 value sets is 3.57 seconds. That is, average time for computing one instance of inverse kinematics of continuum robot with Matlab/Intlab is about 10 msec. In joint space, bellows lengths have a sinusoidal behavior around the desired length of 22mm (Fig. 3). Errors arising in a bellows are minimal when robot bends towards bellows attachment point or in its opposite direction.

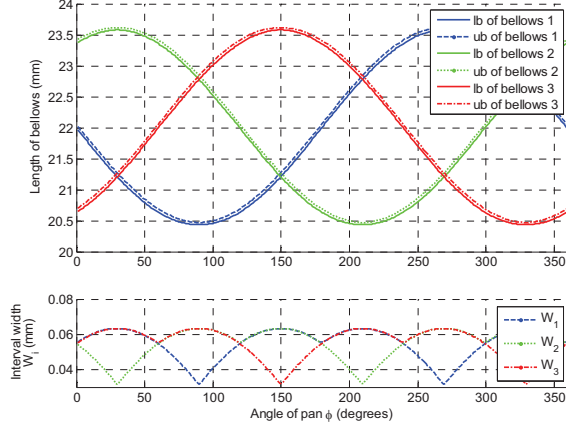


Fig. 3. Computation of the inverse kinematics of continuum robot with uncertainties in bellows' attachments to the base is 1° and in diameter by 1%.

During continuum robot navigation in the aorta, the safe configurations that do not touch aorta walls can be computed according to the existing aorta diameter. Since the

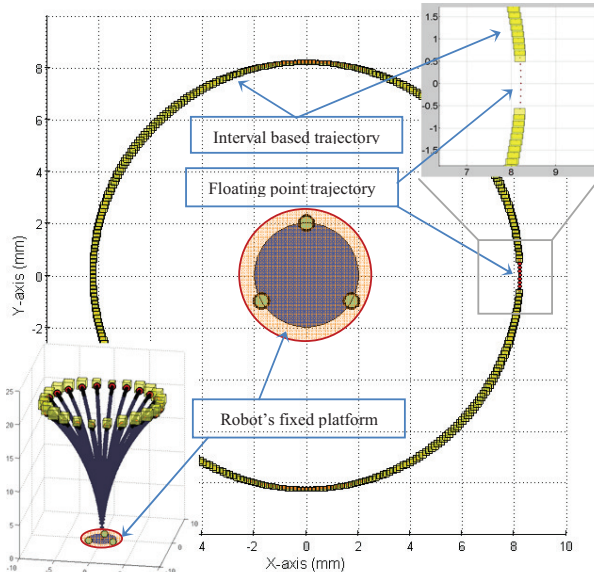


Fig. 4. Projection of the trajectory of the central point of the moving platform of our continuum robot with a bending of 45° and length of 22 mm has a safe diameter of 17 mm. In the bottom left, a 3D trajectory view is given.

diameter of an abdominal aorta for a values. normal adult is 19-25 mm [9], the diameter of the safe configuration of our continuum robot should be smaller than these values. In Fig. 4, projection of the central point of the moving platform of robot is shown, when it is following a circular trajectory. Continuum robot is achieving a safe configuration of diameter 17mm in task space, while allowing the bending till 45° . Yellow boxes contains the uncertainties and their volume increase with the increase in system uncertainties. For an engineer, who is designing a robot for surgeon assistance, information about the safe configurations is very useful.

III. CONCLUSION

In this paper, we have presented a method based on interval analysis that provides the numerically guaranteed result to deal with system uncertainties while computing the continuum robot kinematics. A track of all cumulated uncertainties generated both due to physical errors and rounding errors is kept. On the basis of this information, a robot workspace is computed that informs exactly the continuum robot's safe configurations when robot is navigating inside the body. Proposed approach is validated through simulations and experiments are the part of our future work. This approach of finding of effects of uncertainties in the surgical robotic systems is very important for the patient's safety and should be an essential part of the certification of the kinematic calibration of continuum robots.

REFERENCES

- [1] S. Iqbal, S. Mohammed, and Y. Amirat, "A Guaranteed Approach For Kinematic Analysis of Continuum Robot Based Catheter," in *IEEE Int. Conf. on Robotics and Biomimetics*, Guilin, China, 2009, pp. 1573-1578.
- [2] R. J. Webster, J. M. Romano, and N. J. Cowan, "Mechanics of Precurved-Tube Continuum Robots," in *IEEE Transactions on Robotics*, vol. 25, pp. 67-78, 2009.
- [3] B. A. Jones and I. D. Walker, "Kinematics for Multi-section Continuum Robots," *IEEE Transactions on Robotics*, vol. 22, pp. 43-55, Feb 2006.
- [4] Y. Bailly and Y. Amirat, "Modeling and Control of a Hybrid Continuum Active Catheter for Aortic Aneurysm Treatment," in *International Conference on Robotics and Automation (ICRA 2005)* Barcelona, Spain, 2005, pp. 924-929.
- [5] M. Keuchi and K. Ikuta, "Development of pressure-driven micro active catheter using membrane micro emboss following excimer laser ablation (MeME-X) process," in *IEEE International Conference on Robotics and Automation (ICRA 2009)*. Kobe, Japan, 2009, pp. 4469 - 4472.
- [6] K. Xu and N. Simaan, "An Investigation of the Intrinsic Force Sensing Capabilities of Continuum Robots," in *IEEE Transactions on robotics*, vol. 24, pp. 576-587, 2008.
- [7] D. Daney, Y. Papegay, and A. Neumaier, "Interval methods for certification of the kinematic calibration of parallel robots," in *International Conference on Robotics and Automation (ICRA)*, New Orleans, LA, 2004, pp. 1913-1918.
- [8] L. Jaulin, M. Kieffer, O. Didrit, and E. Walter, *Applied Interval Analysis*, 1 ed. London: Springer, 2001.
- [9] G. Simoni, et al., "Screening for abdominal aortic aneurysms and associated risk factors in a general population," *European Journal of Vascular & Endovascular Surgery*, vol. 10, pp. 207-210, 1995.

Ultrasound Image-Controlled Robotic Cardiac Catheter System

Samuel B. Kesner, *Student Member, IEEE*, and Robert D. Howe, *Senior Member, IEEE*

Abstract—Advances in catheter and medical imaging technology have brought minimally invasive beating heart intracardiac surgery closer to reality. However, current actuated catheter technologies are unable to track fast tissue motion, which is required to accurately perform delicate procedures inside a beating heart. The actuated catheter system presented here compensates for the motion of heart structures such as the mitral valve apparatus by servoing a catheter guidewire inside a flexible sheath. The catheter system is integrated with an ultrasound-based visual servoing system to enable fast tissue tracking. *In vivo* tests show RMS tracking errors of less than 1 mm for following the porcine mitral valve annulus trajectory. These results demonstrate that an ultrasound-guided actuated catheter system can accurately track the fast motion of the mitral valve and that this technology has the potential to revolutionize how surgery is performed inside the heart.

I. INTRODUCTION

While catheters can perform many tasks inside the heart, including measuring cardiac physiological function, dilating vessels and valves, and implanting prosthetics and devices, they do not yet allow clinicians to interact with heart tissue with the same level of skill as in open heart surgery [1]. A primary reason for this is that current catheters do not have the dexterity, speed, and force capabilities to perform complex tissue modifications. Robotic catheter tools have the potential overcome these challenges and greatly expand the range of interventions that can be performed inside the heart under minimally invasive conditions.

Cardiac catheters are long and thin flexible tubes that are inserted into the human vascular system and passed into the heart. Current robotic cardiac catheters do not provide sufficient speeds to compensate for the fast motion of the heart [2]-[4]. Motion compensation is required for many beating heart procedures to prevent the catheter from colliding with internal cardiac structures [5],[6].

In previous work, we have developed robotic devices that compensate for the motion of internal heart structures *in vivo* with a handheld robotic instrument inserted through incisions in the heart wall [6]-[9]. The motion of the tissue target is tracked in real time using 3D ultrasound (3DUS) guidance as described in [8]. This work shows that single degree of freedom (DOF) servoing is sufficient to accurately track the

Manuscript received March 3, 2010. This work is supported by the US National Institutes of Health under grant NIH R01 HL073647. The authors are with the Harvard School of Engineering and Applied Sciences, Cambridge, MA, 02138 USA. R.D. Howe is also with the Harvard-MIT Division of Health Sciences & Technology, Cambridge, MA, 02139 USA. email: howe@seas.harvard.edu

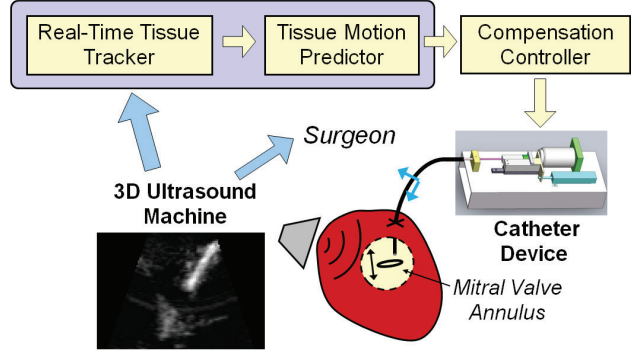


Fig. 1. Ultrasound image-based catheter servoing system.

motion of certain cardiac structures, including the human mitral valve annulus [5],[9]. While this approach enables beating heart procedures to alleviate the risks associated with stopped heart techniques [7], the necessity of creating incisions in the heart wall means that this approach is not minimally invasive.

We propose to apply our successful robotic cardiac motion compensation techniques to catheters in order to minimize the invasiveness. In the envisioned clinical system, a robotic actuation system at the proximal end of the catheter system drives a catheter guidewire inside a flexible sheath. The sheath is manually positioned inside the heart by a clinician using a standard clinical approach, such as introducing the sheath via the femoral vein and across the atrial septum. At the distal end of the catheter inside the heart, the guidewire tip translates in and out of the sheath under ultrasound guidance to compensate for the movement of the cardiac structures and perform repair. Fig. 1 presents a diagram of the image-guided catheter system.

II. SYSTEM DESIGN

The catheter system consists of an actuation system connected to a catheter sheath and guidewire, a 3DUS machine (SONOS 7500, Philips Healthcare, Andover, MA, USA), and a tissue tracking and tool servoing system (Fig. 1). The design parameters for the actuation system were selected to be sufficient to compensate for the human mitral valve motion [5], [9]. The system's principal functional requirements are that it has a single actuated linear degree of freedom with at least 20 mm of travel that can provide a maximum velocity and acceleration of at least 210 mm/s and 3800 mm/s², respectively. The catheter components have the same dimensions and material properties as current clinical cardiac catheters and the system can apply enough force to modify cardiac tissue, approximately 4 N applied along the

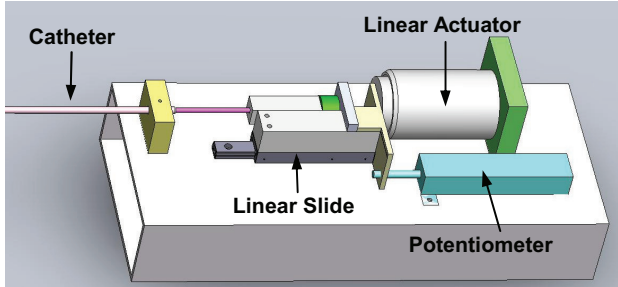


Fig. 2. Actuated catheter system prototype.

major axis of the catheter tool. This is a sufficient amount of force to modify the tissue by driving a surgical staple or suture needle.

The actuation system used in this study (Fig. 2) is composed of a linear voice coil actuator with 50.8 mm of travel and a peak force of 26.7 N (NCC20-18-02-1X, H2W Technologies Inc, Valencia CA), a linear ball bearing slide (BX3-3, Tusk Direct, Inc., Bethel CT), and a linear potentiometer position sensor (A-MAC-B62, Midori America Corp, Fullerton CA). The catheter sheaths are 85 cm long sections of Teflon tubing, and the guidewires are stainless steel close-wound springs.

A PID control system running at 1 kHz is used to control the position of the linear actuator at the base of the catheter. Custom C++ code is used to control the system and make measurements via a data acquisition card (DAQCard-6024E, National Instruments Corp., Austin TX). Commands to the linear actuator are amplified by a bipolar voltage-to-current power supply (BOP 36-12M, Kepco Inc., Flushing NY).

In the ultrasound servoing system, 3D image volumes are streamed via ethernet to an image processing computer. A GPU-based Radon transform algorithm finds the instrument axis in real-time [7]. The target tissue is then located by projecting the axis forward through the image volume until tissue is encountered. This allows the clinician to designate the target to be tracked by simply pointing at it with the catheter. To compensate for the 50-100 ms delay in image acquisition and processing, an extended Kalman filter estimates the current tissue location based on a Fourier decomposition of the cardiac cycle. Previous *in vivo* experiments showed that the rigid instrument system was capable of tracking within the heart with an RMS error of 1.0 mm. See [6]-[9] for a detailed description of the system.

III. IN VIVO EVALUATION

The robotic catheter system was evaluated *in vivo* on a 75 Kg porcine animal model. For this initial study, the actuated catheter was inserted into a beating heart via the top of the left atrium rather than the vasculature to give the surgeon easy access to the mitral valve. The 3D ultrasound probe was placed epicardially. After the device was introduced into the beating heart, the surgeon used the ultrasound image to aim the catheter at the mitral valve annulus. The imaging system was then initialized and tracked the valve motion. See Fig. 3 for a 3DUS image of the catheter *in vivo* and an

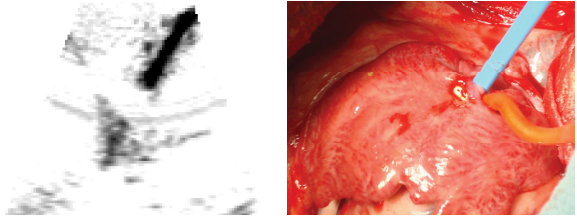


Fig. 3. Left: Ultrasound image showing catheter, mitral valve annulus, and mitral valve leaflets. Right: The catheter tool inserted into the left atrium.

image of the catheter device being inserted into the porcine left atrium.

The catheter system used in this experiment was consisted of a sheath with 1.6 mm inner diameter and a guidewire with a 1.5 mm outer diameter. During the experimental trials, the catheter sheath was constrained outside the heart to a configuration that roughly corresponds to the path from the femoral vein into the left atrium. The catheter was then positioned inside the left atrium so that the tip was 1-2 cm from the mitral valve annulus. The catheter controller performs a simple calibration routine that estimates the magnitude of the friction force in the system. Next, the image processing routines locate the catheter using the Radon transform algorithm, and then project forward to find the target. The catheter is then servoed to maintain a constant distance between the catheter tip and the target.

A. Tracking results

The catheter system was successful in tracking the mitral annulus tissue target. Fig. 3 shows a cross section through a typical ultrasound image volume, showing the catheter, mitral valve annulus, and edge of the valve leaflet. Because of the seals required to prevent backflow of blood out of the heart, friction compensation values as high as 2 N were required for this experiment.

Fig. 4 shows a typical plot of the catheter tip trajectory and the position of the mitral valve annulus. This plot was generated by manually segmenting the position of the catheter tip and valve structure from the 3DUS volumes three times and then averaging the values.

The catheter system tracked the valve motion with RMS errors less than 1.0 mm in all experimental trials. The RMS error for the trial presented in Fig. 4 was 0.77 mm. The tracking error was caused by respiratory motion not captured in the tissue tracking system, performance limitations of the actuated catheter caused by backlash and friction, and the small beat-to-beat variations in the valve motion not compensated for by the image tracking system.

IV. CONCLUSIONS

This work demonstrates that single DOF robotic catheters can achieve the speed and tip position control required for specific intracardiac repair applications such as mitral valve annuloplasty. In addition, this study shows that catheter position can be accurately controlled using real-time image guidance *in vivo*. These results suggest that it is feasible to

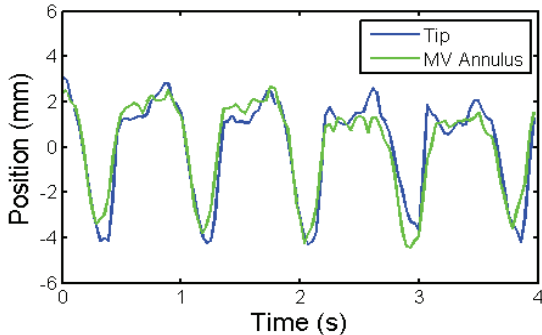


Fig. 4. Trajectory of the catheter tip and the mitral valve annulus found by manual segmentation of 3DUS volumes.

use catheters for beating heart procedures, which will enable intracardiac repairs that are both minimally invasive and avoid the risks of stopped-heart techniques.

While these results are promising, further work is required to allow this technology to be clinically useful. Additional mechanism and controller development is required to allow the catheter to interact with and modify cardiac tissue. Bracing and support mechanisms are required for the catheter to apply substantial forces inside the heart without deflecting away from the tissue. Appropriate end effectors, including tissue resection and stapling tools, are required to perform intracardiac repairs. Future work will also be necessary to extend this motion compensation technology to cardiac surgery applications that require additional degrees of freedom for complex tissue trajectory tracking. In contrast to existing robotic catheter systems that move at roughly manual speeds, fast motion in the lateral directions will be required for these applications.

ACKNOWLEDGMENT

The authors would like to thank Dr. Shelten Yuen for his assistance with system development and Dr. Nikolay Vasilyev and Dr. Pedro del Nido for their assistance with the animal experiments presented here and insights into the clinical applications of this technology.

REFERENCES

- [1] D. S. Baim, *Grossman's Cardiac Catheterization, Angiography, and Intervention*. Lippincott Williams & Wilkins, 2005, pp. 992.
- [2] T. Fukuda, *et al.*, "Micro active catheter system with multi degrees of freedom," in *Proc. IEEE Int. Conf. Robotics & Automation*, 1994, pp. 2290-95.
- [3] J. Jayender, R. V. Patel and S. Nikumb, "Robot-assisted catheter insertion using hybrid impedance control," in *Proc. of IEEE Int. Conf. Robotics and Automation*, 2006, pp. 607-612.
- [4] D. B. Camarillo, C. F. Milne, C. R. Carlson, M. R. Zinn and J. K. Salisbury, "Mechanics Modeling of Tendon-Driven Continuum Manipulators," *IEEE Trans. Robotics*, vol. 24, pp. 1262-73, 2008.
- [5] D.T. Kettler, *et al.*, "An active motion compensation instrument for beating heart mitral valve surgery," in *Proc. of IEEE/RSJ Int. Conf. Intelligent Robots and Systems*, 2007, pp. 1290-95.
- [6] S. G. Yuen, S. B. Kesner, N. V. Vasilyev, P. J. del Nido and R. D. Howe, "3D ultrasound-guided motion compensation system for beating heart mitral valve repair," in *Medical Image Computing and Computer-Assisted Intervention*, LCNS vol. 5241, 2008, pp. 711-719.

- [7] S. G. Yuen, P. M. Novotny and R. D. Howe, "Quasiperiodic predictive filtering for robot-assisted beating heart surgery," in *Proc. IEEE Int. Conf. Robotics and Automation*, 2008, pp. 3875-80.
- [8] P. M. Novotny, J. A. Stoll, P. E. Dupont and R. D. Howe, "Real-time visual servoing of a robot using three-dimensional ultrasound," in *Proc. IEEE Int. Conf. Robotics and Automation*, 2007, pp. 2655-60.
- [9] S. G. Yuen, D. T. Kettler, P. M. Novotny, R. D. Plowes, and R. D. Howe, Robotic "Robotic Motion Compensation for Beating Heart Intracardiac Surgery," *Int. J. Robotics Research*, vol. 28, no. 10, pp. 1355-72, 2009.

Steerable Continuum Robot Design for Cochlear Implant Surgery

Nabil Simaan^{1*}, Member, IEEE Jian Zhang¹, Student Member, IEEE,
J. Thomas Roland Jr.², Spiros Manolidis³

Abstract—Cochlear implant surgery on patients with residual hearing is limited as a result of intra-cochlear trauma caused by the insertion of electrode arrays. Our ongoing work aims at overcoming these limitations by providing a framework for the design, optimal path planning, modeling of intra-cochlear friction, and force feedback for insertion speed control during surgery. This paper presents an optimal design methodology for steerable electrode arrays. The design framework relies on model-based calibration of the electrode arrays followed by optimal insertion path planning and simulation to evaluate a global performance measure that quantifies the shape discrepancy between the electrode array and the curve of the scala tympani throughout the whole insertion process. The aim of the optimization is to design the optimal placement of an actuation strand embedded inside the electrode arrays while minimizing this global performance measure. The design problem is formalized as a constrained optimization problem and validated by simulations and experiments. The simulations show that while complex polynomial paths for the actuation strand may improve the global performance measure, an optimal linear path provides comparable performance and simplifies fabrication.

I. INTRODUCTION

Cochlear implant surgery is currently used for patients suffering from severe hearing loss, but with intact auditory nerves. The surgery substitutes the function of the hair cells as electrical nerve stimulators by inserting a flexible electrode array that is coupled with a subcutaneous implanted electromagnetic receiver and an external sound processor and a generator, Fig. 1.

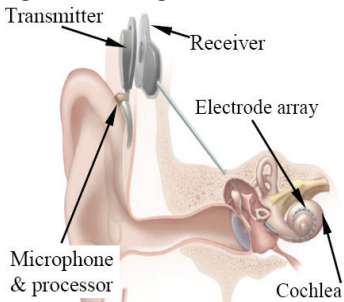


Fig. 1 A typical layout of a cochlear implant system

Currently, patients with residual intact hair cells are not considered as candidates for cochlear implant surgery

Manuscript received March 8, 2010. This work was supported by NSF grant #CBET-0651649. ¹ Department of Mechanical Engineering, Columbia University, New York, NY 10027, USA. E-mails: {jz2181, ns2236}@columbia.edu. ² NYU Medical Center, New York, NY 10016 {john.roland@nyumc.org}. ³ Beth Israel Medical Center, New York, NY 10003 {smanolidis@mac.com}

* Corresponding author.

because of the resultant intra-cochlear trauma during implantation [1-6]. Added limitations include the lack of control on the shape of electrode arrays, the requirement for accurate placement of the electrodes close to the target ganglion cells a target frequency range, and the lack of force sensing and feedback during surgery [7]. These limitations provide the motivation for robotic assistance during cochlear implantation as first proposed in [8].

In our previous works we first proposed and validated the potential of steerable electrode arrays for reduction of insertion forces [9]. Later in [10] developed a steerable electrode array using actuation by a shape memory alloy. Wang et. al, [11], developed strain sensors for measurement of local bending of electrode arrays.

Other groups focused on robotic applications for otology. [12] focused on evaluating registration errors for Bone Anchored Hearing Aids (BAHA). [13, 14] presented robotic devices for facial recess drilling. Other works focused on assistance for stapedotomy [15, 16]. More recently, [17, 18] focused on the design of an insertion tool with force sensing for modiolar-hugging electrodes.

Fig. 2 shows our design of steerable electrode arrays. The design uses an embedded actuation strand inside an elastomeric electrode array. The strand is attached only to the tip of the electrode array. By pulling on the strand, the electrode array assumes minimal energy shapes, Fig. 3.

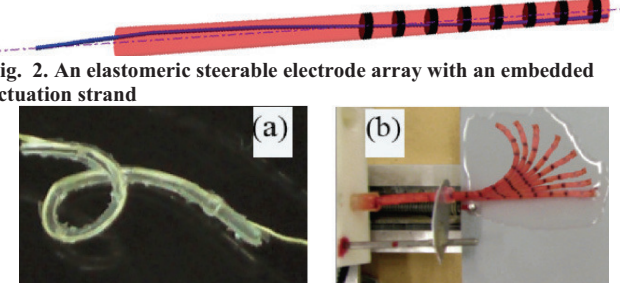


Fig. 2. An elastomeric steerable electrode array with an embedded actuation strand

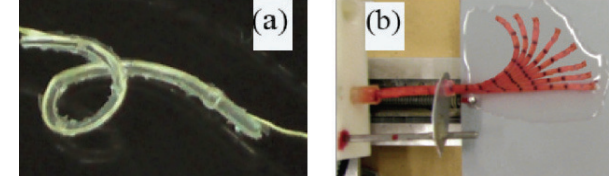


Fig. 3. Prototype steerable electrode arrays: (a) a real size electrode array that bends in 3D. (b) a planar 3:1 scaled-up electrode array.

II. CALIBRATION AND PATH PLANNING

The calibration process of the electrode arrays relates the shape of the electrode array with the amount of pull on the strand. Let \mathbf{q} be the vector of all actuated joints in an n Degrees-of-Freedom (DoF) robot that inserts an electrode array into the scala tympani. Let q_h be the last DoF that refers to the amount of pull on the actuation strand. The shape of a planar-bending electrode array is given by its arc length s and its local tangent $\theta_e(s)$. A calibration process using Kronecker products was described in [8] and using

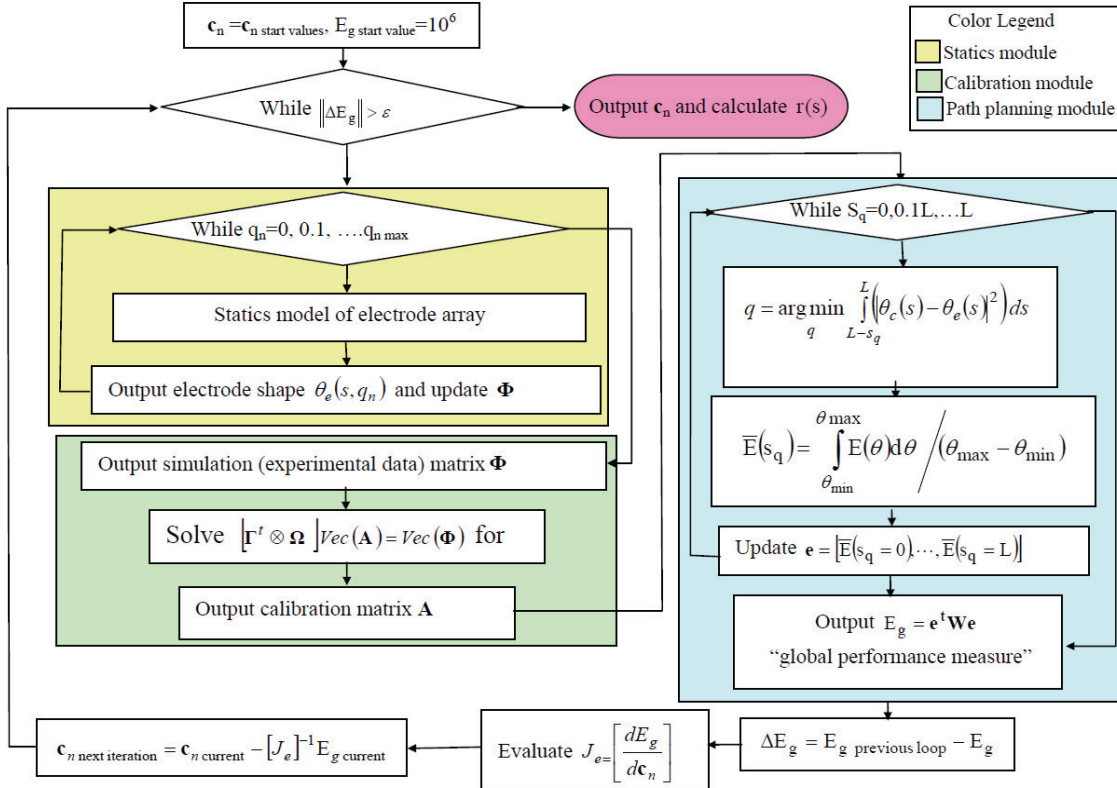


Fig. 4. Algorithm for optimal design and optimal path planning of steerable electrode arrays

splines in [7]. The result of this calibration is a calibration matrix \mathbf{A} that provides the local tangent angle $\theta(s_i, q_{n_j})$ as a function of the electrode arc length, s , and the amount of pull on the actuation strand q_n .

$$\Phi = \Omega(s)\mathbf{A}\Gamma(q_n) \text{ where } \Phi_{i,j} = \theta(s_i, q_{n_j}) \quad (1)$$

For an actuation strand placement $\mathbf{r}(s) = \sum_{j=1}^m c_j f_j(s)$ as

characterized by m modal factors [19] $\mathbf{c} \in \mathbb{R}^m$ and modal functions $f_j(s)$, the calibration matrix $\mathbf{A} = \mathbf{A}(\mathbf{c})$ is unique.

The optimal path planning as presented in [1] is based on the premise that an electrode array that matches the anatomy will minimize its interaction and frictional insertion forces. Let $\theta_c(s)$ represent the shape of the target anatomy (the scala tympani). The insertion path planning is an unconstrained optimization problem:

$$\mathbf{q} = \operatorname{argmin}_{\mathbf{q}} \int_{L-s_q}^L (\theta_c(s) - \theta_e(s))^2 ds \quad (2)$$

In eq. (2) S_q refers to the insertion depth and L designates the length of the electrode array.

The integral shape discrepancy between the electrode array and the cochlea, at each insertion depth s_q , is used as a metric \bar{E} for evaluating the quality of the electrode array and the insertion path plan as given by Eq. (2) and shown in . A global performance measure E_g is then calculated for the whole insertion process from $S_q=0$ to $S_q=L$.

III. STATICS AND OPTIMAL DESIGN OF WIRE PLACEMENT

The calibration matrix \mathbf{A} of a given strand placement $\mathbf{r}(s)$ is a function of the static equilibrium of the electrode array as given by elastic energy minimization or as obtained experimentally. In [8] manual segmentation of images as in Fig. 2b was used. In [7] automatic segmentation was used.

Fig. 5 shows an experimental validation of our electrode design, calibration and statics models. The figure shows an overlay of three electrode shapes for different forces of pulling on the strand (different values of q_n). The figure also shows Matlab-generated curves as predicted by our statics model. The results show good agreement despite some deviation that is a result of imaging segmentation of the wire placement inside the electrode array.

For the purpose of the optimal electrode design, we assume that the shape and material properties of the electrode array are given and we seek to find the optimal strand placement $\mathbf{r}(s)$. This is achieved using automatic calibration of different electrodes for each wire placement $\mathbf{r}(s)$ by using the static model of the electrode array.

The optimal wire placement is then found by solving a constrained optimization problem as given in Eq. (3). The active set algorithm [20] is implemented in Matlab to solve this problem. Eq. (3) $\beta_l(s)$ and $\beta_u(s)$ designate the lower and upper bounds for the cross section width of the electrode array as measured from its centerline.

Fig. 6 shows simulation results using a linear model ($m=2$) and a second order model ($m=3$) for the wire placement. In both simulations, the initial guess for the wire placement was given by using forward recursion from the

base to the electrode tip in order to solve for the best matching equilibrium shape for a fully inserted electrode.

$$\begin{aligned} \operatorname{argmin}_{\mathbf{c}} E_g &= \frac{1}{2} \sqrt{\int_0^L [\bar{\mathbf{E}}(s_q, \mathbf{q}^*)]^T \bar{\mathbf{E}}(s_q, \mathbf{q}^*) ds_q} \quad (3) \\ \text{s.t. } \beta_l(s) &\leq r(s) \leq \beta_u(s) \end{aligned}$$

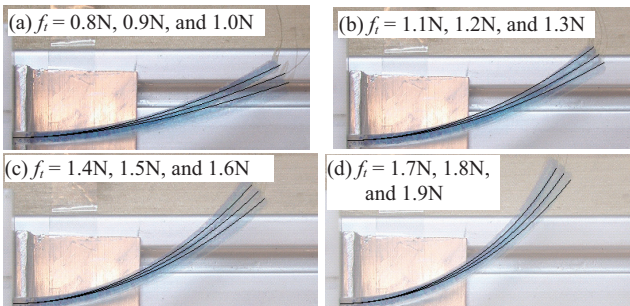


Fig. 5. Overlay of simulation results onto bent electrode arrays. f_i designates the pulling force on the actuation strand

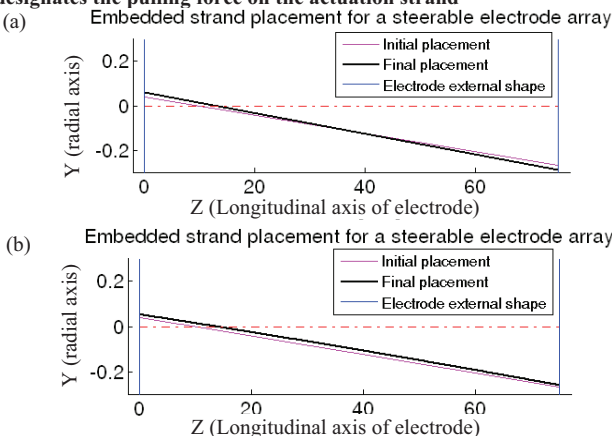


Fig. 6 Optimization algorithm results (a) linear strand placement (b) nonlinear strand placement

Simulations comparing the global performance measure E_g for the optimized linear model of the strand gave a total average error of 0.3434 radians throughout the whole insertion process. The best second-order polynomial wire placement resulted in $E_g=0.3398$ radians. This small difference suggests that an optimized linear strand placement is a reasonable compromise and we plan to construct our electrode arrays using linear strand placement models.

IV. CONCLUSIONS

Modeling of steerable electrode arrays is needed for optimal design of the actuation strand placement. This paper presented the design methodology for optimal steerable cochlear implant electrode arrays. Simulations showed that optimized linear actuation strand placement models produce comparable performance to higher-order strand placements. This justifies the design and construction of steerable electrode arrays with linear strand placement. Future work will focus on optimizing the design of steerable electrodes for 3D target curves and evaluation of insertion forces.

V. REFERENCES

- [1] J. Zhang, T. J. Roland, S. Manolidis, and N. Simaan, "Optimal Path Planning for Robotic Insertion of Steerable Electrode Arrays in Cochlear Implant Surgery," *ASME Journal of Medical Devices*, vol. 3, 2009.
- [2] T. Maeno, S. Hiromitsu, and T. Kawai, "Control of grasping force by detecting stick/slip distribution at the curved surface of an elastic finger," San Francisco, CA, USA, 2000, p. 3895.
- [3] P. Wardrop, D. Whinney, S. J. Rebscher, W. Luxford, and P. Leake, "A temporal bone study of insertion trauma and intracochlear position of cochlear implant electrodes. II: Comparison of Spiral Clarion and HiFocus II electrodes," *Hear Res*, vol. 203, pp. 68-79, May 2005.
- [4] W. Gstoettner, H. Plenk, Jr., P. Franz, J. Hamzavi, W. Baumgartner, C. Czerny, and K. Ehrenberger, "Cochlear implant deep electrode insertion: extent of insertional trauma," *Acta Otolaryngol*, vol. 117, pp. 274-7, Mar 1997.
- [5] T. Roland, "A model for cochlear implant electrode insertion and force evaluation: results with a new electrode design and insertion technique" *The Laryngoscope*, vol. 115, pp. 1325-1339, 2005.
- [6] A. Fishman, Roland, JT Jr, Alexiades, G, Mierzwinski, J, Cohen, NL, "Fluoroscopically assisted cochlear implantation," *Otol Neurotol*, vol. 24, pp. 882-6, 2003 Nov.
- [7] J. Zhang, S. Manolidis, T. J. Roland, and N. Simaan, "Path Planning and Workspace Determination for Robot-Assisted Insertion of Steerable Electrode Arrays for Cochlear Implant Surgery," in *International Conference on Medical Image Computing and Computer-Assisted Intervention (MICCAI'2008)*, 2008.
- [8] J. Zhang, K. Xu, N. Simaan, and S. Manolidis, "A Pilot Study of Robot-Assisted Cochlear Implant Surgery Using Steerable Electrode Arrays," in *MICCAI'06 - the 9th International Conference on Medical Imaging and Computer-Assisted Intervention Copenhagen*, 2006, pp. 30-40.
- [9] J. Zhang, K. Xu, N. Simaan, and S. Manolidis, "A Pilot Study of Robot-Assisted Cochlear Implant Surgery Using Steerable Electrode Arrays," in *MICCAI'06 - the 9th International Conference on Medical Imaging and Computer-Assisted Intervention Copenhagen*, 2006.
- [10] B. Chen, H. Kha, and G. Clark, "Development of a steerable cochlear implant electrode array," in *3rd Kuala Lumpur International Conference on Biomedical Engineering 2006*, 2007607-610.
- [11] J. Wang, M. N. Gulari, and K. D. Wise, "A Parylene-Silicon Cochlear Electrode Array with Integrated Position Sensors," in *Engineering in Medicine and Biology Society, 2006. EMBS '06. 28th Annual International Conference of the IEEE*, 2006, pp. 3170-3173.
- [12] R. Balachandran, R. F. Labadie, and J. M. Fitzpatrick, "Clinical determination of target registration error of an image-guided otologic surgical system using patients with bone-anchored hearing aids," San Diego, CA, United states, 2007, p. SPIE.
- [13] F. M. Warren, R. Balachandran, J. M. Fitzpatrick, and R. F. Labadie, "Percutaneous Cochlear Access Using Bone-Mounted, Customized Drill Guides: Demonstration of Concept In Vitro," vol. 28, 2007, pp. 325-329 10.1097/01.mao.0000253287.86737.2e.
- [14] P. N. Brett, R. P. Taylor, D. Proops, and M. V. Griffiths, "An Autonomous Surgical Robot Applied in Practice," in *Mechatronics and Machine Vision in Practice*, 2008261-266.
- [15] P. N. Brett, D. A. Baker, L. Reyes, and J. Blanshard, "Automatic technique for micro-drilling a stapedotomy in the flexible stapes footplate," *Proceedings of the Institution of Mechanical Engineers, Part H: Journal of Engineering in Medicine*, vol. 209, pp. 255-262, 1995.
- [16] T. Maier, K. Niazmand, T. C. Luth, and G. Straub, "MicroMan - A new Micromanipulator for clinical use in the middle ear surgery MicroMan - Ein Neuartiger Mikromanipulator fur den Einsatz in der Mittelohrchiirurgie," *VDI Berichte*, pp. 67-70, 2008.
- [17] A. Hussong, T. Rau, T. Ortmaier, B. Heimann, T. Lenarz, and O. Majdani, "An automated insertion tool for cochlear implants: another step towards atraumatic cochlear implant surgery," *International Journal of Computer Assisted Radiology and Surgery*, 2009.
- [18] T. Rau, A. Hussong, M. Leinung, T. Lenarz, and O. Majdani, "Automated insertion of preformed cochlear implant electrodes: evaluation of curling behaviour and insertion forces on an artificial cochlear model," *International Journal of Computer Assisted Radiology and Surgery*, 2009.
- [19] G. S. Chirikjian and J. W. Burdick, "A Modal Approach to Hyper-Redundant Manipulator Kinematics," *IEEE Transactions on Robotics and Automation*, vol. 10, pp. 343-354, 1994.
- [20] J. Nocedal and S. J. Wright, *Numerical Optimization*: Springer, 2006.

Modular Needle Steering Driver for MRI-guided Transperineal Prostate Intervention

Hao Su, Kevin Harrington, Gregory Cole, Yi Wang and Gregory S. Fischer

Abstract— This paper presents the design of a modular MRI compatible needle steering driver actuated by piezoelectric actuators for prostate biopsy and brachytherapy. We addressed the design requirements and fabricated the system for close bore interventional MRI surgery. The needle driver simultaneously provides needle cannula rotation and independent cannula and stylet prismatic motion. The 3 degrees-of-freedom (DOF) driver system is proposed to serve as a slave robot to deliver radioactive seeds in an MRI-guided force feedback teleoperation framework. Moreover, it suffices to be a generic robotic platform to provide the needle motion in a diverse array of needle steering scenarios proposed in many literatures.

Keywords: Optical Force Sensor, MRI Compatible, Haptic Feedback, Needle Driver, Prostate Needle Brachytherapy.

I. INTRODUCTION

Prostate cancer continues to be the most common male cancer and the second most common type of cancer [1]. The current “gold standard” transrectal ultrasound (TRUS) for guiding both biopsy and brachytherapy is accredited for its real-time nature and low cost [2]. However, the delivered seeds cannot be effectively observed in image. MRI-based medical diagnosis and treatment paradigm capitalizes on the novel benefits and capabilities created by the combination of high sensitivity for detecting seeds, high-fidelity soft tissue contrast and high spatial resolution. Low dose rate brachytherapy is the permanent implantation of rice grain sized radioactive seeds in a non-uniformly complex pattern into the prostate to cure the cancer with long-term radiation. The major motivation of a robotic system is to increase the seed delivery accuracy while minimize the tissue damage and avoid non-tissue structures by needle steering or minor needle motion correction. The challenges of a robot assisted mechatronic system, however, arise from the manifestation of the bidirectional MRI compatibility requirement [3] and the confined physical space in high-field closed-bore.

Needle steering becomes an interesting and practical technique to address needle based interventional issues in recent years. Bevel needle steering continues to flourish with the combined techniques of nonholonomic modeling and image guided feedback control. Rotation of the needle about its axis may be implemented to “drill” the needle in to limit deflection as described by Masamune, et al. [4] and Wan, et al. [5]. On the other hand, by taking advantage of the intrinsic asymmetry property of bevel needles, the needle driver may

Hao Su, Kevin Harrington, Gregory Cole, Yi Wang and Gregory S. Fischer are with the Automation and Interventional Medicine (AIM) Laboratory in the Department of Mechanical Engineering, Worcester Polytechnic Institute, Worcester, MA, USA. E-mail: haosu@wpi.edu, gfischer@wpi.edu

be used to steer the needle using bevel steering techniques such as those described by Webster, et al. [6] along trajectories defined using techniques described by Alterovitz et al. [7]. Mahvash et al. have [8] experimentally demonstrated that increased needle velocity is able to minimize tissue deformation and damage and reduce position error which is essential for prostate percutaneous therapy. Moreover, as long as the robotic system is immune to work in MRI, it can be applied to many other imaging modalities like ultrasound and CT. To overcomes the loss of needle tip proprioception information, we are developing a teleoperated haptic system with optical force sensor and a 3-DOF robotic needle driver. Our guiding vision is to design a modular needle driver integrable with generic gross positioning stage to enhance MRI-guided prostate brachytherapy and biopsy accuracy and decrease operational time.

II. NEEDLE DRIVER MODULE

Usually, a needle steering system requires insertion and cannula rotation motion. This task becomes more complicated and stringent for a MRI brachytherapy preloaded needle in terms of extra stylet translational motion to mimic the physician gesture that first move the cannula and stylet in a coordinated manner and then retract the cannula to deliver the seeds. Based on an early design of a force sensor [9] and a haptic system [10], this section demonstrates an updated needle driver actuated by piezoelectric motors. This driver can be used for 3 DOF brachytherapy or 2 DOF generic needle steering and fulfills the following design considerations. 1) Cannula rotation about its axis with cannula insertion. The independent rotation and translation motion of the cannula can increase the targeting accuracy while minimize the tissue deformation and damage. 2) Stylet prismatic motion to facilitate seed delivery. 3) Modularity. Easy integration with gross positioning system to provide full 6 DOF motion. 4) Safety. Instead of using mechanical stop, the piezoelectric actuators as frictional motors are capable of creating $10N$ of force, when unpowered they can supply up to $16N$ of holding force per motor. 5) Weight. the total weight of needle driver module and Cartesian positioning module is less than $3.5Kg$. 6) Compatibility. The frames of the robot are built up with acrylic. With limited amount of brass fasteners and aluminum rail, it should be compatible in the bore. 7) Operation in confined space. To fit into the scanner bore, the width of the driver is limited to $7cm$ and the operational space when connected to a base platform is able to cover the traditional TRUS $60 \times 60mm$ temple. 8) Sterilization. We would like to minimize the parts to be

sterilized and the design requires the sterilization of needle clamping part and force sensor holder.

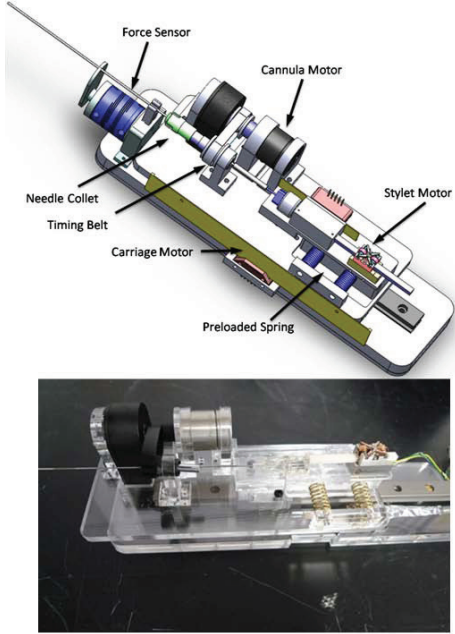


Fig. 1. (Up) CAD model of 3 DOF needle driver and (down) needle driver physical prototype.

To create the force and motion in an MRI compatible system, actuators had to be meticulously selected to create the motion. For this task we selected the piezoelectric motor (PiezoMotor, Uppsala, Sweden). Standard optical encoders (U.S. Digital, Vancouver, WA) have been thoroughly tested in a 3T MRI scanner for functionality and induced effects in the form of imaging artifacts [11]. The encoders have been incorporated into the robot and have performed without any stray or missed counts; the imaging artifact is confined locally to within 2 – 5cm from the encoder.

Current MRI-guided biopsy procedures are performed with the patient outside the scanner bore due to the space constraint. We hope to enable these procedures to be performed inside the bore under real-time imaging without the loss of tactile sensation by integrating with the optical force sensors. A CAD model of the needle driver and the physical prototype are shown in Fig.1 .

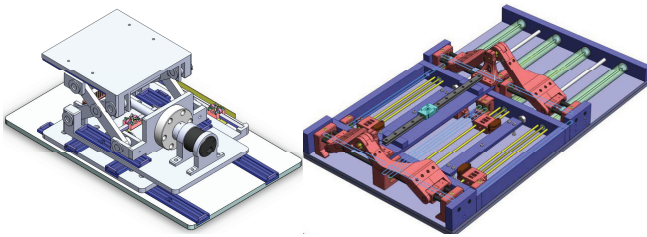


Fig. 2. (Left) A Cartesian positioning stage and (right) a 4 DOF robotic stage.

It is necessary to mention that this driver is modular for percutaneous intervention in the sense that it can be conveniently integrated with generic positioning stage like the Cartesian positioning stage that we have developed (Fig. 2 left) or orientation stage developed by our collaborator [12] shown in Fig. 2 right. The latter stage provides insertion pitch and yaw motion and is especially desirable to overcome pubic arch interference problem.

A. Universal Needle Clamping

To design a needle driver that allows a large variety of standard needles to be used with the system, a new clamping device rigidly connect the needle shaft to the driving motor mechanism is developed. This mechanism is similar to a collet and a brass hollow screw is twisted to fasten the collet thus rigidly lock the needle shaft on the clamping device. The clamping device is connected to the rotary motor through a timing belt that can be freely fastened by moving the motor housing laterally. The clamping device is generic in the sense that we have designed 3 sets of collets and each collet can accommodate a width range of needle diameters. The overall needle diameter range is from 25Gauge to 7Gauge. By this token, it can not only fasten brachytherapy needle but also biopsy needle instead of designing some specific structure to hold the needle handle as those in [13].

B. Needle Loading Mechanism and Force Sensing

Once a preloaded needle or biopsy gun is inserted, the collet can rigidly clamp the cannula shaft. Since the linear motor is collinear with the collet and shaft, we need to offset the shaft to manually load the needle. We designed a brass spring preloaded mechanism that can provide lateral passive motion freedom.

We have developed the force sensor which provides in-vivo measurement of 3 DOF needle insertion forces to render proprioception associated with brachytherapy procedure [10]. Even though the sensor can monitor axial force and two lateral forces, to guarantee fast and convenient needle loading, the sensor is connected with an offset plate to measure the lateral forces while the axial force is measured by another 1 DOF fiber optic force sensor. This setting is preferable than the design that the needle assembly held an off-the-shelf 6-DOF hollow force sensor [14] by complex mechanical fastening.

III. MODULAR SERVO BOARD

The electrical hardware aims to control the piezoelectric motors and interface the encoder and force sensors. Fig. 3 shows the system electrical diagram (left) and the servo board (right). We have described the design of electrical board to drive piezo motor in [10]. The purpose of the servo control board is to provide an independent system that can perform real-time control loops with an interface to a high level path planner for set point inputs. The board, requiring no additional external components to interface with common medium to low power actuators, is intended to provide a platform upon which new and complex control algorithm

could be developed and tested. It is also intended to have on-board connections for quadrature encoder signals and analog voltage sensors. With high speed access to these sensors and actuators, control loops can be changed from application to application with just software modification. While in this design, piezoelectric motor amplifier is used in a similar setting as in [15].

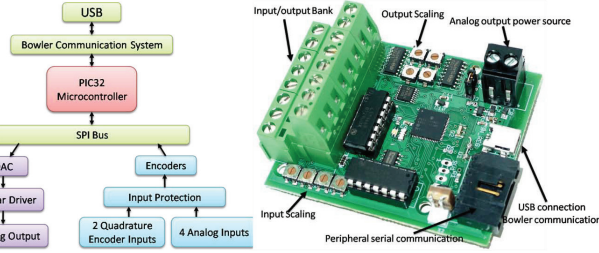


Fig. 3. (Left) system electrical diagram and (right) the servo board.

The final design has a 4 channels, 12 bit voltage digital to analog converter that can update its voltage output at 62.5Hz . Each channel has a linear driver with adjustable gains that can tolerate 0 – 24 volts at 1 amp. There are 4 channels of 10 bit analog inputs while each channel has a voltage divider on it to scale the inputs for the controller. There are also 2 independent quadrature decoders with a count frequency of up to 20MHz and can be accessed over the SPI bus. All input channels have over-voltage protection and can operate from 0 to 12Volts while tolerating from –24 to 24Volts . These services are accessible through the Bowler Communication System (BCS) and a driver layer that breaks out all external I/O to internal function calls. The BCS layer communicates through the USB bus to a host computer. It provides a packaging layer between the operating system software layer and the device.

IV. DISCUSSION

We presented a novel needle driver and a plurality of MRI compatible mechatronic devices consisting of a optical force sensor and a linear stage. The needle driver can provide needle cannula rotation and stylet translation motion while the cannula translation is engendered by the 3-axis stage. The design is capable of positioning needle and increase the operation autonomy and thus reduce operation time.

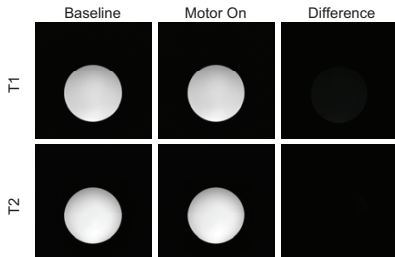


Fig. 4. Representative results showing the difference in images obtained of baseline and motor running conditions.

We are in the process of electrical test and building a fully functional prototype to evaluate the MRI-compatibility and targeting accuracy. Our recent compatibility test with

the same actuator [11] and control hardware in the scanner room has confirmed that no pair showed a significant signal degradation with a 95% confidence interval shown in Fig. 4. Further MRI tests aims to confirm the mutual compatibility of the robot structure. Detailed quantitative performance experiments and results would be reported soon.

V. ACKNOWLEDGEMENTS

This work is supported in part by the Congressionally Directed Medical Research Programs Prostate Cancer Research Program (CDMRP PCRP) New Investigator Award W81XWH-09-1-0191 and Worcester Polytechnic Institute internal funds. We are grateful for the generous sample support from Igus, Inc (Providence, RI).

REFERENCES

- [1] A. Jemal, R. Siegel, E. Ward, Y. Hao, J. Xu, and M. J. Thun, "Cancer statistics, 2009," *CA Cancer J Clin*, vol. 59, pp. caac.20006–249, May 2009.
- [2] J. C. Presti, "Prostate cancer: assessment of risk using digital rectal examination, tumor grade, prostate-specific antigen, and systematic biopsy," *Radial Clin North Am*, vol. 38, pp. 49–58, Jan 2000.
- [3] K. Chinzei and K. Miller, "Towards mri guided surgical manipulator," *Med Sci Monit*, vol. 7, no. 1, pp. 153–163, 2001.
- [4] K. Masamune, G. Fichtinger, A. Patriciu, R. C. Susil, R. H. Taylor, L. R. Kavoussi, J. H. Anderson, I. Sakuma, T. Dohi, and D. Stoianovici, "System for robotically assisted percutaneous procedures with computed tomography guidance," *Comput Aided Surg*, vol. 6, no. 6, pp. 370–383, 2001.
- [5] G. Wan, Z. Wei, L. Gardi, D. B. Downey, and A. Fenster, "Brachytherapy needle deflection evaluation and correction," *Med Phys*, vol. 32, pp. 902–909, Apr 2005.
- [6] R. J. Webster III, J. Memisevic, and A. M. Okamura, "Design considerations for robotic needle steering," in *Proc. IEEE International Conference on Robotics and Automation ICRA 2005*, pp. 3588–3594, 2005.
- [7] R. Alterovitz, M. Branicky, and G. Ken, "Motion planning under uncertainty for image-guided medical needle steering," *International Journal of Robotics Research*, vol. 27, no. 11–12, pp. 1361 – 74, 2008.
- [8] M. Mahvash and P. Dupont, "Fast needle insertion to minimize tissue deformation and damage," in *Proc. IEEE International Conference on Robotics and Automation ICRA 2009*, pp. 3097 – 3102, 2009.
- [9] H. Su and G. Fischer, "A 3-axis optical force/torque sensor for prostate needle placement in magnetic resonance imaging environments," *2nd Annual IEEE International Conference on Technologies for Practical Robot Applications*, (Boston, MA, USA), pp. 5–9, IEEE, 2009.
- [10] H. Su, W. Shang, G. Cole, K. Harrington, and F. S. Gregory, "Haptic system design for mri-guided needle based prostate brachytherapy," *IEEE Haptics Symposium 2010*, (Boston, MA, USA).
- [11] Y. Wang, G. Cole, H. Su, J. Pilitsis, and G. Fischer, "Mri compatibility evaluation of a piezoelectric actuator system for a neural interventional robot," in *Annual Conference of IEEE Engineering in Medicine and Biology Society*, (Minneapolis, MN), pp. 6072–6075, 2009.
- [12] S.-E. Song, N. B. Cho, G. Fischer, N. Hata, C. Tempany, G. Fichtinger, and I. Iordachita, "Development of a pneumatic robot for mri-guided transperineal prostate biopsy and brachytherapy: New approaches," in *Proc. IEEE International Conference on Robotics and Automation ICRA 2010*, 2010.
- [13] Z. Tse, H. Elhawary, M. Rea, I. Young, B. Davis, and M. Lamperth, "A haptic unit designed for magnetic-resonance-guided biopsy," *Proceedings of the Institution of Mechanical Engineers, Part H (Journal of Engineering in Medicine)*, vol. 223, no. H2, pp. 159 – 72, 2009.
- [14] H. S. Bassan, R. V. Patel, and M. Moallem, "A novel manipulator for percutaneous needle insertion: Design and experimentation," *IEEE/ASME Transactions on Mechatronics*, vol. 14, no. 6, pp. 746 – 761, 2009.
- [15] G. A. Cole, J. G. Pilitsis, and G. S. Fischer, "Design of a robotic system for mri-guided deep brain stimulation electrode placement," in *Proc. IEEE International Conference on Robotics and Automation ICRA 2009*, May 2009.

Distributed Parameter Statics of Magnetic Catheters

İlker Tunay, Member, IEEE

Abstract—We discuss how to use special Cosserat rod theory for deriving distributed parameter static equilibrium equations of magnetic catheters. These medical devices are used for minimally-invasive diagnostic and therapeutic procedures and can be operated remotely or controlled by automated algorithms. The magnetic material can be lumped in rigid segments or distributed in flexible segments. The position vector of the cross-section centroid and quaternion representation of an orthonormal triad are selected as DOF. The strain energy for transversely isotropic, hyperelastic rods is augmented with the mechanical potential energy of the magnetic field and a penalty term to enforce the quaternion unity constraint. Numerical solution is found by 1D finite elements. Material properties of polymer tubes in extension, bending and twist are determined by experiments.

I. INTRODUCTION

A magnetic catheter is an interventional device containing permanent or permeable magnets, navigated in a patient's body lumens by steering at the distal tip using an external magnetic field \mathbf{B} and by changing the inserted length L at the proximal end by an advancer. In contrast to manually manipulated catheters which are bent at the tip using pull wires and twisted by a handle at the proximal end to change the plane of bending, magnetic catheters do not need torque transmission via the shaft since the field can rotate the tip. Combined with a localization system that measures tip position and orientation; an X-ray or ultrasound imaging system; other physiological sensors such as ECG, pressure or force; end-effectors such as ablation electrodes, biopsy probes; and a software platform that adds visualization, automation and control, these catheters can be teleoperated by human physicians at a workstation placed in a control room which may be adjacent to the surgical room or placed in a remote location. With the help of varying degrees of automation from the software, the efficacy and efficiency of minimally-invasive medical procedures may potentially be improved with likely less risk for the patient and less X-ray exposure to the physician.

Typically, the body of a catheter is made from an extruded thermoplastic polymer which may be irradiated to increase cross-linking, making it more "elastomeric." The body may be reinforced with coils or braids to improve kink resistance and pushability and loaded with a radiopaque substance for fluoroscopy. The mechanical properties of the resulting material must be determined experimentally. These properties are not isotropic, depend heavily on temperature (and sometimes on water absorption if uncoated) and manufacturer's specifications are not adequate for precise engineering purposes. The material is viscoelastic and can go into the plastic range if care is not taken.

This work was entirely supported by Stereotaxis, Inc.

İ. Tunay is with Stereotaxis, Inc., 4320 Forest Park Ave, Suite 100 St. Louis, Missouri, 63108, USA, itunay@ieee.org

Mechanical modeling of these devices is valuable for multiple purposes: Visualization at the user interface; simulation for training and pre-procedure planning; design optimization; and automatic control. Here we will restrict our model to spatially uniform, externally generated magnetic fields. Time variation of the actuation (\mathbf{B} field plus advancer) and surrounding tissues are assumed to be much slower than the dynamics of the catheter. Therefore, static equilibrium configurations can approximate a moving time average of dynamic configurations and seem to be adequate for most medical catheterization applications. Also we restrict this work to permanent magnetic materials whose volumetric magnetization does not depend on the external field. We allow both rigid magnets placed at arbitrary intervals along the device body and magnetic materials distributed with axially varying density along the body. Although we call our device a "catheter," the proposed modeling method is directly applicable to guide wires, endoscopes, sheaths, blood vessels or other elongate objects.

Our formulation follows the (special Cosserat) rod theory described in [1], [2] and references therein. The kinematic formulation is intrinsically one-dimensional (1D), as opposed to reduction from 3D elasticity. For our application there are two motivating factors: First, the resulting finite-element model (FEM) uses a 1D domain parametrized by the arc length s in the reference configuration and thus yields significant computational savings compared to 3D FEM; second, it is time consuming and expensive to identify the anisotropic material properties of polymers in 3D. Instead, the 1D formulation allows us to determine the constitutive relationships between strains and internal forces by experimenting on manufactured (but not assembled) tubing segments.

II. STATIC MODEL

When a magnetic catheter with discrete rigid magnets is in free-space, extending from a sheath or support, its centroid curve is planar, there is no twist, and curvatures of homogeneous segments completely determine the equilibrium configuration [3]. When there is contact with tissue only at the tip, then a closed-form solution is still possible using Jacobi elliptic functions [4]. However, for distributed magnetic materials with arbitrary magnetization direction, and when the catheter makes contact at multiple locations, twisting and shear deformation occur in addition to bending. At every point in the domain six degrees-of-freedom (DOF) are required as functions of the reference arc length s . These can be selected as the strain variables: Two for bending $\kappa_1(s), \kappa_2(s)$, two for shear $\nu_1(s), \nu_2(s)$, one for extension $\nu_3(s)$, and one for twist $\kappa_3(s)$. Alternatively, the position vector of the cross-section centroids $\mathbf{r}(s)$ and an orthonormal triad $\{\mathbf{d}_i(s)\}$, $i = 1, 2, 3$ may be used. First two vectors of the triad are called "directors" and they span the cross-section. Denote by

differentiation with respect to s . This triad rotates as

$$\mathbf{d}'_i = \boldsymbol{\kappa} \times \mathbf{d}_i, \quad \boldsymbol{\kappa} \stackrel{\text{def}}{=} \sum_i \kappa_i \mathbf{d}_i. \quad (1)$$

The rotational DOF may also be represented by a proper orthogonal matrix $R(s) \in SO(3)$, transforming the standard basis $\{\mathbf{e}_i\}$ of \mathbb{R}^3 to the local basis of the directors. In the case of straight rods with negligible shear and extension, the latter method leads to an efficient, custom FE discretization based on beam elements [5], which is particularly useful for control design [6]. However, representing the three rotational DOF with six variables in $\mathbf{d}_1, \mathbf{d}_2$ and three orthonormality constraints (or nine variables and six constraints for R) necessitates special integration methods at every step of the solution to maintain these constraints since standard methods like Runge–Kutta are inappropriate [7]. If one wishes to use commercial or standard FE packages instead, then a useful reduction to four variables is afforded by using unit quaternions $q = q_0 + \mathbf{q}$, with norm $\sqrt{q_0^2 + \mathbf{q} \cdot \mathbf{q}} = 1$. Other alternatives include keeping the directors as main variables, but transforming them to and from quaternions only for the configuration update [8]; expressing strain variables in quaternions and using coordinate projection at every step [9] to enforce the unity constraint; deriving the equations of motion in quaternion algebra and using index reduction for the resulting differential-algebraic system followed by a stiff integration method [10]; using \mathbf{r} , R and strain variables all together in a two-point shooting scheme for the resulting first order ODE's [11].

We prefer a commercial general-purpose FE environment, such as Comsol® for our rod model not only to save time in programming but also for the ability to couple this structural mechanics problem to other physics (fluid, thermal, etc.). For this reason, we choose quaternions to represent rotations as

$$\begin{aligned} R &= [\mathbf{d}_1, \mathbf{d}_2, \mathbf{d}_3] \\ &= (q_0^2 - \mathbf{q} \cdot \mathbf{q}) I_{3 \times 3} + 2\mathbf{q} \otimes \mathbf{q} + 2q_0 Q, \end{aligned} \quad (2)$$

where Q is the skew-symmetric matrix corresponding to \mathbf{q} . Denoting the alternating symbol by ε , the strain variables in terms of the DOF (\mathbf{r}, q) are

$$\kappa_i = \frac{1}{2} \sum_{j,k} \varepsilon_{ijk} \mathbf{d}'_j \cdot \mathbf{d}_k, \quad (3)$$

$$\nu_i = \mathbf{r}' \cdot \mathbf{d}_i. \quad (4)$$

The unity constraint is enforced by adding a penalty term

$$P = \frac{1}{2} (q_0^2 + \mathbf{q} \cdot \mathbf{q} - 1)^2 \quad (5)$$

to the total potential energy. Indeed, this approach is not only mathematically convenient but also equivalent to scaling the directors in the deformed configuration corresponding to uniform distention of the cross-section. A hollow tube filled with pressurized fluid, such as blood vessels would have this behavior.

Since catheter tubes are made by extrusion it is reasonable to assume that the material is transversely isotropic. In this case,

the most general hyperelastic strain energy per unit reference length, up to quadratic order is [12]

$$\begin{aligned} W &= \frac{1}{2} [E^b (\kappa_1^2 + \kappa_2^2) + E^t \kappa_3^2 \\ &\quad + E^s (\nu_1^2 + \nu_2^2) + E^e (\nu_3 - 1)^2], \end{aligned} \quad (6)$$

where E^b , E^t , E^s , E^e are stiffness in bending, twist, shear and extension respectively, which may depend on s . If the reference configuration is not straight but has nonzero initial curvatures κ_i^r , then (6) still applies via the substitution $\kappa_i \leftarrow (\kappa_i - \kappa_i^r)$. The constitutive relations for the internal contact force \mathbf{n} and moment \mathbf{m} vectors are

$$\mathbf{n} = \sum_i n_i \mathbf{d}_i, \quad n_i = \frac{\partial W}{\partial \nu_i}, \quad (7)$$

$$\mathbf{m} = \sum_i m_i \mathbf{d}_i, \quad m_i = \frac{\partial W}{\partial \kappa_i}. \quad (8)$$

For a rod magnetized in the direction perpendicular to its cross-section with magnetic moment per length $\mu(s)$, the mechanical potential energy per length is

$$U_m = -\mu(s) \mathbf{d}_3(s) \cdot \mathbf{B}, \quad (9)$$

and the (energy) functional to be minimized by (\mathbf{r}, q) is

$$S(\mathbf{r}, q) = \int_0^L (W + U_m + c_u P) ds, \quad (10)$$

in which the constant c_u is selected large. Common boundary conditions are geometric at the proximal end $\mathbf{r}(0) = 0$, $q_0(0) = 1$, $\mathbf{q}(0) = 0$ and an applied force or torque at the distal end $s = L$. If there are other external conservative forces or moments acting along the rod body or at the ends, the potential energies corresponding to those can be added to (10). The ODE's describing the static equilibrium are found by standard calculus of variations since (\mathbf{r}, q) are unconstrained except for the boundary conditions at $s = 0$. Indeed, the weak form can be used directly. Symbolic computation in Mathematica® is used for this purpose. These equations were translated to Matlab®, calling Comsol® FE functions to mesh the domain, to discretize via cubic Hermite elements to maintain differentiability, and to solve by repetitively using pure Newton's method in a continuity scheme. Comparison to standard 3D FEM indicated that 40-fold reduction in the total FE DOF is possible without sacrificing accuracy.

The stiffness parameters in (6) were estimated by experiments for tube segments with uniform material and geometric properties. All tests were done at body temperature. Extension stiffness E^e was estimated in pulling tests with constant elongation rate. Viscoelastic behavior is evident in Fig. 1 showing dependence of pulling force on strain rate. The difference in force between increasing the length (upper part of the loop) and decreasing the length (lower part of the loop) indicates the energy lost to internal viscous forces of the polymer. The standard 3-parameter spring–dashpot model relating stress σ , strain ϵ and their time rates $\dot{\sigma}, \dot{\epsilon}$

$$\dot{\epsilon} = \frac{\dot{\sigma} + \frac{E_2}{\eta} \sigma - \frac{E_1 E_2}{\eta} \epsilon}{E_1 + E_2} \quad (11)$$

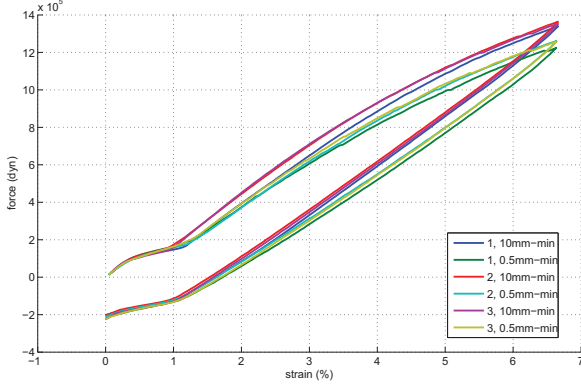


Fig. 1. Extension force (dyn) vs. strain (%) at various elongation rates for catheter tube.

using viscous damping parameter η captures both creep and stress relaxation behavior, although three parameters may not be sufficient for quantitatively describing a particular material. Since we are interested in statics, we fitted the experimental data to the steady-state value of the ramp response of force to elongation. The bending stiffness E^b was estimated by attaching small magnets to one end of a tube and deflecting it in a magnetostatic field. At the strain range we were testing, the linearity of the response was very good and E^b did not depend much on tube length, as seen in Fig. 2. The twist stiffness E^t was estimated by rotating one end of a tube to a fixed angle and measuring the torque at the other end by a precision torque meter. Figure 3 indicates that for short tubes the deflection is going outside the linear range. But for magnetic catheters torsional deformation is fairly small, and the linear fit is sufficient for our purposes. Estimating the shear stiffness E^s is not straightforward because creating a configuration with pure shear deformation with constant strain requires a constant body torque to be applied along the whole length of the tube, not just at the boundaries, which is not practical. Instead, a three-point bend test may be used which will combine shear with planar bending and extension. Using numerical optimization, E^s may be estimated that fits the FE simulation to the experimental data in a least-squares sense.

ACKNOWLEDGMENT

The authors would like to thank Stereotaxis for supporting this work entirely. From this company, Bella Bloom performed the experiments.

REFERENCES

- [1] S. Antman, *Nonlinear Problems of Elasticity*, 2nd ed. New York, US: Springer-Verlag, 2005.
- [2] J. Simo, "A finite strain beam formulation. the three dimensional dynamic problem. part i," *Comput. Meths. Appl. Mech. Eng.*, vol. 49, pp. 55–70, 1985.
- [3] I. Tunay, "Position control of catheters using magnetic fields," in *Proc. IEEE International Conference on Mechatronics 2004 (ICM'04)*, Istanbul, Turkey, June 2004, pp. 392 – 397.
- [4] ——, "Modeling magnetic catheters in external fields," in *Proc. 26th Annual Int. Conf. IEEE Engineering in Medicine and Biology Society (EMBC'04)*, vol. 3, San Francisco, California, September 2004, pp. 2006 – 2009.
- [5] W. Lawton, R. Raghavan, S. Ranjan, and R. Viswanathan, "Ribbons and groups: a thin rod theory for catheters and filaments," *Journal of Physics A*, vol. 32, pp. 1709–1735, 1999.
- [6] İ. Tunay, S.-Y. Yoon, K. Woerner, and R. Viswanathan, "Vibration analysis and control of magnet positioner using curved-beam models," *IEEE Trans. on Control Systems Technology*, vol. 17, no. 6, pp. 1415–1423, November 2009.
- [7] J. Park and W.-K. Chung, "Geometric integration on euclidean group with application to articulated multibody systems," *IEEE Trans. on Robotics*, vol. 21, no. 5, pp. 850 – 863, 2005.
- [8] J. Simo and L. Vu-Quoc, "A three dimensional finite-strain rod model. part ii," *Comput. Meths. Appl. Mech. Eng.*, vol. 58, pp. 79–116, 1986.
- [9] J. Spillmann and M. Teschner, "CORDE: Cosserat rod elements for the dynamic simulation of one-dimensional elastic objects," in *Proc. Symposium on Computer Animation*, San Diego, California, August 2007.
- [10] H. Lang, J. Linn, and M. Arnold, "Multibody dynamics simulation of geometrically exact Cosserat rods," in *Proc. Multibody Dynamics*, Warsaw, Poland, June 2009.
- [11] B. Jones, R. Gray, and K. Turlapati, "Three dimensional statics for continuum robotics," in *Proc. Intl Conf. on Intelligent Robots and Systems*, St. Louis, Missouri, October 2009.
- [12] T. Healey, "Material symmetry and chirality in nonlinearly elastic rods," *Math. Mech. Solids*, vol. 7, pp. 405–420, 2002.

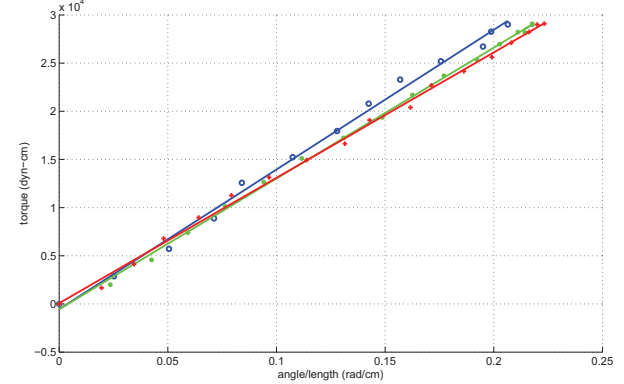


Fig. 2. Magnetic bending torque (dyn-cm) vs. tip angle/length (rad/cm) for tubes of length 3 cm (blue), 4.5 cm (green) and 6 cm (red); experimental results (markers) and fitted lines (solid).

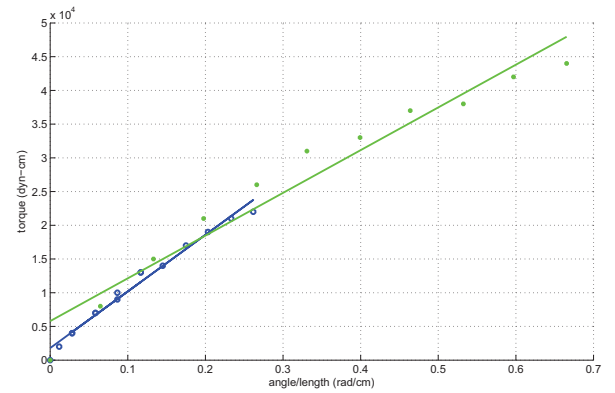


Fig. 3. Twisting torque (dyn-cm) vs. tip angle/length (rad/cm) for tubes of length 6 cm (blue), 2.6 cm (green); experimental results (markers) and fitted lines (solid).

A Pilot Study on Using a Flexible Cannula Robot for Micro-Vascular Stenting

Wei Wei¹ Student Member, IEEE, Howard F. Fine², Stanley Chang³, Nabil Simaan^{1*}, Member, IEEE

Abstract— Micro-stenting is a potentially revolutionary approach to surgical treatment of micro-vascular retinal disorders that do not resolve using pharmaceutical treatment. This paper presents a novel flexible cannula robot called a Stent Deployment Unit (SDU) that enables micro-stent placement in ophthalmic surgery. The clinical motivation for this work is highlighted in context of micro-vascular retinal surgery. The proposed SDU allows intraocular adjustment of the approach angle and the position of the stent with respect to the retina. The feasibility of this robot is experimentally evaluated on chick chorioallantoic membranes (CAM) and on agar vascular models. Experiments show dependency on the approach angle with respect to the vasculature and on the mobility of the vasculature. Successful placement of stents was achieved in both experimental media. To the best of our knowledge, this work is the first to demonstrate successful stent deployment in a scale suitable for retinal surgery. We believe this technique has the promise of enabling effective vascular treatments for blinding conditions such as central and branch retinal vein occlusion.

I. INTRODUCTION

OPHTHALMIC surgery is one of the most delicate surgical fields and presents many challenges to surgeons. Common ophthalmic surgical procedures include intraocular lens placement for cataract, trabeculectomy (a surgical procedure used to relieve intraocular pressure) and tube shunt placement for glaucoma, and vitrectomy (a surgery to remove the vitreous humor from the eye) for a number of retinal disorders including retinal detachment, epiretinal membrane and macular hole [1].

The challenges of ophthalmic surgery include a lack of intraocular distal dexterity of the tools, limited force feedback due to the dominating friction between the tool and the sclera [2], lack of depth perception, and eye mobility. Microsurgery of the retina also demands a level of accuracy and bimanual dexterity not common to other surgical fields. For example, a positioning accuracy of 5-10 μ m is required for procedures such as epiretinal membrane peeling and retinal venous cannulation, and intraocular trauma (e.g. retinal hemorrhage [3]) can adversely affect surgical outcomes.

Recently, robot-assisted ophthalmic surgery has been proposed to address the aforementioned challenges [4-9]. Despite these efforts and the success of stenting procedures

Manuscript received March 8, 2010. ¹Department of Mechanical Engineering, Columbia University, New York, NY 10027, USA. E-mails: {ww2161, ns2236}@columbia.edu. ²Robert Wood Medical Center, New Brunswick, NJ 08901 {hfine@yahoo.edu}. ³Edward Harkness Eye Institute, Columbia University New York, NY 10032 {sc434@columbia.edu}

* Corresponding author.

in cardiac vascular applications [10, 11], no previous work exists on robotic assistance for micro-vascular stenting in ophthalmic retinal surgery. The main hindrance to micro-vascular stenting is the lack of instruments that address the challenges of this procedure. Micro-vascular stenting requires high precision and intraocular dexterity of surgical tools – a constraint not common to other retina applications. The use of existing catheters is not possible due to size limitations, lack of precision, and dexterity deficiency. To date, the feasibility of micro-stent deployment in retina applications remains unexplored and novel dexterous surgical devices are needed.

This paper proposes to use a novel flexible cannula robot to assist micro-vascular stenting procedures. These robots were first proposed by [12, 13]. Our target surgical application is to provide a physical treatment for Central Retinal Vein Occlusion (CRVO) and Branch Retinal Vein Occlusion (BRVO). Retinal vein occlusion is an obstruction to the outflow of blood that typically occurs at a site where an atherosclerotic artery crosses over a retinal vein, compressing the thin-walled vein [14], and it usually leads to blindness. In this work, preliminary experimental results of using the proposed robot to deliver micro stents in mockup blood vessel models are presented. Successful stent delivery shows the feasibility of our proposed approach.

II. ROBOT DESIGN AND EXPERIMENT SETUP

A. Robot Design

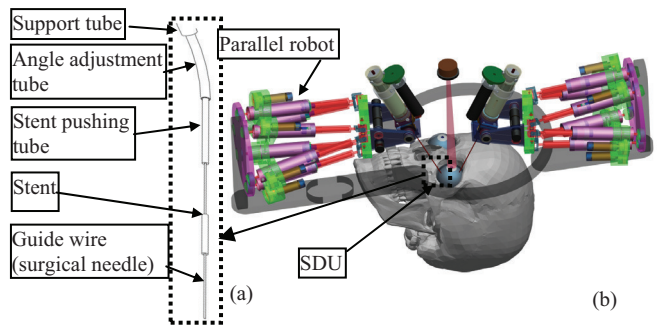


Figure 1. Robot design: (a) SDU, (b) dual-arm robotic system for ophthalmic surgery.

Stent deployment in retinal surgery requires a high-precision miniature design that allows controllable adjustment of the stent approach angle with respect to the retina and axial adjustment of the deployed stent inside the blood vessel. Our proposed design for the SDU (Figure 1(a)) relies on the use of compliant members while eliminating backlash stemming from using pivots or gears. The design is comprised from three concentric NiTi elements. The outer-

most tube is called the angle adjustment tube since it is pre-shaped with a circular radius of 5mm. This tube bends at a specified angle when it is extended outside of its stainless steel support tube. The angle adjustment tube contains a concentric flexible NiTi tube, which serves as a stent pushing element in order to deliver the stent in position. The stent pushing tube contains a NiTi guide wire with a sharp tip. This guide wire is used to create an incision in the blood vessel and to guide the positioning of the stent. These three Degrees-of-Freedom (DoF) for controlling the angle adjustment tube, stent pushing tube, and guide wire correspond to adjusting the approach angle with respect to the retina, delivery of stent, and puncture of the blood vessel as well as the guidance of stent delivery. The 3-DoF SDU will eventually be used as part of a complete dual-arm retinal micro-surgery robotic system of Figure 1(b) [9].

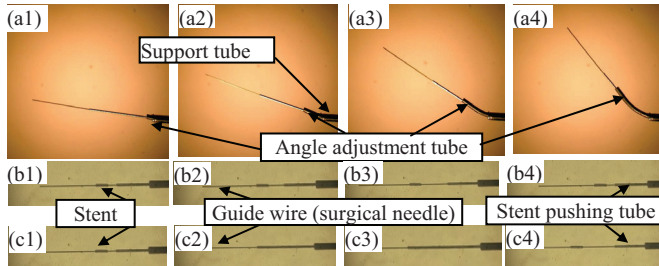


Figure 2. Motion demonstration of the SDU: (a) using angle adjustment tube to change the surgical tool orientation, (b) extending and retracting the guide wire (surgical needle), (c) using the stent pushing tube to deliver the stent.

Figure 2(a1-a4) shows the use of the angle adjustment tube to change the angle of the guide wire. Figure 2(b1-b4) demonstrates the use of the guide wire for stent placement. At the same time, the guide wire serves as a surgical needle to puncture the blood vessel. Figure 2(c1-c4) shows the stent pushing tube used to deliver the stent by pushing it off the guide wire. In physical dimensions, the angle adjustment tube is 550 μm in diameter. The stent pushing tube and the stent have an inner diameter of 100 μm and outer diameter of 200 μm . The guide wire has a diameter of 70 μm .

B. Experiment Setup

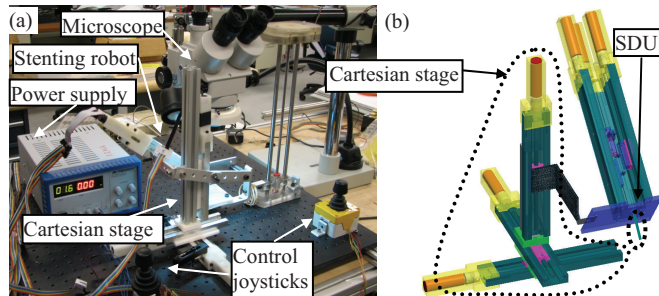


Figure 3. Experiment setup overview: (a) experiment setup, (b) Cartesian stage and SDU.

The experiment setup of Figure 3(a) was constructed to evaluate stent deployment. Figure 3(b) shows the preliminary design of the SDU assembled to a Cartesian stage. Although the eventual goal of this work is to use the dual-arm robotic system of Figure 1(b) to manipulate the SDU, the current work evaluates the efficacy of the SDU

regardless of the robot embodiment used to manipulate it inside the eye.

Two analogue joysticks were used as 3-DoF user interfaces to provide control of the Cartesian stage and the SDU. For the Cartesian stage joystick, the tilting angles about the joystick y- and x-directions were used to control the translations along the x-y plane. Rotation of the joystick (according to the right-hand rule) about its longitudinal axis was used to control translation along the z-direction. For the SDU joystick, tilting about its y axis was used to control the guide wire, and tilting about x-axis was used to control the stent pushing tube. Rotation about the longitudinal axis of the joystick rod was used to control the angle adjustment tube. In the experiment, Matlab® xPC target real-time toolbox was used for control.

III. STENT DEPLOYMENT EXPERIMENTS

Experiments were performed on channels made in agar [15] and on chick chorioallantoic membranes (CAM) - a common animal model for retinal blood vessels. The CAM's were harvested at 18 days, to ensure blood vessel size similar to that of adult human retinal veins (approximately 160 μm as they exit the optic nerve head [16]).

A. Agar Experiments

Experiment Preparation: A 1/8"-1/4" thick layer of solid agar was first prepared on a Petri dish. A hole was created on the side of the dish and a 500 μm wire was advanced into the agar. Upon removing the wire, a channel formed as a mockup blood vessel. Although the channel size is larger than the size of human retinal veins (100-160 μm), this experiment was used for initial validation of our approach.

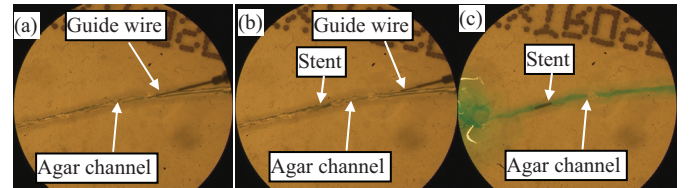


Figure 4. Agar stenting experiment: (a) wire piercing the agar surface, (b) stent delivered, (c) indocyanine green dye injected to demonstrate channel patency.

Method and Results: The SDU was adjusted for the optimal approach angle and for making contact with the top surface of the agar, as shown in Figure 4(a). The vessel poking wire (guide wire) was then slowly advanced into the channel to help lead the stent. Once the wire reached the target region of the channel, the stent pushing tube was extended to push the stent off the guide wire and deliver it at the target place. Finally, both the stent pushing tube and the guide wire were retracted from the channel. Figure 4(b) shows the stent inside the channel. To verify that the stent allowed fluid transport, green dye was injected using a micropipette, Figure 4(c).

Discussion: In this experiment, the agar medium was stiffer than a blood vessel; therefore, the approach angle of the guide wire might be different from that for human retina. The advantage of using agar in the experiments is that it

represents the immobility of the retinal vasculature more faithfully compared to CAM.

B. CAM Experiments

Experiment Preparation: The CAM was first flattened in water and then stretched across a piece of foam. The human retina and the CAM have obvious similarities, including comparable thickness (retina is 100-300 μm while CAM is 20-100 μm) and analogous vasculature. The relevant vessels within the CAM can measure from 40 to 350 μm in diameter; this size agrees with the size of human retinal blood vessels.

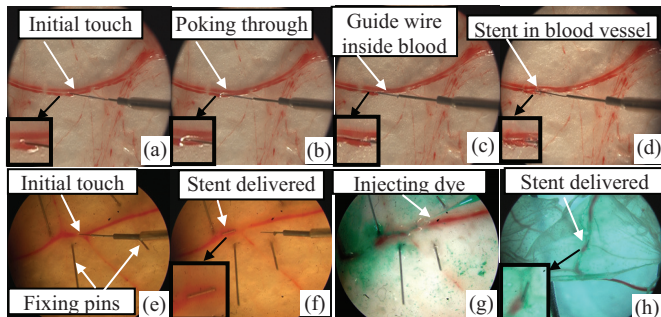


Figure 5. Chicken membrane experiment 1: (a) initial touch, (b) poking procedure, (c) stent guiding, (d) stent delivered. Chicken membrane experiment 2: (e) initial touch, (f) stent delivered, (g) injecting dye, (h) verification of the stent inside the blood vessel.

Method and Results: The initial trial utilized a similar approach as the agar experiments. The guide wire was advanced to the blood vessel, as shown in Figure 5(a). Next, the wire was used to pierce the blood vessel wall, Figure 5(b). After the guide wire was advanced into the blood vessel lumen, Figure 5(c), the stent pushing tube was used to deploy the stent at the target position, Figure 5(d).

In this trial, due to the mobility of the CAM sliding on the foam, the blood vessel was stretched, as observed in Figure 5(d) where the actual delivery position of the stent was to the left of the original vessel piercing location. In order to partially alleviate this problem, the second trial utilized pins to fixate the CAM to the foam base, as shown in Figure 5(e). In this trial the stent was deployed at the target location, Figure 5(f). Injection of indocyanine green dye to demonstrate patency of the stent within the blood vessel was inadvertently under the membrane, as in Figure 5(g). However, confirmation of correct placement of the stent within the blood vessel was clear upon floating the membrane in a water bath, as shown in Figure 5(h).

Discussion: In this experiment, the CAM was fixed to the foam base using pins because the human retina is held in position by its adhesion with the underlying cell layer - the retinal pigment epithelium. The difficulty in injecting indocyanine green dye into the CAM vessel was secondary to ex vivo fixation artifact and obstruction in the dead tissue, which is not the case in live human eyes.

IV. CONCLUSIONS

This paper proposed a novel flexible cannula robot that enables a new surgical approach for micro-vascular retinal surgery. This new approach relies on the use of stenting as a potentially revolutionary surgical treatment for retinal

vascular occlusions. A miniature design of a disposable Stent Deployment Unit (SDU) was validated for micro-vascular stent deployment in agar and chick chorioallantoic membranes. To the best of our knowledge, this work is the first to demonstrate successful stent deployment in a scale suitable for retinal surgery. The proposed technique has the potential to surgically treat retinal vein occlusions, a blinding condition which currently has no medical or surgical cure. We believe that our preliminary results suggest that robot-assisted stenting may play a transformative role in ophthalmic surgery as it currently does in other clinical disciplines such as cardiac surgery. Future work will include integration of the SDU in a dual-arm robotic system for micro-surgery of the eye and verification on animal eyes.

REFERENCES

- [1] J. D. Gottsch, W. J. Stark, and M. F. Goldberg, *Ophthalmic Surgery*, 5th ed.: Hodder Arnold Publishers, 1999.
- [2] A. D. Jagtap and C. N. Riviere, "Applied Force during Vitreoretinal Microsurgery with Handheld Instruments," in 26th Annual International Conference of the IEEE EMBS, San Francisco, CA, 2004, pp. 2771-2773.
- [3] R. L. McIntosh, Q. Mohamed, S. M. Saw, and T. Y. Wong, "Interventions for Branch Retinal Vein Occlusion: An Evidence-Based Systematic Review," *Ophthalmology*, vol. 114, pp. 835-854, 2007.
- [4] H. Das, H. Zak, J. Johnson, J. Crouch, and D. Frambach, "Evaluation of A Telerobotic System to Assist Surgeons in Microsurgery," *Computer Aided Surgery*, vol. 4, pp. 15-25, 1999.
- [5] I. Fleming, M. Balicki, J. Koo, I. Iordachita, B. Mitchell, J. Handa, G. Hager, and R. Taylor, "Cooperative Robot Assistant for Retinal Microsurgery," in MICCAI, 2008, pp. 543-551.
- [6] K. W. Grace, "Kinematic Design of An Ophthalmic Surgery Robot and Feature Extracting Bilateral Manipulation," Ph.D. dissertation, Dept. Mech. Eng., Northwestern Univ., Chicago, IL, 1995.
- [7] K. Ikuta, T. Kato, and S. Nagata, "Development and Experimental Verification of Micro Active Forceps for Microsurgery," in International Symposium on Micromechatronics and Human Science, Nagoya, Japan, 1996, pp. 229-234.
- [8] C. N. Riviere, W. T. Ang, and P. K. Khosla, "Toward Active Tremor Canceling in Handheld Microsurgical Instruments," *IEEE Trans. on Robotics and Automation*, vol. 19, pp. 793-800, 2003.
- [9] W. Wei, R. E. Goldman, H. F. Fine, S. Chang, and N. Simaan, "Performance Evaluation for Multi-Arm Manipulation of Hollow Suspended Organs," *IEEE Trans. on Robotics*, vol. 25, pp. 147-157, 2009.
- [10] C. T. Dotter and M. P. Judkins, "Transluminal Treatment of Arteriosclerotic Obstruction, Description of A New Technic and a Preliminary Report of Its Application," *Circulation*, vol. 30, pp. 654-670, 1964.
- [11] G. Lim, K. Park, M. Sugihara, K. Minami, and M. Esashi, "Future of Active Catheters," *Sensors and Actuators*, vol. 56, pp. 113-121, 1996.
- [12] P. Sears and P. Dupont, "A Steerable Needle Technology Using Curved Concentric Tubes," in IEEE/RSJ International Conference on Intelligent Robots and Systems (IROS 2006) Beijing, China, 2006.
- [13] R. J. Webster, A. M. Okamura, and N. J. Cowan, "Toward Active Cannulas: Miniature Snake-Like Surgical Robots," in IEEE/RSJ International Conference on Intelligent Robots and Systems (IROS), 2006.
- [14] T. H. Williamson, "Central Retinal Vein Occlusion: What is the Story?," *British Journal of Ophthalmology*, vol. 81, pp. 698-704, 1997.
- [15] E. J. Chung, W. R. Freeman, and H. J. Koh, "Visual Acuity and Multifocal Electroretinographic Changes After Arteriovenous Crossing Sheathotomy for Macular Edema Associated with Branch Retinal Vein Occlusion," *Retina*, vol. 28, pp. 220-225, 2008.
- [16] S. Hayreh, "Classification of Central Retinal Vein Occlusion," *Ophthalmology*, vol. 90, pp. 458-474, 1983.

Closed-Loop Control of Needle Steering for Percutaneous Kidney Access

N. A. Wood¹, K. Shahrou², M. C. Ost², C. N. Riviere¹

¹The Robotics Institute, Carnegie Mellon University, Pittsburgh, PA 15213

²Department of Urology, University of Pittsburgh, Pittsburgh, PA 15213

Abstract—The authors present ongoing work on the use of a variable curvature flexible needle system to gain access to the kidney for medical interventions. A nonlinear control law is introduced which drives the needle to track a predetermined planar path using duty-cycled spinning. Renal access is simulated both in simulation and *in vitro* testing which validate the control method proposed.

I. INTRODUCTION

Percutaneous renal access is used in multiple clinical situations including urinary drainage, management of renal tumors during biopsy, and treatment of stones. The most important step in percutaneous renal procedure is to have an appropriate renal access that meets the goals of the surgery. However, percutaneous renal access has multiple limitations. Percutaneous access in nephrolithotomy has a steep learning curve that limits its use among urologists despite a proven benefit of an access created by urologists compared to that created by interventional radiologists [1, 2]. Even with extensive experience, percutaneous renal access can be difficult to obtain in many instances when the renal tumor of interest is small or intraparenchymal or when the kidney has an abnormal location or orientation.

Percutaneous access carries the risk of injuring adjacent organs such as the lungs, colon, liver, spleen, and duodenum [3]. Moreover, radiation exposure to the operating surgeon during percutaneous nephrolithotomy has been estimated to be highest in comparison to other procedures as more fluoroscopy time is used by a factor of 10 [4]. These disadvantages drive us to look for alternative approaches to the current technology that is based on the rigid needle with fluoroscopic guidance in order to gain a percutaneous access to the kidney. A flexible needle that can be guided preemptively and precisely to the target region in the kidney may decrease exposure to radiation and simplify the procedure.

Considerable work has been done which exploits the tendency of a bevel-tip needle to deflect during insertion and by controlling the orientation of the bevel one may control the trajectory of the needle [5]. This work builds on that by controlling the curvature of a needle to follow a predetermined path to simulate renal access in simulation and *in vitro* testing.

II. METHODS

A. Needle Steering via Duty-Cycled Spinning

Duty-cycled spinning of a bevel tipped needle allows for proportional control of the curvature of bevel tipped needles during insertion. This method works by alternating between

periods of (i) insertion without rotation, in which the needle follows a path of maximum curvature, and (ii) insertion with rotation, in which the needle moves straight. Assuming constant velocities, duty cycle, DC , is defined as the ratio of the rotation period, τ_{rot} , to the cycle period, T , where the cycle period is the sum of the rotation period and the translation period, τ_{trans} .

$$DC = \frac{\tau_{rot}}{T} = \frac{\tau_{rot}}{\tau_{rot} + \tau_{trans}} \quad (1)$$

The effective curvature, κ , of the path a needle follows under duty-cycled spinning is then defined as linear function of the duty cycle and the maximum nominal curvature, κ_{max} , of the needle-tissue combination.

$$\kappa = \kappa_{max} (1 - DC) \quad (2)$$

Using the relationship in (2) the needle can be driven to follow a path of any curvature up to the maximum value [6].

Implementation of this method of needle steering is accomplished by moving a fixed distance each cycle, Δs , and having a fixed rotational velocity, ω . A motion cycle is then fully defined by

$$\tau_{rot} = \frac{2\pi}{\omega}, \quad \tau_{trans} = \frac{\tau_{rot}(1-DC)}{DC}, \quad u = \frac{\Delta s}{T}, \quad (3)$$

where u is translational velocity.

B. Path Tracking

Duty-cycled control, in conjunction with paths that have curvatures smaller than the maximum curvature of the needle, allows for path tracking to be implemented. By constraining the normal of the needle-tip bevel to a plane while not rotating, the system can be approximated with a planar model. Previous work [7] has shown that the path a needle tip follows in tissue can be modeled as a bicycle in which the needle tip is located between the front and rear wheels, and less accurately as a unicycle with constrained angular velocity. For simplicity in implementation of control at this stage, a unicycle model is assumed to describe the motion of the needle tip.

$$\frac{d}{ds} \begin{bmatrix} x \\ y \\ \theta \end{bmatrix} = \begin{bmatrix} \cos \theta \\ \sin \theta \\ \kappa \end{bmatrix} \quad (4)$$

The tracking control law implemented here is based on the Stanley method [8], which was used by Stanford

University's DARPA Grand Challenge autonomous vehicle. The nonlinear function steers the front wheel of a kinematic bicycle model, ϕ , to correct for heading error, θ_e , and crosstrack error, e_{ct} , where k is a gain parameter.

$$\phi(t) = \theta_e(t) + \tan^{-1} \frac{k e_{ct}(t)}{v_x} \quad (5)$$

Slight modifications are made to this control law for implementation on the unicycle model. In order to directly control the curvature of the unicycle model, the steering angle from (5) is converted to curvature using the relationship

$$\kappa = k_2 \tan \phi, \quad (6)$$

where for a bicycle model the parameter k_2 is one over the wheelbase, but in this case is considered a tuning parameter. The Stanley method defines crosstrack error as the distance from the front wheel to the nearest point on the desired path, which will be considered to be the distance from the needle tip to the nearest point on the path. Because of the nature of the duty-cycled spinning, the velocity term in the control, v_x , is replaced by distance per cycle, Δs .

$$\kappa = k_2 \tan \left(\theta_e + \tan^{-1} \frac{k_1 e_{ct}}{\Delta s} \right) \quad (7)$$

C. Experimentation

In order to test the proposed control system, shown in Fig. 1, simulation and *in vitro* tests were conducted. Start and goal configurations were defined using a percutaneous nephrolithotomy medical training model (Limbs & Things). The goal position was set at the center of a minor calyx with the orientation parallel with the blood vessels.

The needle used in the experiment was a 0.6 mm diameter nitinol wire with a bevel of 8° and bent to an angle of 6° at a point 5 mm from the tip. The tissue phantom used in experiments was gelatin (Knox gelatin, Kraft Foods Global Inc., Tarrytown, NY) mixed at a ratio of 1.3 cm³ gelatin to 20 cm³ boiling water. The minimum radius path for this needle-tissue combination is 135 mm. Control gains used for both tests were $k_1 = 1.0$ and $k_2 = 0.01$. Rotational velocity, ω , was set to 1 rev/s, and step size, Δs , was set to 1mm.

1) *Simulation Model*: The 3D model for a needle under duty-cycled spinning used for simulation was previously shown in [6].

2) *Path Planning*: Planar trajectories for the needle are calculated in a manner similar to the inverse kinematic method presented in [9]. The major difference is that in the case of 100% duty cycle the path has zero curvature, allowing for Dubins paths. The minimum allowable path radius used was 200 mm.

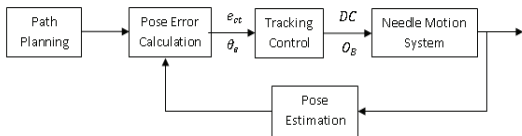


Figure 1. Experimental system control loop.

3) *Pose Estimation*: Real-time needle tip location in 2D is determined through image processing of video from a camera (Dragonfly, Point Grey Research Inc.) mounted 25 cm directly above the tissue phantom and is assumed to be normal to the plane in which the needle operates. Prior to the needle being introduced into the tissue, a background image is initialized. This background image is then subtracted from each image taken during testing leaving only the needle as the image foreground. The position of the needle tip is then determined by finding the distal most point of the foreground object. Needle tip orientation is determined from successive needle tip locations. In simulation, perfect sensors are assumed.

III. RESULTS

Results from simulation of the needle system are shown in Fig. 2 and Fig. 3. Results from *in vitro* testing of the needle system are shown in Fig. 4-7. In both simulation and testing, the needle tracked the desired path well, with the mean crosstrack error for the *in vitro* test being 0.46 mm. The major difference between the simulated and test results are in the control output, where, the test control outputs contain a significant amount of noise.

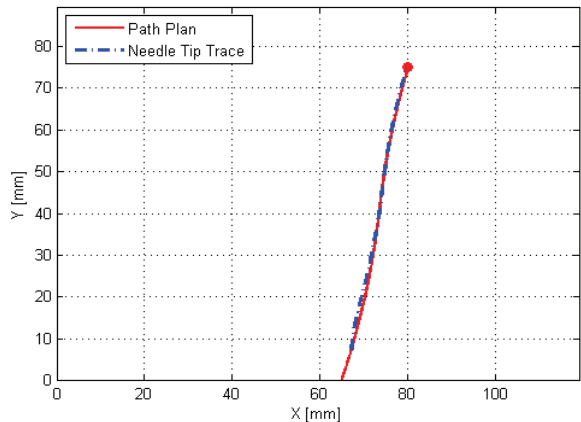


Figure 2. Simulated path tracking results

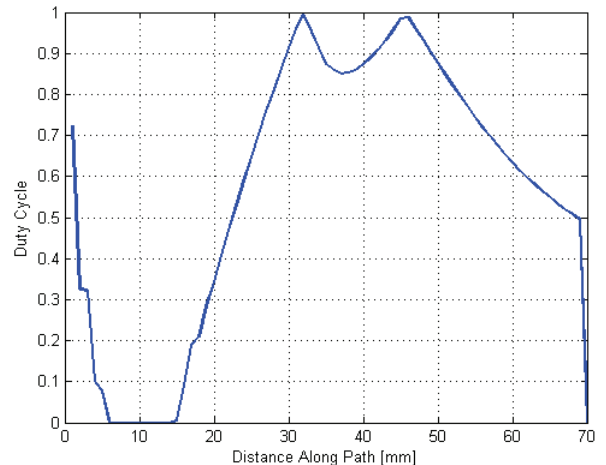


Figure 3. Simulated path tracking control output

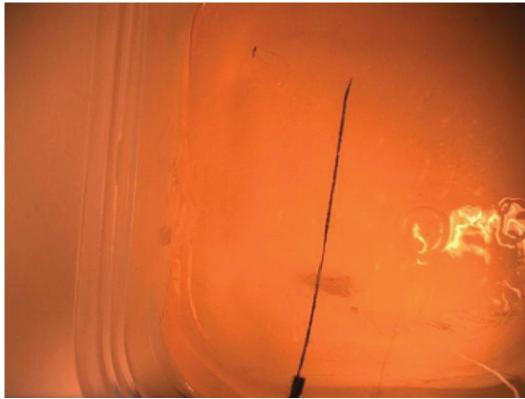


Figure 4. *In vitro* test in gelatin phantom.

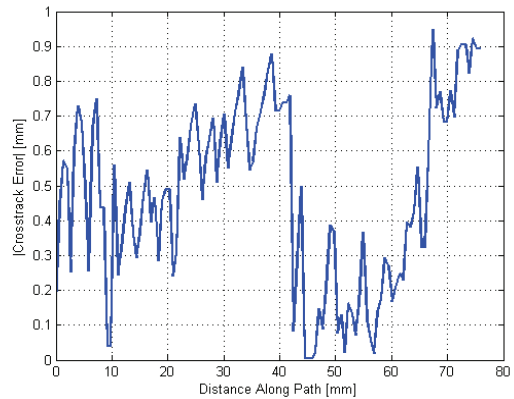


Figure 7. *In vitro* test cross track error magnitude.

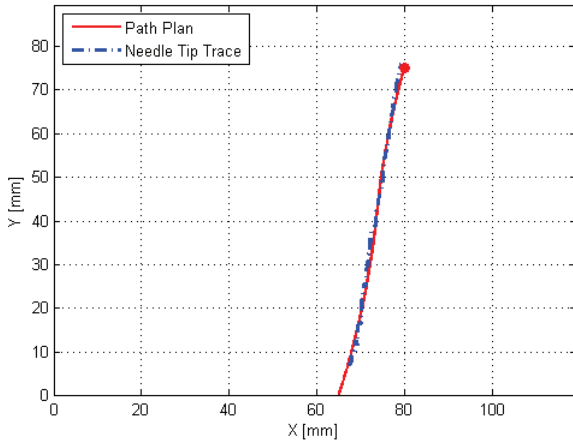


Figure 5. *In vitro* path tracking results.

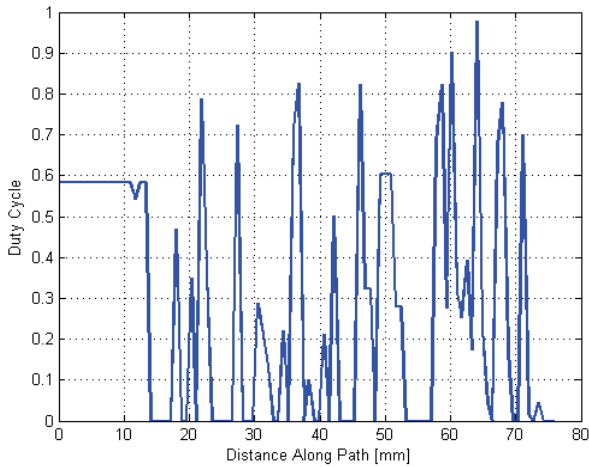


Figure 6. *In vitro* path tracking control output.

IV. DISCUSSION

These preliminary results show promise in path tracking using duty-cycled driving of steerable needles for access to the kidney. Although the unicycle model is assumed in the control derivation, the control law appears to work as intended. Several things are currently being addressed to further the preliminary work presented here. Significant sensor noise is apparent in the test results that may require refinement of the tracking algorithm and filtering. Also, the needle used for these experiments was relatively stiff, but performed well for the relatively mild trajectories tested. Look-ahead tracking algorithms and the full bicycle model are also being investigated.

REFERENCES

- [1] V.G. Bird, B. Fallon, and H.N. Winfield, "Practice patterns in the treatment of large renal stones," *Journal of Endourology*, vol. 17, 2003, pp. 355-363.
- [2] J.D. Watterson, S. Soon, and K. Jana, "Access related complications during percutaneous nephrolithotomy: urology versus radiology at a single academic institution," *The Journal of Urology*, vol. 176, 2006, pp. 142-145.
- [3] M.S. Michel, L. Trojan, and J.J. Rassweiler, "Complications in percutaneous nephrolithotomy," *European Urology*, vol. 51, 2007, pp. 899-906.
- [4] G. Hellawell, S. Mutch, G. Thevendran, E. Wells, and R. Morgan, "Radiation exposure and the urologist: what are the risks?," *The Journal of Urology*, vol. 174, 2005, pp. 948-952.
- [5] N. Abolhassani, R.V. Patel, and M. Moallem, "Needle insertion into soft tissue: a survey," *Medical Engineering & Physics*, vol. 29, 2007, pp. 413-431.
- [6] D.S. Minhas, J.A. Engh, M.M. Fenske, and C.N. Riviere, "Modeling of needle steering via duty-cycled spinning," *Proceedings of the 29th Annual International Conference of the IEEE Engineering in Medicine and Biology Society*, 2007, pp. 2756-2759.
- [7] R.J. Webster, J.S. Kim, N.K. Cowan, G.S. Chirikjian, and A.M. Okamura, "Nonholonomic modeling of needle steering," *International Journal of Robotics Research*, vol. 25, 2006, pp. 509-525.
- [8] S. Thrun, et al., "Stanley: the robot that won the DARPA grand challenge," *Journal of Field Robotics*, vol. 23, 2006, pp. 661-692.
- [9] V. Duindam, J. Xu, R. Alterovitz, S. Sastry, and K. Goldberg, "3D motion planning algorithms for steerable needles using inverse kinematics," *Algorithmic Foundation of Robotics VIII*, Springer Berlin / Heidelberg, 2009, pp. 535-549.

Stochastic Modeling and Path Planning for Steerable Needles

Wooram Park and Gregory S. Chirikjian

Abstract—In this paper we introduce stochastic modeling and path planning for flexible needles with bevel tips. When flexible needles are repeatedly inserted into soft tissue, the trajectories of the multiple insertions are slightly different to one another. A stochastic needle model can predict the stochastic behavior of the needle insertion. Based on the stochastic model of needle steering, the probability density function (PDF) for the needle tip pose is obtained. The mean and covariance of the PDF are estimated using an error propagation algorithm which has second order accuracy. Then we apply the path-of-probability (POP) algorithm to path planning of flexible needles with bevel tips. The probability density function for the needle tip pose plays an important role in the POP algorithm.

I. INTRODUCTION

When medical needles are inserted into tissue, the needles and the tissue undergo deflection and deformation, respectively. The deflection of a needle can be negligible if the needle is very stiff and/or very short. However, since the deflection cannot be completely avoided, special manipulation of the needle is required to prevent or compensate the deflection.

A number of recent works have been reported in the topic of the steerable flexible needles with bevel tips that are inserted into soft tissue for minimally invasive medical treatments [1], [2], [5], [8], [9], [12], [13], [15]. In this research, the needle deflection is not avoided or compensated. Rather, the deflection is used to steer the needle. A flexible needle is rotated with the angular speed $\omega(t)$ around its tangent while it is inserted with translational speed $v(t)$ in the tangential direction. Due to the bevel tip, the needle will not follow a straight line when $\omega(t) = 0$ and $v(t)$ is constant. Rather, in this case the tip of the needle will approximately follow a circular arc with curvature κ when the needle is very flexible. The specific value of the constant κ depends on parameters such as the angle of the bevel tip and the properties of the tissue. Building in arbitrary $\omega(t)$ and $v(t)$, a nonholonomic kinematic model predicts the time evolution of the position and orientation of the needle tip [15].

Due to the uncertainty in the needle insertion, repeated insertions of the flexible needle give an ensemble of slightly different needle trajectories. A stochastic model for flexible needles with bevel tips has been developed to capture this uncertainty in the insertion [9]. This model has been also used for probability-based path planning [9], [10], [12], [13]. Using this stochastic model, we apply the path-of-probability

This work was supported by NIH Grant R01EB006435 “Steering Flexible Needles in Soft Tissue.”

Wooram Park and Gregory S. Chirikjian are with the Department of Mechanical Engineering, Johns Hopkins University, 3400 N. Charles St., Baltimore, MD, USA. {wpark7, gregc}@jhu.edu

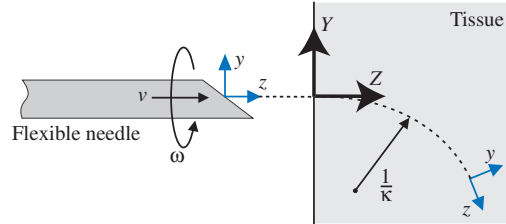


Fig. 1. The definition of parameters, inputs and frames in the nonholonomic needle model. $Y-Z$ denotes the world frame and $y-z$ denotes the body-fixed frame attached to the needle tip.

(POP) algorithm to the needle path planning. We can obtain the probability density function (PDF) of the needle tip pose using the stochastic model and then generate needle paths using the POP algorithm with the PDF. This path planning method for the flexible needles can be built on the top of other path planners in order to have paths avoiding obstacles.

II. KINEMATIC MODEL FOR NEEDLE STEERING

Let us consider a reference frame attached to the needle tip as shown in Fig. 1. The z axis denotes the tangent to the needle tip trajectory, and the x axis is orthogonal to the direction of infinitesimal motion induced by the bevel tip. The needle bends in the $y-z$ plane. A nonholonomic kinematic model for the evolution of the frame at the needle tip was developed in [9], [15] as:

$$\xi = (g^{-1}\dot{g})^\vee = \begin{pmatrix} \kappa v(t) & 0 & \omega(t) & 0 & 0 & v(t) \end{pmatrix}^T \quad (1)$$

where κ is the curvature of the needle trajectory, $g \in \text{SE}(3)$ is the body frame attached to the needle tip, and $\xi \in \mathbb{R}^6$ is the body velocity of the frame, g . The two inputs, $\omega(t)$ and $v(t)$ are the rotating and insertion velocities, respectively.

In practice, we obtain an ensemble of slightly different trajectories when we repeatedly insert a needle at the different insertion locations of a soft medium used to simulate soft tissue [15]. The deviation between the trajectories at the insertion location can be negligible and will increase as the insertion length increases. A simple stochastic model for the needle [9], [10] is obtained by letting:

$$\omega(t) = \omega_0(t) + \lambda_1 w_1(t), \quad \text{and} \quad v(t) = v_0(t) + \lambda_2 w_2(t).$$

Here $\omega_0(t)$ and $v_0(t)$ are what the inputs would be in the ideal case, $w_i(t)$ are uncorrelated unit Gaussian white noises, and λ_i are noise parameter constants. The actual sources of the uncertainty include the stochastic behavior of the tissue deformation and the needle deflection as well as the velocity noise. However, only considering velocity noise is a practical assumption because this system is ‘reachable’ [9]

and the velocity noise parameters are expected to capture the stochastic behaviors from various sources as a whole. The noise parameters can be determined using multiple insertions [11]. A nonholonomic stochastic needle model is defined as

$$\xi = (g^{-1}\dot{g})^\vee dt = (\kappa_0 v_0(t) \ 0 \ \omega_0(t) \ 0 \ 0 \ v_0(t))^T dt + \begin{pmatrix} 0 & 0 & \lambda_1 & 0 & 0 & 0 \\ \kappa\lambda_2 & 0 & 0 & 0 & 0 & \lambda_2 \end{pmatrix}^T \begin{pmatrix} dW_1 \\ dW_2 \end{pmatrix} \quad (2)$$

where $dW_i = W_i(t+dt) - W_i(t) = w_i(t)dt$ are the non-differentiable increments of a Wiener process $W_i(t)$. The needle model (2) is a stochastic differential equation (SDE) on SE(3). As shorthand, we write this as

$$(g^{-1}\dot{g})^\vee dt = \mathbf{h}(t)dt + Hd\mathbf{W}(t). \quad (3)$$

Similar models arise in various applications [4], [16].

III. PATH PLANNING OF STEERABLE NEEDLES

In this section, a path planning method for steerable needles is introduced. The planning method which is adapted from the path-of-probability (POP) algorithm utilizes the probability density of the needle tip pose to determine the intermediate insertions of the needle. The method to compute the probability density function is first discussed and then our path planning method will be introduced. In addition, several examples are provided.

A. Probability density function

Corresponding to the SDE (3) is the Fokker-Planck equation that describes the evolution of the probability density function $\rho(g; t)$ of the ensemble of needle tip positions and orientations at each value of time, t [4]:

$$\frac{\partial \rho(g; t)}{\partial t} = - \sum_{i=1}^d h_i(t) \tilde{E}_i^r \rho(g; t) + \frac{1}{2} \sum_{i,j=1}^d D_{ij} \tilde{E}_i^r \tilde{E}_j^r \rho(g; t) \quad (4)$$

where $D_{ij} = \sum_{k=1}^m H_{ik} H_{kj}^T$ and $\rho(g; 0) = \delta(g)$. In (4), the ‘right’ Lie derivative \tilde{E}_i^r is defined for any differentiable function $f(g)$ as

$$\tilde{E}_i^r f(g) = \left(\frac{d}{dt} f(g \circ \exp(tE_i)) \right) \Big|_{t=0}.$$

For a small amount of diffusion, the solution for the Fokker-Planck equation (4) can be approximated by a shifted Gaussian function [10], [12], [13]:

$$\rho(g, t) = \frac{1}{(2\pi)^3 |\det(\Sigma(t))|^{\frac{1}{2}}} e^{(-\frac{1}{2}\mathbf{y}^T \Sigma(t)^{-1} \mathbf{y})}, \quad (5)$$

where $\mathbf{y} = \log(m(t)^{-1} \circ g)^\vee$, and $m(t)$ and $\Sigma(t)$ are the mean and the covariance of this PDF, respectively. This approximation is based on the fact that for small diffusion the Lie derivative is approximated as $\tilde{E}_i^r f(g) \approx \frac{\partial f}{\partial x_i}$ [10]. Using this, the Fokker-Planck equation (4) becomes a diffusion equation in \mathbb{R}^6 . Therefore, (5) is the solution for the diffusion equation. The probability density function (5) plays an important role in the path planning algorithm that appears in [10], [12], [13].

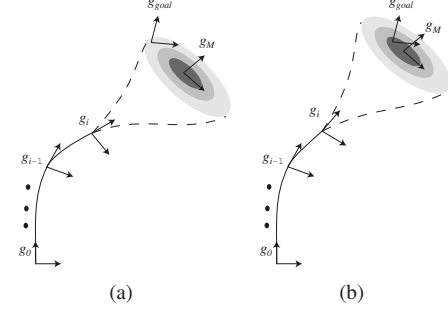


Fig. 2. The path-of-probability algorithm at the i th step. (a) Evaluation of one candidate move, g_i , with low resulting probability of reaching the goal, (b) an candidate move, g_i , resulting in high probability of reaching the goal.

The mean and the covariance of the PDF can be computed using the second order propagation [14]. If a PDF, $\rho_i(g)$ has mean μ_i and covariance Σ_i for $i = 1, 2$, then with second order accuracy, the mean and covariance of $(\rho_1 * \rho_2)(g)$ are respectively [14]

$$\mu_{1*2} = \mu_1 \circ \mu_2 \quad \text{and} \quad \Sigma_{1*2} = A + B + F(A, B), \quad (6)$$

where $A = Ad(\mu_2^{-1})\Sigma_1 Ad^T(\mu_2^{-1})$, $B = \Sigma_2$ and $F(A, B)$ is given in [14]. Consequently, we can obtain the mean and covariance for a relatively large t with given mean and covariance for a small t using this propagation formula. These can then be substituted into (5) to obtain a closed-form estimate of the probability density that the needle will reach any particular pose at any value of time.

B. Path planning method

For needle path planning, we adapt the path-of-probability algorithm introduced in [6]. A similar trajectory planning method can be also found in [7].

In this algorithm, we find the whole trajectory by serially pasting together several intermediate paths. Fig. 2. shows the concept of this algorithm. We aim to find a path that starts at $g_0 = I_{4 \times 4}$ and ends at g_{goal} using M intermediate steps. The homogeneous transformation matrix, $g_i \in \text{SE}(3)$ ($i = 1, 2, \dots, M$), represents the position and orientation of the i^{th} frame with respect to the $(i-1)^{th}$ frame as shown in Fig. 2. Suppose that the $(i-1)$ intermediate steps ($g_1, g_2, \dots, g_{i-1} \in \text{SE}(3)$) have already been determined. The intermediate step, g_i is determined to maximize the probability that the remaining steps reach the goal. In Fig. 2, the shaded ellipses depict the probability density functions when we consider the remaining $(M-i)$ steps. In other words, when we consider $(M-i)$ intermediate steps after g_i , the expected final pose will be in the dark area which has higher probability than the bright area. Comparing the two simplified cases in Fig. 2, if the previous intermediate steps (g_1, g_2, \dots, g_{i-1}) are the same for both cases, we should choose g_i shown in Fig. 2(b) because it yields a higher probability that the final pose is the goal pose. The determination of the intermediate steps can be formulated as

$$g_i = \arg \max_{g \in S} \rho((g_1 \cdots g_{i-1} \circ g)^{-1} \circ g_{goal}; \tau_i), \quad (7)$$

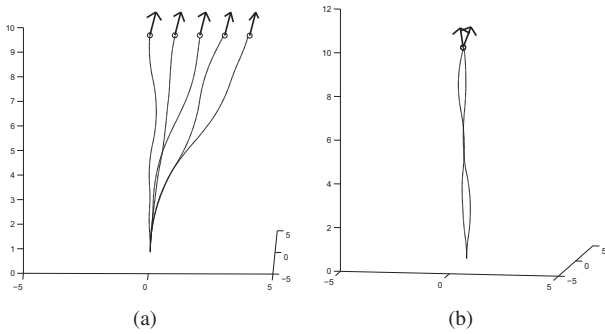


Fig. 3. Path planning using the POP algorithm with a spline for several desired targets.

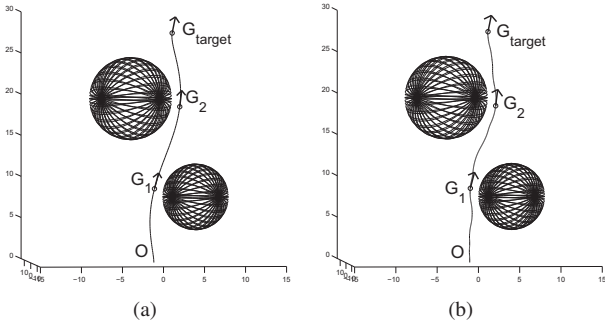


Fig. 4. (a) A long spline with a target and two obstacles, (b) a path generated by the POP algorithm with a spline in a piecewise fashion.

where τ_i is the remaining time to hit the goal and S is the set of possible intermediate poses.

This planning method can be mounted on the top of other path planners. To demonstrate it, we generate splines that connect the starting and the target pose of the needle tip. Then we make the needle to follow the splines using our path planner. Fig. 3 shows several paths generated by our path planning method [13]. Fig. 4 shows an example of a path generated in a piecewise fashion for the environment with obstacles [13]. Suppose that we have a desired target (G_{target}) and two spherical obstacles and that an obstacle-avoiding spline connecting the starting and target pose is obtained in some way as shown in Fig.4(a). Next we choose two poses (G_1 and G_2) that the needle should pass through in order to avoid the obstacles. Then, we can obtain a path from O to G_1 using our path planning method with a spline. We repeat it from G_1 to G_2 , and from G_2 to G_{target} . The result is a trajectory from O to G_{target} via G_1 and G_2 as shown in Fig.4(b).

IV. CONCLUSION

In this work, a stochastic model for the flexible needle with the bevel tip is developed by adding a noise term in a deterministic model for the needle. This model captures the uncertainty of the needle insertion. Using the stochastic model, we approximate the probability density function of the needle tip pose as a shifted Gaussian function. The mean and the covariance for the probability density function are

computed using the propagation formula with the second order accuracy.

Our path planning method generates the paths for the flexible needle using the probability density function. The method is an adapted version of the path-of-probability algorithm. The planning algorithm can be merged with other path planners to give obstacle-avoiding paths.

ACKNOWLEDGEMENTS

This work was supported by NIH Grant R01EB006435 "Steering Flexible Needles in Soft Tissue."

REFERENCES

- [1] R. Alterovitz, K. Goldberg, and A. Okamura, "Planning for steerable bevel-tip needle insertion through 2D soft tissue with obstacles," *IEEE International Conference on Robotics and Automation*, pp. 1652-1657, 2005.
- [2] R. Alterovitz, T. Simeon, and K. Goldberg, "The Stochastic Motion Roadmap: A Sampling Framework for Planning with Markov Motion Uncertainty," *Robotics Science and Systems*, June 2007.
- [3] G. S. Chirikjian and A. B. Kyatkin, *Engineering Applications of Noncommutative Harmonic Analysis*. CRC Press, 2000.
- [4] G. S. Chirikjian, *Stochastic Models, Information Theory, and Lie Groups, Vol. 1*, Birkhäuser, 2009.
- [5] V. Duindam, R. Alterovitz, S. Sastry and K. Goldberg, "Screw-based motion planning for bevel-tip flexible needles in 3D environments with obstacles," *IEEE International Conference on Robotics and Automation*, pp. 2483-2488, May 2008.
- [6] I. Ebert-Uphoff, and G. S. Chirikjian, "Inverse kinematics of discretely actuated hyper-redundant manipulators using workspace densities," in *IEEE International Conference on Robotics and Automation*, pp. 139-145, April 1996.
- [7] R. Mason, J. W. Burdick, "Trajectory planning using reachable-state density functions," in *IEEE International Conference on Robotics and Automation*, pp. 273- 280, Washington, D.C., May 2002.
- [8] S. Misra, K. B. Reed, B. W. Schafer, K. T. Ramesh, and A. M. Okamura, "Observations and models for needle-tissue interactions," *IEEE International Conference on Robotics and Automation*, pp.2687-2692, 2009.
- [9] W. Park, J. S. Kim, Y. Zhou, N. J. Cowan, A. M. Okamura, and G. S. Chirikjian, "Diffusion-based motion planning for a nonholonomic flexible needle model," *IEEE International Conference on Robotics and Automation*, pp. 4600-4605, 2005.
- [10] W. Park, Y. Liu, Y. Zhou, M. Moses, G. S. Chirikjian, "Kinematic state estimation and motion planning for stochastic nonholonomic systems using the exponential map," *Robotica*, 26(4):419-434, 2008.
- [11] W. Park, K. B. Reed, A. M. Okamura and G. S. Chirikjian, "Estimation of model parameters for steerable needles," *IEEE International Conference on Robotics and Automation*, 2010.
- [12] W. Park, Y. Wang and G. S. Chirikjian, "Path planning for flexible needles using second order error propagation," *International Workshop on Algorithmic Foundations of Robotics*, Mexico, December, 2008.
- [13] W. Park, Y. Wang and G. S. Chirikjian, "The path-of-probability algorithm for steering and feedback control of flexible needles," *International Journal of Robotics Research* (available online doi:10.1177/0278364909357228)
- [14] Y. Wang and G. S. Chirikjian, "Nonparametric second-order theory of error propagation on motion groups," *International Journal of Robotics Research*, 27(11-12):1258-1273, 2008.
- [15] R. J .Webster III, J. S. Kim, N. J. Cowan, G. S. Chirikjian, and A. M. Okamura, "Nonholonomic modeling of needle steering," *International Journal of Robotics Research*, 25(5-6):509-525, 2006.
- [16] Y. Zhou and G. S. Chirikjian, "Probabilistic models of dead-reckoning error in nonholonomic mobile robots," *IEEE International Conference on Robotics and Automation*, pp. 1594-1599, 2003.

A 4-DOF Bendable Endoscope Mechanism For Single Port Access Surgery

Hyun-Soo Yoon

Department of Electric, Electronic, Control and
Instrumentation Engineering
Hanyang University
Ansan, Gyeonggi-do, Korea
nada5140@hanmail.net

Abstract - Different from a straight endoscope mechanism used for Laparoscopic surgery, single port access (SPA) surgery requires multi degrees of freedom endoscope mechanism. This work presents a 4-DOF bendable endoscope mechanism that employs a spring as its backbone. This design is slim-sized, light-weighted, and easy to implement a camera at the distal end. The suggested mechanism consists of two modules in which each has 2 DOF. A mechanism integration method with a small-sized camera as well as design principle of the endoscope is introduced. The performance of the suggested mechanism is verified by experiments.

Index Terms - Endoscope, Single port access surgery.

I. INTRODUCTION

Minimally invasive surgery has been a key issue in recent clinical practices. Specifically, the da vinci robot system has been used successfully because it ensures minimum invasion, accurate operation, and fast recovery. Even though it is less invasive as compared to conventional open surgery and Laparoscopic surgery, it is still making multiple holes in the skin by using multi-ports in operation. Recently, single port access (SPA) surgery is becoming a hot issue. As shown in Fig. 1, only one port is employed instead of using multiple ports. In such design, not only the manipulators but also endoscope mechanism should have some degrees of freedom for dexterous manipulation.

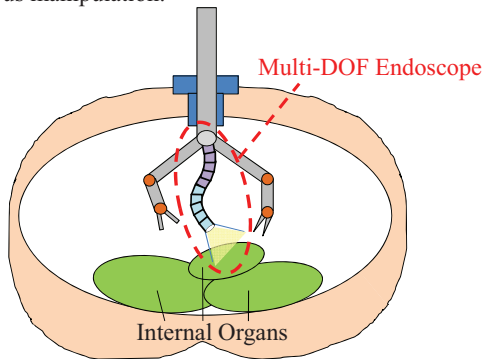


Fig. 1. Single Port Access Surgery

To date, NOTES (Natural Orifice Transluminal Endoscopic Surgery) is an initial attempt of SPA surgery. Abbott, et al [1]

Youngjin Choi and Byung-Ju Yi

Department of Electronic Systems Engineering
Hanyang University
Ansan, Gyeonggi-do, Korea
bj@hanyang.ac.kr

developed an endoluminal robotic system which features a visualization method and two instruments, each having at least 6 degrees-of freedom plus an end effector gripping action. Its initial prototype was created by EndoVia Medical. Swanstrom *et al.* [2] partnered with USGI Medical developed a new manually operated, flexible but rigidly lockable, access instrument using shape lock technology. However, real clinical implementation of NOTES is still in its infancy.

Recently, SPA surgery has been intensively applied to Laparoscopic area. Xu, *et al.* [3] proposed a robotic effector platform for SPA surgery, which consists of two flexible arms and one endoscope system using optical fibers. Osaki, *et al.* [4] proposed a single-trocår assemblable retractor-hand for Laparoscopic surgery. Azuma, *et al.* [5] developed a gripper and a micro-arm for Endoscopic sub mucosal dissection. The micro structures were fabricated and assembled by STAMP. Peter, *et al.* [6] designed an insertable surgical imaging device with pan, tilt, zoom, and lighting. Ko, *et al.* [7] proposed a 3 DOF endoscopic mechanism for Laparoscopic surgery. OLIMPUS EVIS LUCERA 260 [8] is a flexible endoscope with bendable distal end, but the whole body is not lockable.

Based on the analysis of the previous endoscope mechanisms for SPA surgery, they have less degree of freedom as compared to that of end-effector mechanisms. Thus, the visible area is smaller as compared to the endoscope used for the da vinci system. To cope with such problem, multi-degree of freedom endoscope mechanism is indispensable for providing the surgeon with a wide and detailed view of the operation area. Such design allows inspection of a large workspace and even invisible area occluded by the manipulators, organs, or tissues. This work focuses on design of a 4 DOF endoscope mechanism for SPA surgery.

II. A 4-DOF FLEXIBLE CONTINUUM MECHANISM

A. Structure

Up to now, various multi-moduled continuum robots and flexible surgical robots have been developed [9-14]. Salemi, *et al.* [9] and Kurokawa, *et al.* [10] presented self-reconfigurable modular robots. Jones and Walker [11] conducted kinematic modeling for the same model. However, these mechanisms were designed without considering the safety issue in the human-robot interaction where the soft structure is of significance. Webster III, *et al.* [12] developed

a miniature snake-like surgical robot. Sears and Dupont [13] presented a steerable needle using curved concentric tubes. These mechanisms are structurally flexible, but not backdrivable. Choi, *et al.* [14] also proposed a 2 DOF soft endoscope mechanism by employing a spring as its backbone. However, the degree of freedom is limited by using just one module.

This paper is an extension of Choi, *et al.* [14]. The proposed mechanism consists of two modules and each module has 2 DOF. The special features of the mechanism are the flexibility and the backdrivability of the whole body by using a spring backbone. That implies that when the mechanism contacts the human tissues or organs, the actuators driving the mechanism reacts to the external force exerted on the endoscope mechanism. Thus, even in the case of collision with human body, this device can ensure safety. The second advantage is the availability of the hollow space inside the spring through which wires used for the camera and the lighting device installed at the distal end can be inserted without stiffening the whole mechanism by providing some slack length of the wires. The third advantage is its light weight and slim structure.

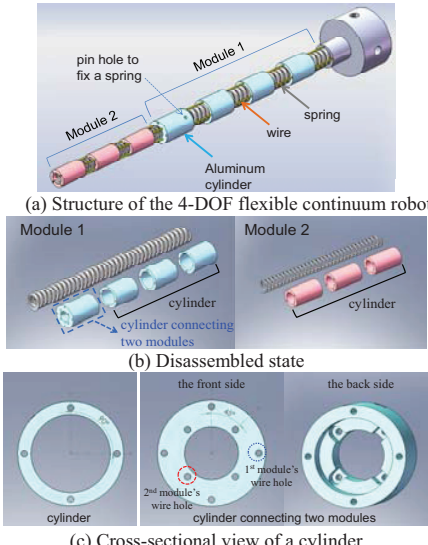


Fig. 2. Structure of the 4-DOF flexible continuum robot

Fig. 2 shows the structure of the suggested mechanism. Each module consists of a backbone spring and multiple aluminum cylinders. To control each module, cylinders are connected by wires through four holes pierced in the cylinders. By pulling and releasing the four wires, the 4 DOF motion can be obtained.

B. Kinematics for one module

1. Spatial model

The motion of each module can be described by two rotation variables (β, γ). Initially, the continuum mechanism is rotated with respect to the global Y_A axis by β . Next; the whole mechanism is rotated about the global Z_A axis by γ .

Fig. 3 shows the configuration of the spatial model being rotated.

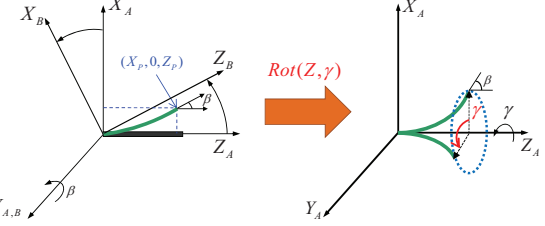


Fig. 3. The bent and rotated shape of the spatial model

Using the rotation matrices, the forward kinematics of the whole mechanism is expressed as

$$\begin{bmatrix} X \\ Y \\ Z \end{bmatrix} = \begin{bmatrix} X_{p1}c\gamma_1 + X_{p2}A + Z_{p2}c\gamma_1s\beta_1 \\ X_{p1}s\gamma_1 + X_{p2}B + Z_{p2}s\gamma_1s\beta_1 \\ Z_{p1} + X_{p2}C + Z_{p2}c\beta_1 \end{bmatrix}, \quad (1)$$

where

$$A = c\gamma_2(c^2\gamma_1c\beta_1 + s^2\gamma_1) + s\gamma_1c\gamma_1s\gamma_2(c\beta_1 - 1),$$

$$B = s\gamma_2(s^2\gamma_1c\beta_1 + c^2\gamma_1) + s\gamma_1c\gamma_1c\gamma_2(c\beta_1 - 1),$$

$$C = -s\beta_1c(\gamma_1 - \gamma_2).$$

The position of two-moduled mechanism is obtained by superposition of those of the two individual modules.

- Coupling of two wires

Each module can be controlled by using two motors. Fig. 4 shows the concept of the coupling of two wires.

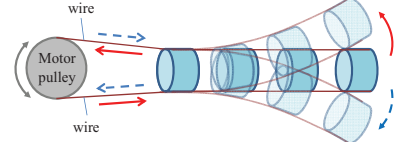


Fig. 4. Coupling of two wires

The relation between the two opposite wires is obtained as

$$\begin{aligned} \Delta d_3 &= -\Delta d_1, \\ \Delta d_4 &= -\Delta d_2. \end{aligned} \quad (2)$$

That is, when the mechanism is bending and rotating, two opposite wires have the same amount of the length change with an opposite sign.

III. IMPLEMENTATION

A. Hardware

Table I shows the specification of the robot module. To prevent interference between the first and second modules, the spring constant of the second module is smaller than that of the first module.

TABLE I: Specification of each module

Module	Specification				
	Diameter	Length	Cylinder material	Cylinder Length	Number of nodes
1 st Module (Base)	8mm	69mm	Al6061	10mm	4
2 nd Module	6mm	45mm	Al6061	10mm	3

B. Experimental Work

1. Position control

Using the two-moduled continuum robot, initially we perform a basic experiment in which the output positions of the end point are controlled. Fig. 5 shows that the robot follows the given straight-line trajectories along the X- and, Y-axis, respectively. The special feature of this robot is its soft structure by using a spring as a backbone as shown in Fig. 6.

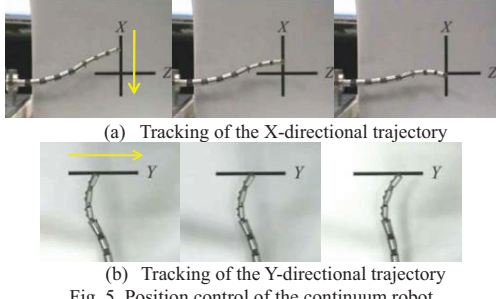


Fig. 5. Position control of the continuum robot



Fig. 6. Soft mechanism

2. Endoscope Mechanism

Fig. 7 shows the CCD camera used for this endoscope and its image. Its dimension and resolution are listed in Table II. Though currently it is a mono camera, a stereo image can be obtained by using two cameras. Fig. 8 shows the endoscope system that integrates the camera and the flexible mechanism. A small-sized LED is employed for lighting.

TABLE II : Specification of camera

Effective pixels	76,800
Resolution	320 x 240
Video outputs	Composite (PAL/NTSC)
Dimension	<Camera head> Diameter: 3mm
Power input	DC 5V
Field of View	60 degrees

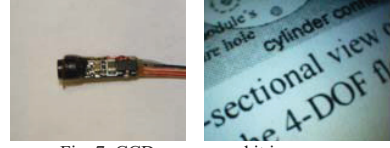


Fig. 7. CCD camera and its image

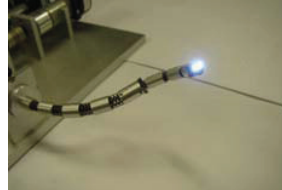


Fig. 8. 4 DOF endoscope mechanism

IV. CONCLUSIONS

In this work, we presented a 4-DOF endoscope mechanism. The special feature of this robot is its soft structure by using a spring as a backbone. As compared to contemporary prototypes reported in the literature, this device is applicable to SPA surgery which requires dexterous multi-degree of freedom. As a future work, we plan to optimize this device so that it is applicable to different surgical areas such as Laparoscopic and sinus surgeries.

ACKNOWLEDGEMENT

This work was partially supported by the Korea Science and Engineering Foundation (KOSEF) grant funded by the Korea government (MEST) (NO. 2009-0059948), partially supported by the Ministry of Knowledge Economy (MKE) and Korea Industrial Technology Foundation (KOTEF) through the Human Resource Training Project for Strategic Technology, and the outcome of a Manpower Development Program for Energy & Resources supported by the Ministry of Knowledge and Economy (MKE).

REFERENCES

- [1] D.J. Abbott, C. Becke, R.I. Rothstein, and W.J. Peine, "Design of an Endoluminal NOTES Robotic System," in *Proc. of IEEE/RSJ Int'l. Conf. on Intelligent Robots and Systems*, 2007.
- [2] L.L. Swanstrom, R. Kozarek, and P.J. Pasricha, "Development of a New Access Device for Transgastric Surgery," *Journal of Gastrointestinal Surgery*, vol. 9, no. 8, 2005.
- [3] K. Xu, R.E. Goldman, J. Ding, P.K. Allen, D.L. Fowler, and N. Simaan, "System Design of an Insertable Robotic Effector Platform for Single Port Access (SPA) Surgery," In *Proc. of IEEE/RSJ Int'l. Conf. on Intelligent Robots and Systems*, 2009.
- [4] M. Osaki, T. Takayama, T. Omata, T. Ohya, K. Kojima, K. Takase, and N. Tanaka, "Single-Trocar Assemblable Retractor-Hand for Laparoscopic Surgery," In *Proc. of Int'l. Conf. on Robotics and Automation*, 2009.
- [5] D. Azuma, J. Lee, K. Narumi, and F. Arai, "Fabrication and Feedback Control of an Articulated Microarm," In *Proc. of Int'l. Conf. on Robotics and Automation*, 2009.
- [6] T.H. Peter, K. Allen, N.J. Hogle, and D.L. Fowler, "Insertable Surgical Imaging Device with Pan, Tilt, Zoom, and Lighting," In *Proc. of Int'l. Conf. on Robotics and Automation*, 2008.
- [7] S-Y. Ko and D-S. Kwon, "A Surgical Knowledge Based Interaction Method for a Laparoscopic Assistant Robot," In *Proc. of Int'l. Workshop on Robot and Human Interactive Communication (RO-MAN 2004)*.
- [8] OLIMPUS EVIS LUCERA260
<http://olympusmedical.co.kr/OMhtml/hmMain/main.php>
- [9] B. Salemi, M. Moll, and W.-M. Shen, "SUPERBOT: A Deployable, Multi-Functional, and Modular Self-Reconfigurable Robotic System," in *Proc. IEEE/RSJ Int'l. Conf. on Intelligent Robots and Systems*, pp. 3636-3641, 2006.
- [10] H. Kurokawa, K. Tomita, A. Kamimura, E. Yoshida, S. Kokaji, and S. Murata, "Distributed Self-reconfiguration Control of Modular Robot M-TRAN," in *Proc. IEEE Int'l. Conf. on Mechatronics & Automation*, pp. 254-259 , 2005.
- [11] B. A. Jones and I.D. Walker, "Kinematics for multi section continuum robots," *IEEE Trans. Robotics*, vol.22, no.1, pp. 43-57, 2006.
- [12] R. J. Webster III, A. M. Okamura, and N. J. Cowan, "Toward Active Cannulas : Miniature Snake-like Surgical Robots," in *Proc. IEEE/RSJ Int'l. Conf. on Intelligent Robots and Systems*, pp. 2857-2863, 2006.
- [13] P. Sears and P. Dupont, "A Steerable Needle Technology Using Curved Concentric Tubes," in *Proc. IEEE/RSJ Int'l. Conf. on Intelligent Robots and Systems*, pp. 2850-2856, 2006.
- [14] D.-G. Choi, B.-J. Yi, and W.K. Kim, "Design of a Spring Backbone Micro Endoscope," in *Proc. IEEE/RSJ Int'l. Conf. on Intelligent Robots and Systems*, pp. 1815-1821, 2007.

Robotization of a ureteroscope for efficient semi-automatic vaporization of kidney stones

Benoit Rosa, Pierre Mozer, and Jérôme Szewczyk
Email : firstname.name@isir.upmc.fr

I. INTRODUCTION

Kidney stones is a very frequent pathology. Estimations say that about 10% of people over 40 years of age in industrialized countries are affected, with a recurrence rate of 53% [1]. Among the techniques recommended by the European Association of Urology to treat this pathology [2], ureteroscopy allows the surgeon to treat stones of sizes up to 20 mm with a mini-invasive approach.

When the stone is larger than 4 mm it cannot pass the ureter and therefore must be treated inside the kidney. The operation process is the following: after introduction of the device into the kidney via natural ways, the surgeon navigates to find the stone and places it properly. A laser fiber is then introduced in the operating channel to eliminate the stone. A red light passes through the fiber to show the surgeon where the fiber points to. When the fiber points towards the stone, the surgeon pushes a pedal activating the power laser. The surgeon should ideally smoothly sweep the surface of the stone to vaporize it, but the the poor maneuverability of the device - it can only be bent on one plane from the outside - and backlash in the transmission mechanism make the operation uneasy. As a result, stones are often fragmented and brought to the outside one by one with a basket wire. Moreover, this operation is time consuming (about 1 hour to treat a stone of 1 cm diameter).

We propose to assist the surgeon in the vaporization task in order to reduce the operating time and avoid fragmentation of stones. The operation remains the same until the push on the laser pedal. At this stage our system handles the vaporization task automatically, under control of the surgeon: the next impact points of the laser appear on the video image, and the surgeon can stop the process if a laser shot is to be made outside the stone. This is allowed by the fact that the laser shooting rate is around 1 Hz.

The system we developed is depicted on Fig. 1. The actuation of the system relies on shape memory alloy (SMA) [3], [4]. The control of the system is made through a visual servoing scheme based on the ureteroscopic images. Those images are segmented to extract a safe region inside

B. Rosa, P. Mozer, and J. Szewczyk are with UPMC Univ Paris 06, UMR 7222, ISIR, F-75005, Paris, France.

P. Mozer is also with AP-HP, Pitié-Salpêtrière Hospital, Department of Urology, F-75013, Paris, France.

the stone which is used to plan a sweeping movement of the fiber.

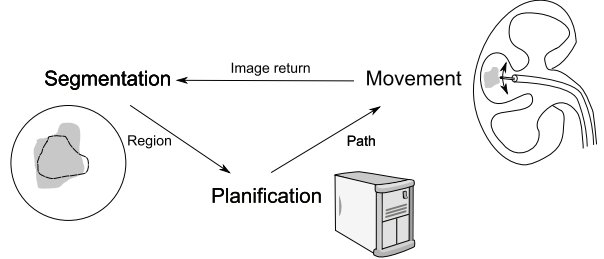


Fig. 1. The proposed command scheme

II. ACTUATION THROUGH SMA WIRES

A. Integration

Nickel-Titanium wires were used as actuators. This material has the property to change its cristallographic organization when heated, resulting in a shortening of the wire of 4 to 8% of its total length. Hence, wires integrated to the distal tip of a catheter can bend it, as showed on Fig. 2.

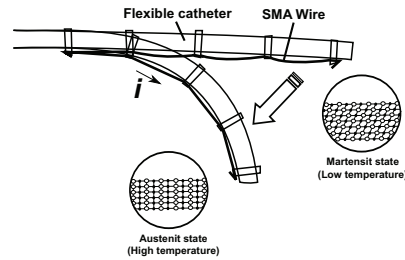


Fig. 2. Bending of a catheter using the shape memory effect of a SMA wire.

Using this principle, three SMA wires were mounted at 120 degrees on the distal tip of a ureteroscope as showed on Fig. 3. They were attached at their two extremities and passed inside two bushings to allow translation of the wire while keeping it close to the ureteroscope. Their length was calculated to reach the limits of a 20mm wide stone with the ureteroscope at 1 cm distance from the stone. A security factor of 2 was chosen, which led to wires of 2.5 cm length. 175 µm diameter wires were used. The outer diameter of

the prototype was 4 mm, which is the inner diameter of the ureteral sheaths commonly used for ureteroscopy.

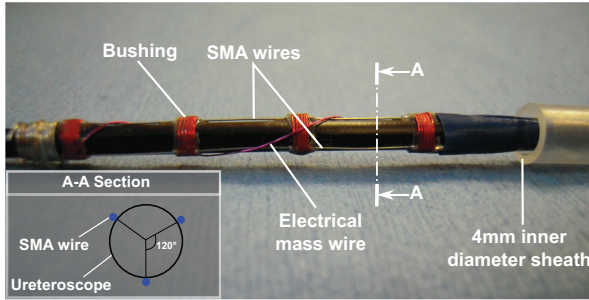


Fig. 3. Integration of the SMA wires to the distal tip of the ureteroscope

B. Validation

A validation was made at the urology department of Pitié-Salpêtrière Hospital (Fig. 4). The prototype was found to be effective to reach the extreme points of a 13 mm kidney stone. Comparisons between actuation by the urologist and actuation using the SMA wires resulted in a much smoother movement of the tip of the ureteroscope in the second case.

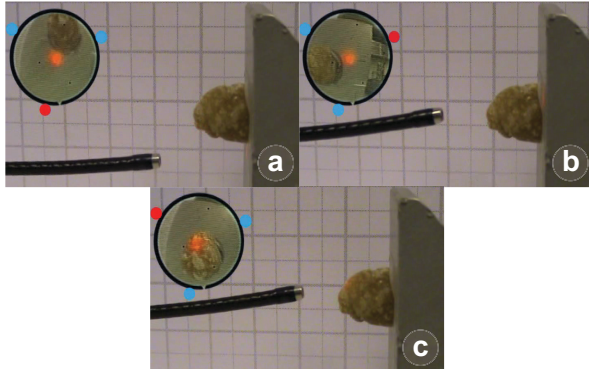


Fig. 4. Validation of the limits of the mechanical system. The upper left view is the endoscopic view, the blue points are the cold SMA wires and the red point is the hot SMA wire. a: movement down. b: movement right. c: movement left

III. COMMAND

To command a smooth sweeping of the surface of the stone, a careful planning of the movements of the ureteroscope tip is needed. For that, we implemented an image based control of the SMA actuators. It relies on an efficient stone edge detection algorithm.

A. Segmentation of the ureteroscopic images

The segmentation of ureteroscopic images is very difficult. First of all, kidney stones come in different chemical compositions, resulting in different shapes, colours, and textures [5]. Moreover, the fiber bundle of the ureteroscope is also fragile, and black dots frequently appear on the image. An algorithm was developed taking these constraint into accounts. It was kept very simple because of

the fact that this particular problem was never handled in the past.

A region growing algorithm was used. The algorithm starts as the surgeon pushes the laser pedal. The fiber then points towards the stone. A detection of the red spot gives the starting point for the region growth. The algorithm parameters tuning and validation were made on a dataset composed of 903 images coming from 10 videos presenting 4 different compositions of stones with sizes varying from 9 to 19 mm. The images were manually segmented by an expert to serve as ground truth, using common performance indicators such as F-score, compactness, and Yasenoff measure. The algorithm parameters were tuned to obtain good results on different kinds of kidney stones. The algorithm has a computational time which allows to run it at a video framerate of 25 frames/s. An example of segmented image is shown on Fig. 5.

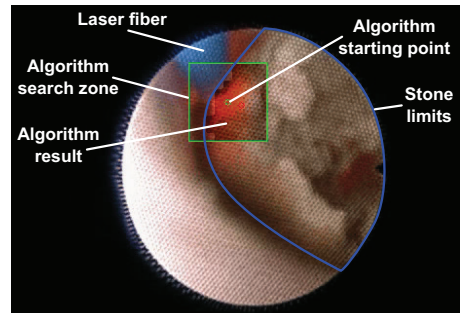


Fig. 5. Example of segmentation obtained with the developed algorithm

B. Visual servoing

A visual servoing scheme was developed. It doesn't rely on any formal relation between the heating current and the shortening of an SMA wire. Equations linking the temperature to the shortening of the wire exist, but our system doesn't embed a temperature sensor. Therefore, the relation between the electrical current in input and the resulting movement has been determined experimentally, and has been integrated in the control scheme. The movement of the ureteroscope results from a vectorial composition of the movements produced by the SMA wires individually (Fig. 6). The regulation was made through a simple PD regulator. A simple testing was developed in which the ureteroscope was actuated to bring a designated point at the center of its image. The system was able to carry out any displacement in its field of view with good accuracy.

C. System bandwidth

The algorithm frequency is greater than 30 Hz and the video is acquired at 25 Hz. Hence, the system bandwidth is mainly limited by the dynamic of the SMA wires. The heating and cooling times of the SMA wires were found to be 0.4s and 1.0 s respectively. However, the proposed control scheme aims at limiting the influence of the cooling time as

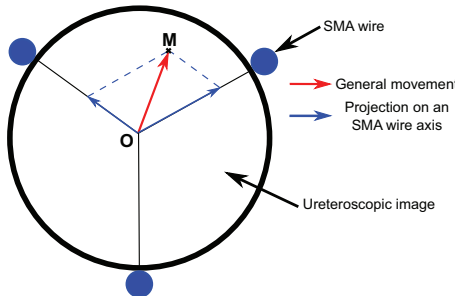


Fig. 6. Composition of movements to reach the point M on the ureteroscopic image

it never lets the system evolving under the sole effect of the natural convection. Exploiting the antagonistic positionning of the SMA wires (Fig. 3), it always maintains the system under the control of one active SMA wire at least, whatever the commanded displacement is. Additionally, a cooling water can be used by the surgeon during the ureteroscopy in order to facilitate the cooling of the wires. Hence, the system bandwidth can be considered to be more than 2.5 Hz, which is sufficient, compared to the laser shooting rate of 0.8 Hz.

IV. CONCLUSION AND FUTURE WORK

An SMA based active ureteroscope prototype was proposed to solve the problem of effective vaporization of kidney stones. An algorithm for kidney stones segmentation based on ureteroscopic images was developed and tuned for a general use. The system was successfully commanded using visual servoing.

The integration of a path planning with the command of the ureteroscope distal tip movement through visual servoing is the last step towards a complete operating prototype.

REFERENCES

- [1] R. Bartoletti, T. Cai, N. Mondaini, F. Melone, F. Travaglini, M. Carini, and M. Rizzo, "Epidemiology and risk factors in urolithiasis," *Urol. Int.*, vol. 79 Suppl. 1, pp. 3–7, 2007.
- [2] H. Tiselius, P. Alken, C. Buck, M. Gallucci, T. Knoll, K. Sarica, and C. Trk. (2009) Guidelines on urolithiasis. European Association of Urology. [Online]. Available: http://www.uroweb.org/fileadmin/tc_eauguidelines/2008/Full/17%20Urolithiasis.pdf
- [3] J. Szewczyk, R. Blanc, A. Gaston, and P. Bidaud, "Active catheters for neuro-radiology." Chambery, France: 2nd Surgetica Conf., 2007.
- [4] Y. Haga, Y. Tanahashi, and M. Esashi, "Small diameter active catheter using shape memory alloy," in *Proc. IEEE Int. Workshop Micro Electro Mechanical Systems*, 1998, pp. 419–424.
- [5] D. B. Leusmann, "A classification of urinary calculi with respect to their composition and micromorphology," *Scand. J. Urol. Nephrol.*, vol. 25, pp. 141–150, 1991.